EUROPEAN COMMISSION

European Research Area

Long-term Performance of Engineered Barrier Systems PEBS

Contract (grant agreement) number: ***FP7 249681***

DELIVERABLE (D-N°:D2.3-3-2)

Laboratory tests at the interfaces

Results of Small Cells with mortar-bentonite-magnetite

Author(s):

J. Cuevas, M.J. Turrero, E. Torres, R. Fernández, A.I. Ruiz, A. Escribano

Date of issue of this report: **31/10/13**

Start date of project: **01/03/10** Duration: **48** Months

Revised	Approved

Project co-funded by the European Commission under the Seventh Euratom Framework Programme for Nuclear Research &Training Activities (2007-2011)		
Dissemination Level		
PU	Public	X
RE	Restricted to a group specified by the partners of the PEBS project	
CO	Confidential, only for partners of the PEBS project	

EURATOM

Contents

LIST OF FIGURES

LIST OF TABLES

1 INTRODUCTION

The Deep Geological Repository (DGR) is currently the most accepted management option for the isolation of high level radioactive wastes. The DGR is based on a multibarrier system, which will limit the release of mobile radionuclides to the biosphere. In the multibarrier approach in a clay formation as geological barrier, the engineered barrier system (EBS) around the solid waste consists basically of a metallic canister surrounded by a bentonite buffer. The space between the clay barrier and the host geological formation will be filled with concrete. To give confidence in the function of the EBS, the European Commission has supported during the last decades scientific research programs, some of them focused on chemical processes taking place in the EBS (ECOCLAY I and II, NF-PRO and PEBS), since they can affect the feasibility of the barriers.

The main aim of the project PEBS (Long-term Performance of the Engineered Barrier System) is to evaluate the sealing and barrier performance of the EBS with time, through development of a comprehensive approach involving experiments, model development and consideration of the potential impacts on long-term safety functions. The experiments and models cover the full range of conditions from initial emplacement of wastes (high heat generation and EBS resaturation) through to later stage establishment of near steady-state conditions, i.e. full resaturation and thermal equilibrium with the host rock.

As part of this broad objective, a set of experiments were conducted to assess THM-C processes at the EBS. Alteration of bentonite buffer by iron from the C-steel alteration products and alkaline solutions from cement/concrete may be critical to system performance through changes in physical and chemical properties of these barrier materials (Savage, 1997). The aim of the experimental study presented in this report was obtaining evidences on the physical and geochemical processes occurring by the combine effects of cementitious materials from the concrete degradation and magnetite from steel corrosion on the bentonite barrier during storage and disposal of radioactive wastes. The tests try to reproduce the repository conditions prevailing 1000 to 3000 years after emplacement.

2 EXPERIMENT CONCEPTUAL APPROACH

To cover one of the main objectives of the project: *"The experiments and models cover the full range of conditions from initial emplacement of wastes (high heat generation and EBS resaturation) through to later stage establishment of near steady-state conditions"*, it was agreed to design experiments to reproduce the repository conditions prevailing 1000 to 3000 years after emplacement of wastes. This range of times was proposed after the calculations of bentonite saturation, alkaline front, diffusion front, spatial distribution of major ions concentration and interaction of corrosion products and bentonite reported in Samper et al. (2010). Furthermore, the experiments should consider the interfaces present in the EBS, the concrete-bentonite interface at the hydration zone and the iron-bentonite interface on the opposite side, at the heat focus.

The design of the experiments was discussed jointly by UDC-UAM-CIEMAT and a summary of the main decisions adopted concerning some key aspects related to the evolution of the EBS is provided in this document.

Temperature

Temperatures at the canister (r = 0.35 m) and at the bentonite-granite interface (r = 1.15 m) were computed by ENRESA (2003) and are shown in Figure 1. After considering the time evolution of temperatures represented in Figure 1 and the selected time range it was agreed that the experiments would run isothermal at 60 ºC.

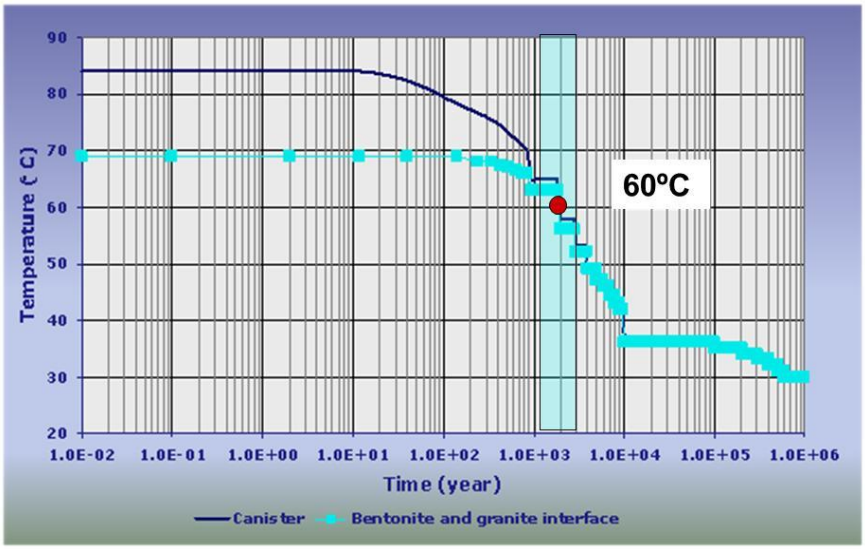

Figure 1: Time evolution of temperatures at the canister and bentonite-granite interface (ENRESA, 2003)

Exchangeable cation population

Based on long-term scope modeling (Samper et al., 2010) it was assumed that, close to the concrete interface (12 cm), in 3000 years of repository life, bentonite is going to be depleted in magnesium and in consequence enriched in potassium, sodium and calcium (Figure 2). Consequently, it was agreed to run the experiments with a pre-treated FEBEX bentonite (depleted in magnesium) and with the natural FEBEX bentonite for comparison purposes.

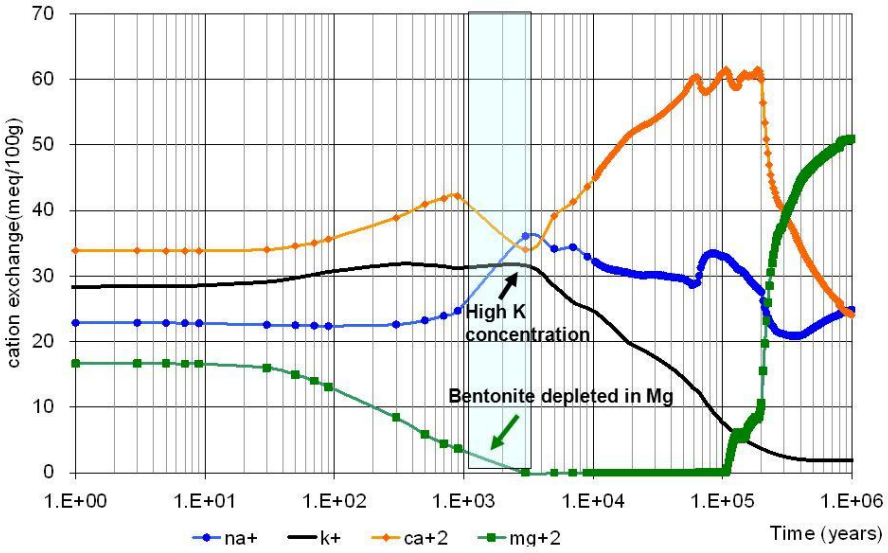

Figure 2: Computed time evolution of concentrations of interlayer exchanged cations ions at a point within the bentonite buffer close to bentonite-concrete interface (r = 1.125 m) (Samper et al., 2010).

Concrete-bentonite interface

A lime mortar was prepared in order to provide a source for calcium and alkalinity presumed to be an active process during concrete degradation after 1000-3000 years of repository operation.

Canister-bentonite interface

The result of chemical reactions between the C-steel canister and the bentonite and its environment is corrosion. Corrosion process will occur by a complex mechanism beginning with oxygen and/or water combined with the effect of temperature. The release of Fe^{2+} by corrosion can result in several corrosion products depending on the surrounding conditions. According to PA simulations, after 1000 to 3000 years of operation, anaerobic saturated conditions are expected nearby the canister surface. Under these conditions the passivation of the steel surface will occur due to the formation of a black protective film against further corrosion. According to thermodynamics, magnetite will be the prevailing corrosion product. Magnetite is the end-member of the transformation of ferrous hydroxide and for cast iron and C-steel. Smart et al. (2002) reported that, under anaerobic conditions, a duplex magnetite film is formed. This film comprises an inner adherent layer formed by a solid-state process and a thicker outer layer formed by dissolution-precipitation. A powder of magnetite in contact with bentonite was used in the experiments.

3 MATERIALS

3.1 Natural FEBEX Bentonite

The FEBEX bentonite was extracted from the Cortijo de Archidona deposit (Almería, Spain) and the processing at the factory consisted on disaggregation and gently grinding, drying at 60 °C and sieving by 5 mm. The physical-chemical properties of the FEBEX bentonite, as well as its most relevant thermo-hydro-mechanical and geochemical characteristics obtained during the projects FEBEX I and II are summarized in the final reports of the project (ENRESA, 2000, 2006). A summary of the results obtained is given below.

The montmorillonite content of the FEBEX bentonite is above 90 wt.% (92 ± 3 %). The smectitic phases are actually made up of a smectite-illite mixed layer, with 10-15 wt.% of illite layers. Besides, the bentonite contains variable quantities of quartz (2 ± 1 wt.%), plagioclase (3 ± 1 wt.%), K-felspar (traces), calcite (1 ± 0.5 wt.%), and cristobalite-tridimite (2 ± 1 wt.%).

The cation exchange capacity is 102 ± 5 meq/100g, the main exchangeable cations being calcium 36 ± 2 meq/100g, magnesium 37 ± 3 meq/100g and sodium 26 ± 2 meq/100g. The predominant soluble ions are chloride, sulfate, bicarbonate and sodium.

The external specific surface area is 61 ± 2 m^2/g and the total specific surface area is about 725 m^2/g.

3.2 Pre-treated FEBEX Bentonite

In order to fabricate a bentonite depleted in magnesium and enriched in potasium (FEBEX K, Na, Ca – from now on FEBEX Pre-treated), 500 g of natural FEBEX bentonite were soaked for 24 h in 5L of 1MKCl-1MNaCl-0.5M $CaCl_2$ aqueous solution in a polypropylene 10 L tank. The suspension was led to settle 24 h, then it was partially decanted (approx 2/3 of the solution can be removed without loose of suspended material), and the conditioning solution was renewed two times repeating the procedure described. After this, the aqueous phase was renewed two more times, this time using distilled water after the corresponding 24 h settling. The obtained slurry was allowed to air dry during three weeks and then grinded to pass a 1 mm sieve with a hammer mill.

The pre-treated FEBEX bentonite has a 13.0 ± 0.1 weight % water content under laboratory environmental condition (30-40 % RH) and its final distribution of exchangeable cations and the BET specific surface can be compared to natural FEBEX in Table I.

Pre-treated FEBEX bentonite showed a decrease in CEC, calculated as the sum of the charges of exchangeable cations, which has led us to investigate, in terms of K-exchange, its impact on a presumably mineralogical transformation of the smectite component of bentonite. The XRD randomly oriented powder patterns of pre-treated and natural bentonite have similar peak intensities considering the non-basal asymmetric hk0 reflections (4.49, 2.57, 1.70 Å d-spacings) or

060 (1.50 Å). By contrast 00l reflections are different. The FEBEX K, Na, Ca – form shows a broad 001 d-spacing in a 15-13 Å range thus combining Ca and K typical d-spacings. This is consistent with its exchangeable cations composition. Nevertheless a 10-- Å peak (illite) is more noticeable in pre-treated than in natural bentonite (Figure 3).

Table I: Exchangeable cations and BET surface (SBET) for the natural and pre-treated FEBEX bentonites.

FEBEX	Na^+ (cmol(+)/Kg)	K^+ (cmol(+)/Kg)	Ca^{2+} (cmol(+)/Kg)	Mg^{2+} (cmol(+)/Kg)	Total (cmol(+)/Kg)	SSA BET (m^2/g)
Natural	26 ± 2	2.3 ±0 .1	36 ± 2	37 ± 3	102± 5	56 ± 0.5
Pre-treated	6.5 ± 0.3	31 ±0.5	43 ± 2	1.8 ± 0.2	81± 2	58 ± 2

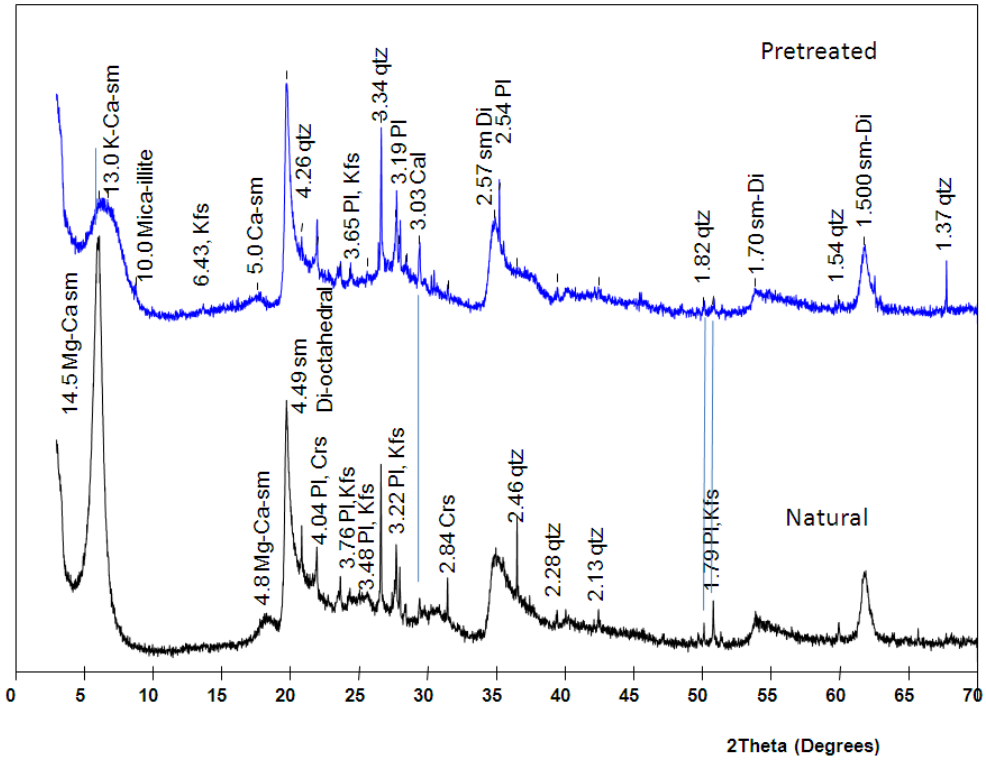

Figure 3: Bulk sample randomly oriented XRD powder patterns of Natural and Pre-treated FEBEX bentonite. Numbers are d-spacings in Å. Sm: smectite, Sm-Di-dioctahedral smectite ; qtz: quartz, Kfs: K-feldspar, Pl: Plagioclase, Cal: calcite.

In order to study in detail the smectite component there were prepared, by duplicate, oriented aggregates by pipetting a < 2 µm size fraction suspension on a glass slide (Moore and Reynolds,

1989). Once the oriented films were air dried in the lab, one of the replicas was treated with ethylene-glycol vapor in order to strain the 001 montmorillonite lattice plane from its dry state (13 Å in the case of K-dominated form or 15 Å in the case of Ca-Mg form) to 17 Å (ethylene- glycol (EG) spacing for all cations-smectite species). The XRD patterns from natural or pre-treated samples are shown in Figure 4. Pre-treated FEBEX was partially collapsed by the K-exchange treatment as far as 001 and 002 d-spacings are not completely expanded, visibly broaden (d_{001}= 16.2 Å) and with non regular positions: d_{002} has to be placed at half d-spacing regarding d_{001} (i.e. 8.5 and 17 in natural FEBEX). This means that the 2:1 smectite structure behaves as a mixed layer mineral (MLM) including illite-like and smectite structures. The proportion of collapsed layers (illite) has been calculated with the expert program MLM from Plancon and Drits (1999) as 40 % illite/60 % smectite type, the layers randomly distributed. In fact they are not true illite as far as a re-saturation of cation exchange positions with Mg and re-expansion in the presence of EG vapor yielded a regular smectite d-spacing behavior, so the effect is reversible. Nevertheless, a significant decrease of CEC can be explained by the collapsing effect of potassium, which is not completely reversible to the cesium exchange practiced in the displacement method prepared to determine the distribution of exchangeable cations.

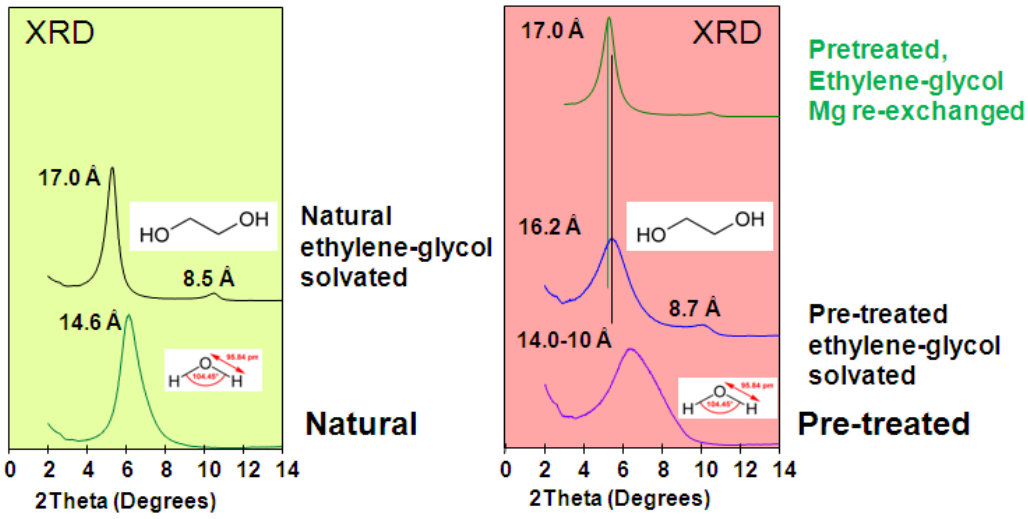

Figure 4: XRD patterns from oriented aggregates prepared with a separated < 2µm size fraction of each of the bentonites.

3.3 Mortar

A lime mortar was prepared in order to provide a source for calcium and alkalinity presumed to be an active process during concrete degradation.

The lime mortar was formulated as a 2:1 quartz-sand (< 0.5 mm particles diameter)/CaO (quicklime binder) mixture similar to some formulations provided in Stefanidou and Papayianni (2005). CaO was obtained by calcining $Ca(OH)_2$ Panreac™, P.A. grade reagent at 950 ^oC, which was allowed to quench inside a glove box in which a deposit with NaOH pellets acted as a trap for CO_2. The mix was then amassed inside by hand with a Water/binder ratio = 1, in a polypropylene cup. After the exothermic reaction for CaO hydration, the hydrated mix was pressed inside PVC mold rings of 50 mm diameter allowing it to harden for one month in a deposit free of CO_2. The characteristics of this mortar, once it was water saturated, are summarized in Table II.

Table II: Characteristics of lime mortar prepared for the experiments.

Porewater pH	Water content weight %	Dry density	Calculated porosity V %	Hg intrusion porosity(*) v%	$Ca(OH)_2$ weight %
12.6	22.9	1.55	35.4	33.3	39.8

*: As measured in a Micromeritics™ AutoPore IV 9500 V1.05 apparatus

3.4 Magnetite characteristics

20 g of magnetite (Fe_3O_4) powder (1-5 µm) provided by Atlantic Equipment Engineers ref. (CAS-1317-61-9) was used for the experiments. The physical characteristics of the magnetite as received are: Density: 4.8-5.1 g/cm^3 at 25 °C and molecular weight: 231.53 g.

3.5 Spanish reference argillaceous formation water composition

The water used to hydrate the cells is an artificial clay water (Na^+-Ca^{2+}-SO_4^{2-} type water) (Table III) obtained in the laboratory after the analysis and synthesis of the water of a Spanish reference clayey formation (Turrero et al., 2001, 2006).

Table III: Main chemical species (M) in the synthetic water obtained from the Spanish Reference Argillaceous Formation.

Chemical species	Concentration (M)
Fe	1.1E-05
Na	1.3E-01
K	8.2E-04
Ca	1.1E-02
Mg	8.2E-02
Si	2.7E-04
SO_4^{2-}	7.0E-02
Cl^-	2.3E-02
HCO_3^-	1.8E-03
pH= 7.54	

4 EXPERIMENTAL SETUP

A total of six experiments were performed simultaneously:

- Two experiments with bentonite, one with natural FEBEX bentonite and the other with pre-treated FEBEX bentonite. These experiments were planned as blanks.
- Two experiments with mortar-bentonite-magnetite, one with natural FEBEX bentonite and the other with pre-treated FEBEX bentonite.
- One experiment with mortar-pre-treated FEBEX bentonite.
- One experiment with magnetite-pre-treated FEBEX bentonite.

The tests were performed in cylindrical cells with an internal diameter of 5 cm and an inner length of 2.5 cm. They are made out of Teflon to prevent as much as possible lateral heat conduction. The upper closing of the cells is made by means of a stainless steel plug. The hydration is made through that plug with water taken from a stainless steel pressurized deposit. A porous stainless-steel filter with pore size of 0.45 μm is placed between the plug and the sample. The plug has concentric grooves in the plane in contact with the filter that allow a better distribution of the water (Figure 5). The bottom part of the cells is a plane stainless steel. A Teflon disc is placed between the sample and the stainless steel. A schematic diagram of the setup and a picture of the cells are shown in Figure 5 and Figure 6.

Blocks of FEBEX bentonite were compacted with its hygroscopic water content (14%) at a nominal dry density of 1.65 g/cm^3 and placed inside each cell according to the scheme in Figure 5. In the cells 3 and 4 the magnetite powder was placed giving rise to a layer thickness of ≈ 2.0 mm. On top of this, the bentonite block (≈ 18 mm) was inserted, then the mortar (≈ 5 mm) and a porous filter over it.

Hydration from the deposit started as soon as setting-up of the cells finished. The deposit was initially pressurized with nitrogen at 5 bars. It was periodically weighed, and this allowed checking water intake.

The six cells were mounted at a time, starting operation on 15/03/2011. All of them were set up and run in the same way with the only difference of the materials inside.

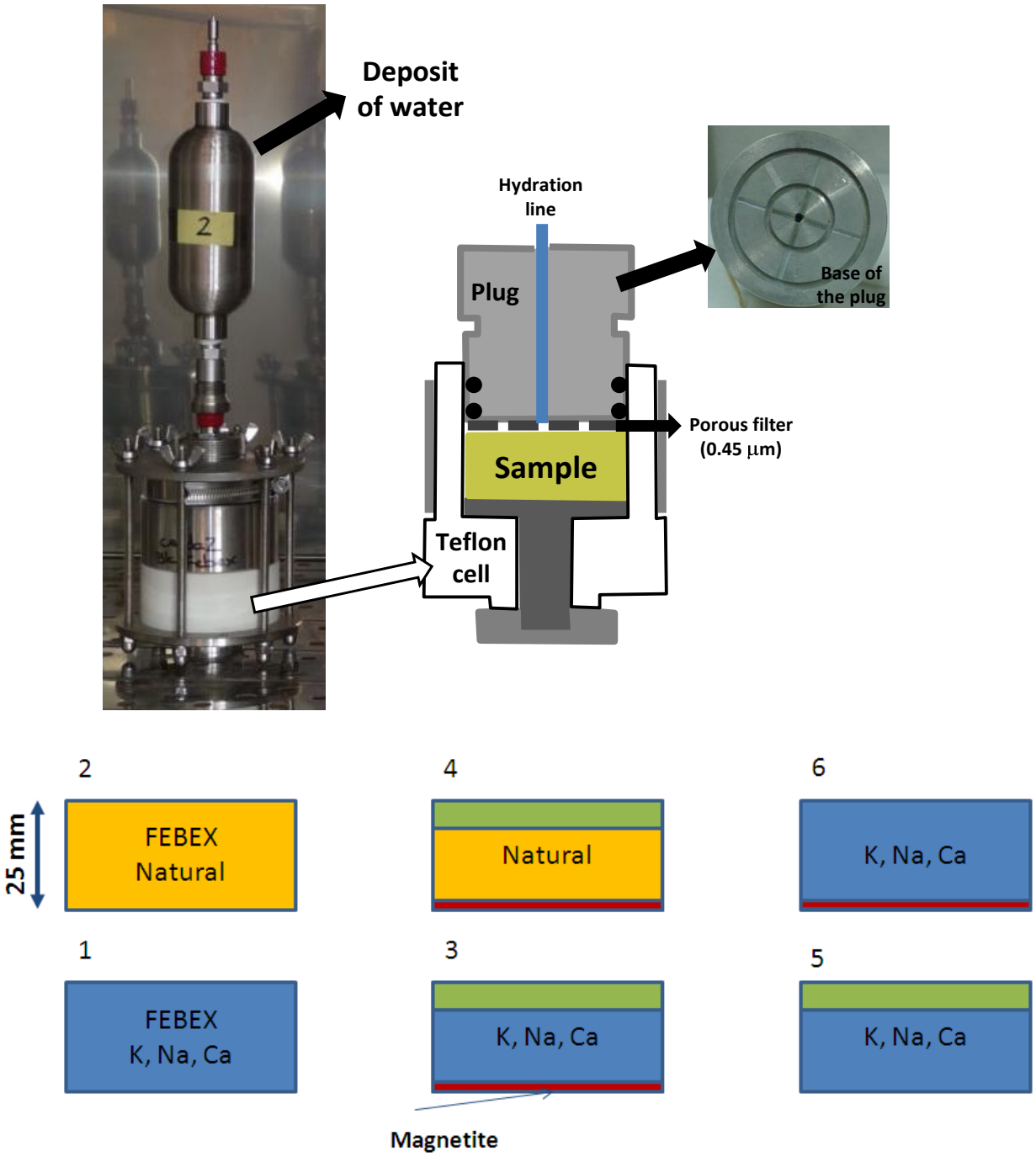

Figure 5: Top: Picture showing the final configuration of the experiment and a scheme of the cell. Botton: Scheme of the six samples for the experiments performed in small cells.

Figure 6: Final configuration of the experiment, with the six cells inside an oven adjusted at 60 ^{o}C.

The tests were in operation for 18 months. Apparently, no operational problems occurred with cells 2, 4, 5 and 6 during that period. However, cells 1 and 3 had water leakage from the beginning of operation. Leakage was successfully solved in cell 3 in 2 weeks but it was not the case for cell 1 that kept little leakage during the whole life of the tests, which was evident in the white precipitate formed at the bottom part of the cell.

4.1 Dismantling, Cutting and Sampling

The small cells experiments were dismantled in September-October 2012. The aspect of the bentonite cylinders after dismantling was expected to be a compact block (including mortar and magnetite interfaces). This was true for the mortar and bentonite but not for the magnetite, which readily separates and part of it disaggregates in powder (e.g. cell 3, Figure 7).

The pre-treated bentonite (1 in Figure 5) was first dismantled in order to gain experience for a first cutting plan, sampling procedure and amounts of material needed for the analysis (Figure 8).

The operations performed during the dismantling of the cells were as follows:

1. Demolding and inmediate weighting of the block, preserving inert conditions by operating the process inside a glove box filled with nitrogen gas (Figure 7).

2. Isolation of the block using Parafilm® paper. This was assured outside the glove box by wrapping the block with textile adhesive strands.

3. Cutting as it is designed in the drawing of Figure 8, which it is illustrated by the photographs in Figure 9.

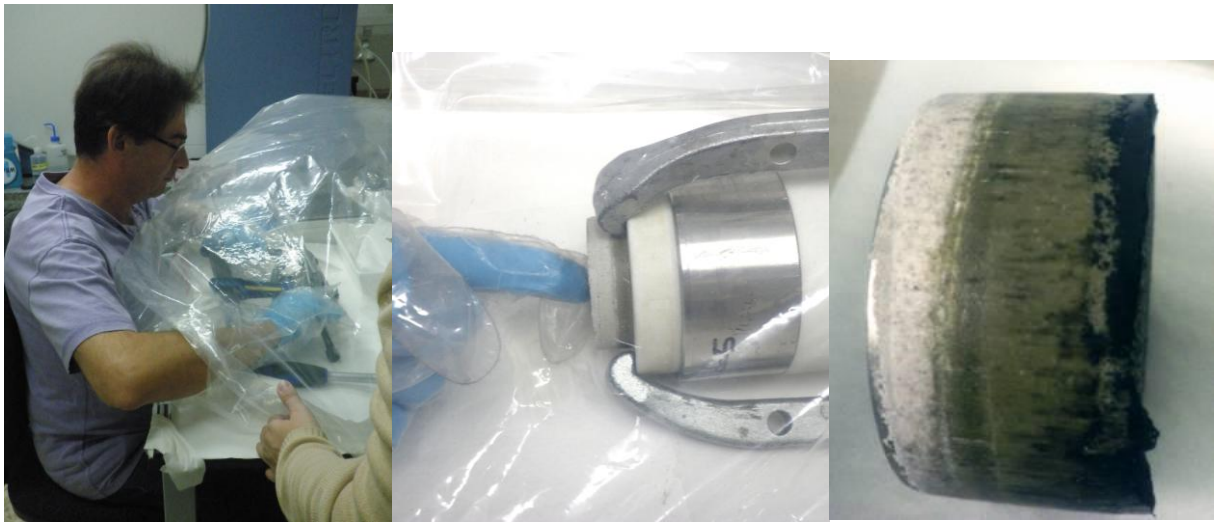

Figure 7: Pictures showing the extraction of the material from the Teflon cell. The dismantling was made inside a plastic globe box filled with nitrogen (left) to minimize alteration of the samples by contact with atmosphere. On the right, picture shows one of the cells with mortar and magnetite interfaces once dismantled. Magnetite has dissagregated and a dark area just at the interface with mortar is observed.

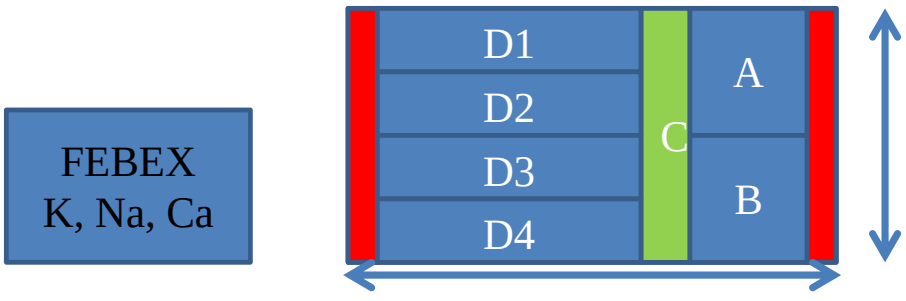

Figure 8: Cutting design for small cell 1. A, B: samples for water content and density. C: longitudinal cut for preparing polished sections for microscopy inspection and analysis. D: transversal sections to determine porosity, mineralogy, external specific surface, exchangeable cations and soluble salts. The transversal sections have been modified in other cells in order to include mortar or magnetite sections (to be described later on). In red: approx 2.5 mm exterior ring to be avoided in by scrapping the surface before preparation operations.

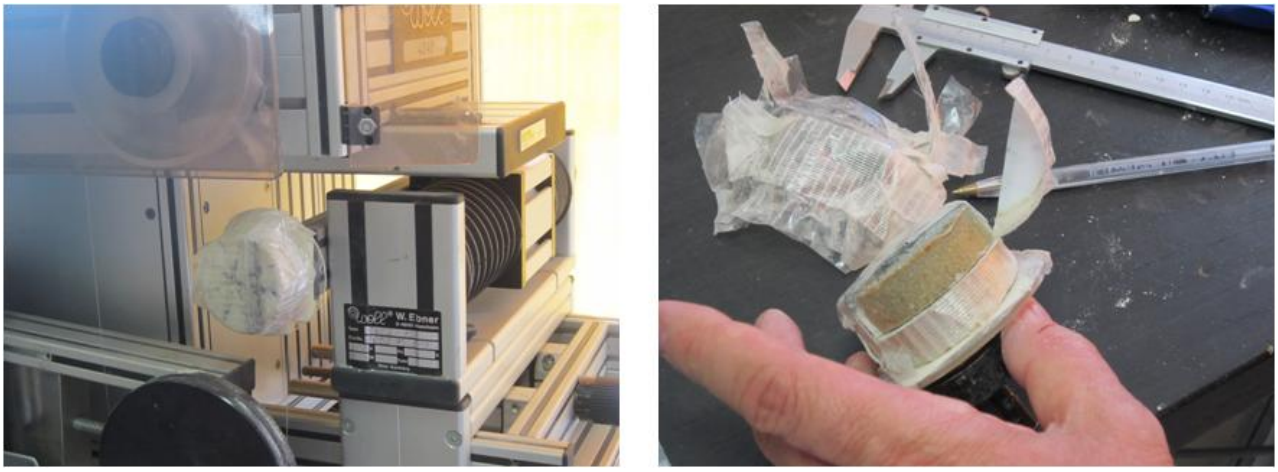

Figure 9: Photographs showing the protected block during the process of cutting in the diamond wire saw.

The cutting was done with small modifications for the different cells, taken into account that they have different thicknesses of bentonite and that they include interfaces. Figure 10 shows the different cuttings performed considering to have enough quantities to carry out the analyses. The cutting machine failed in the middle of cells 2, 3 and 4. Then, it was not possible to maintain the integrities of some of the longitudinal sections as far as we had to end the cuttings with a hand conventional thin wire saw. Finally, after several failed repairs we had to wait to December 2012 to be able to use the diamond wire cutting saw and to practice the planned cuts for cells 5 and 6. The wire saw allowed us to cut the bentonite without breaking the sample and without risk of heating and drying the samples. The bentonite density (1.65 g/cm^3 on average) is high enough to make the samples relative stiff so they cannot be cutted with cutter blades without breaking them in pieces. The thicknesses reported of the sampled slices are approximated (± 2 mm).

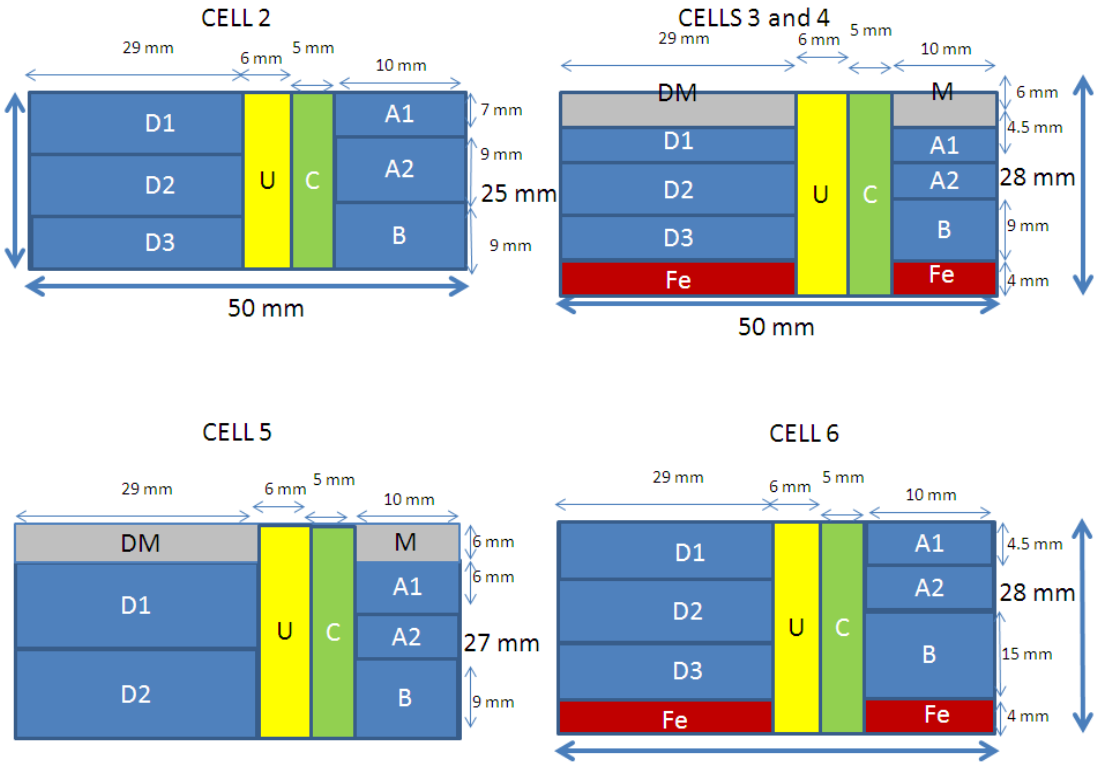

Figure 10: Drawing of the different sampling schemes performed on small cells. A, B: samples for water content and density. C: longitudinal cut for preparing polished sections for microscopy inspection and analysis. D: transversal sections to determine porosity, exchangeable cations and soluble salts. U: longitudinal section to perform a detailed sampling for mineralogy and external specific surface determinations.

4.2 Methods of analysis

4.2.1 Dry density and water content

The method used to determine the bulk density was the paraffin coating method (Blake and Hartge, 1986) applied to the small slices cutted from the bentonite blocks extracted from the cells. It is based on the Arquimedes principle as the paraffin coated specimen is weighted both on air and immersed in pure water. The weights difference is the volume of the sample assuming density 1 for water, so density can be calculated as the ratio of the specimen weight on air to the volume. The volume occupied by paraffin is calculated from its density (0.910 g/cm^3) and used to correct the measurement. The specimen is coated in paraffin by immersing the sample with the aid of steel tongs at 70 $^{\circ}$C in pure liquid paraffin just a few seconds. Then, it is rapidly dry with a fan.

Once the bulk density has been determined, the paraffin coated sample is cleaned of paraffin using cutter blades. The water content is then determined by heating the cleaned specimen at 110 $^{\circ}$C in an oven until constant dry weight (48 h).

4.2.2 Polished sections for textural and elemental analysis at the interfaces

The sections labeled C in Figure 10 were prepared for embedding in LR-White© resin following the procedure described by Cobeña et al. (1999) adapted from Kim et al. (1995) to bentonite sections. Once the 5 mm thick bentonite-interface slice is cutted (hermethically coated by paraffin paper) and separated under free-CO_2 atmosphere (glove box with alkaline traps, see Figure 11), the slice is immersed in liquid nitrogen inside a polycarbonate box filled with porous filter paper at the inner base. After approximately 2 h, the freeze box is placed in a vacuum chamber until 10^{-6} mmHg is achieved (three days). Then it is placed in a dessicator containing P_2O_5 powder (dry conditions), and several droplets of the liquid resin are added through the filter paper at the base of the longitudinal section. The slice is not covered with resin at the top to permit the entrance of the liquid from the base to the top by capillarity under vacuum conditions. The box is periodically refilled with resin if it is needed. After 24 h the slice is completely covered with resin and the top is filled with filter paper platelets that absorb an excess of liquid resin. Then the box is closed rejecting gas bubbles and it is tightly wrapped first by a thin paper and secondly with plastic (PVC) adhesive strands in order to prevent the entrance of humidity and oxygen. The box is finally introduced in an oven at 60 ^{o}C during 48 h for the resin curing process. The hardened sample is again cut at the level of the filter paper, and this surface is polished for SEM-EDX textural and elemental analysis. Figure 12 shows the polished aspect of longitudinal fragments of 3, 4, 5 and 6 cells. Cell 4 and partially cell 3 is visibly fragmented because of the cutting problems mentioned in section 4.1. Figure 13 compares a well preserved dry (without resin) fragment of cell 3 (separated for XRD sampling) to a well embedded slice of cell 5. Bentonite darkens as it is observed in the whole cell 6, without mortar and in most parts of cells 3 and 4 (bentonite here was presumably not totally well embedded). A bright bentonite band of 4-5 mm characterizes the bentonite at the mortar interface. This is also more or less well traced in polished section of cells 3 and 4 in Figure 12.

Figure 11: Separation of the pre-cutted slices in a glove box. Small cell 5. On the left: aspect of the thin section slice inside a polycarbonate box.

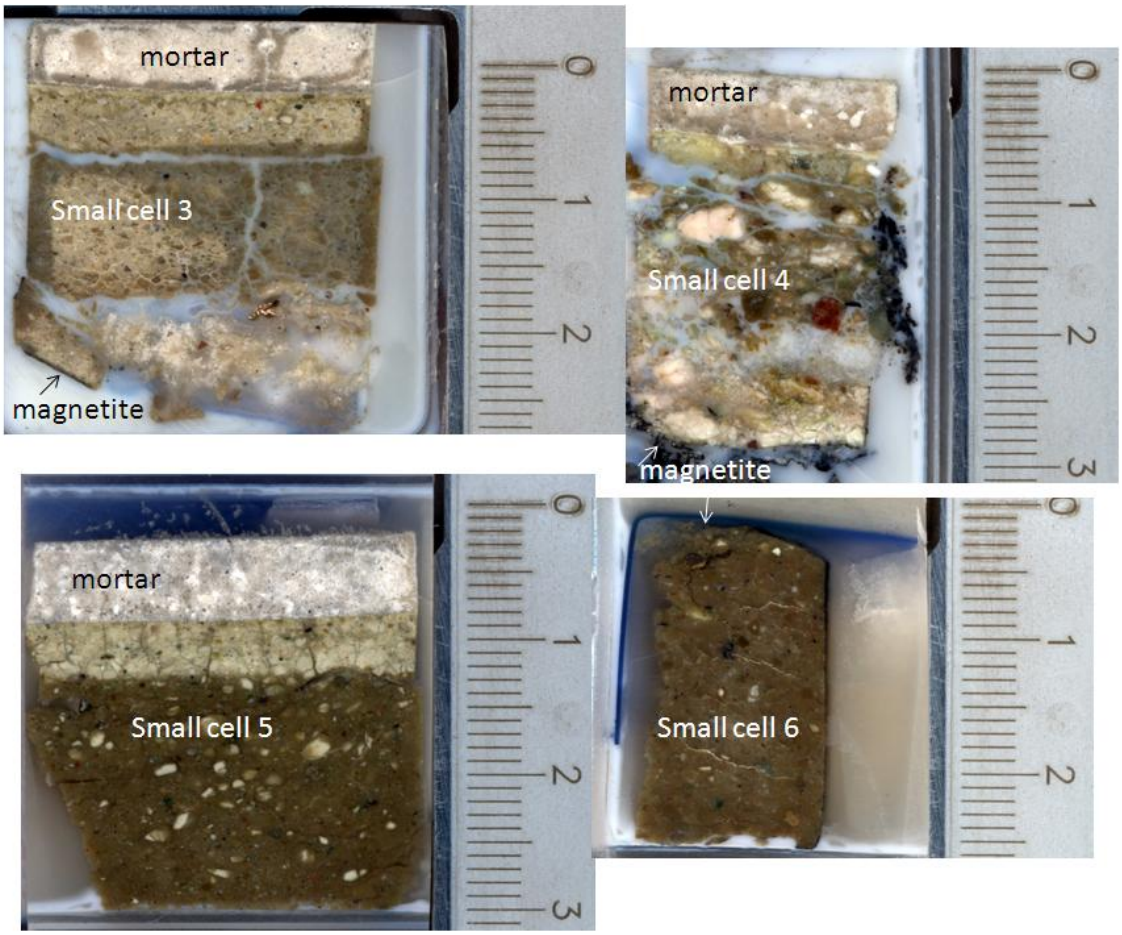

Figure 12: Aspect of the interface small cells slices cut for polished sections prepared for SEM-EDX analyses.

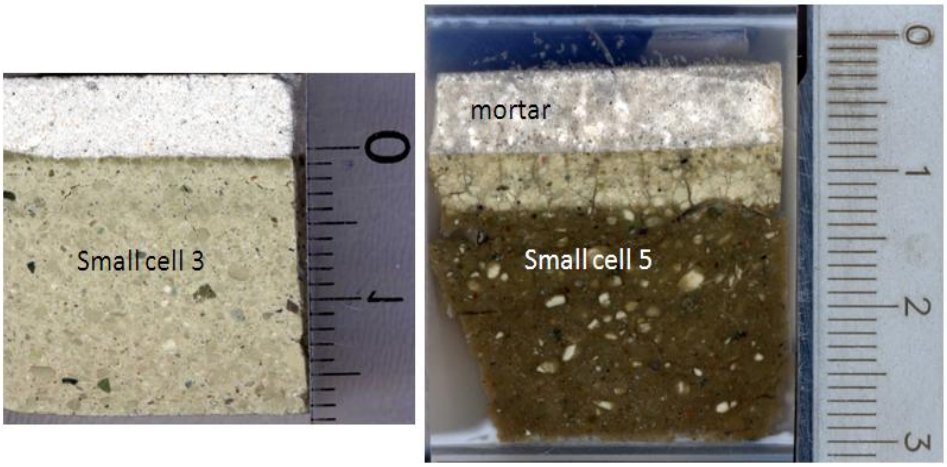

Figure 13: Comparison of a dry polished section to an embedded polished section from lime mortar bentonite interfaces experiments.

4.2.3 Textural and elemental analyses at the interfaces

Textural and elemental analysis was performed by scanning electron microscopy (SEM) coupled with energy dispersive of X-rays detector (EDX). The study of micrometric features (mineral morphologies and inter-relationships) was sometimes performed in fresh fractured samples at the interfaces. However, the detailed study of texture and chemistry was performed in the longitudinal polished sections under backscattering electron mode and by means of chemical profiles analysis using EDX. The profiles of the chemical composition along the column axis were measured by SEM-EDX with a Hitachi S-3000N microscope and an INCAx-sight analyzer from Oxford Instruments. The spatial resolution around magnetite or mortar interfaces was 0.05 mm using a rectangular slit 1 mm wide in order to acquire a representative analysis, taken into account the heterogeneity of the grains that composed the material (Figure 14). In the bulk bentonite or within the mortar, the analyses were taken every 0. 5 mm. In all cases the analysis was performed by integration at least 5000 counts/s in the targeted area.

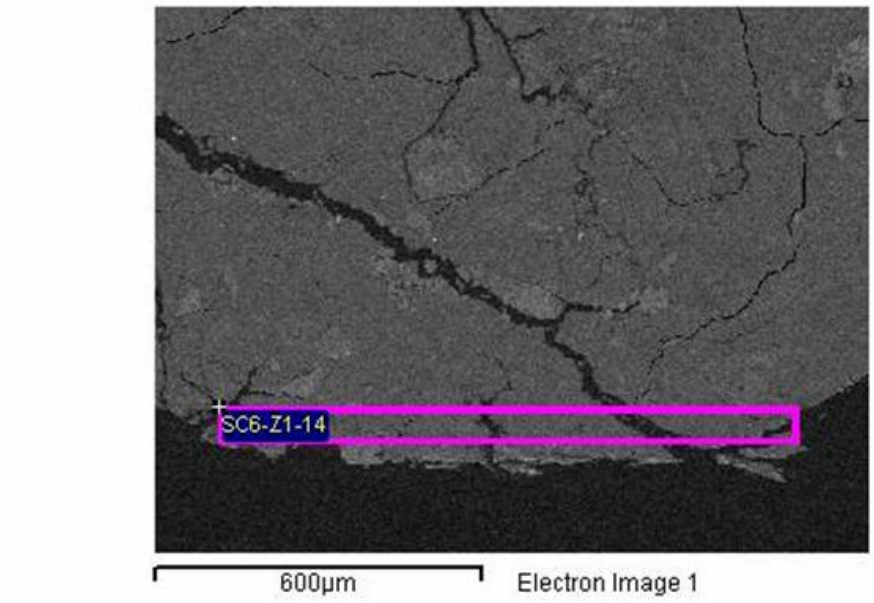

Figure 14: Example of the slit size (0.05mm x 1mm) used for integrate energies dispersive of X-Rays for chemical analysis at the interfaces (magnetite interface of cell 6).

4.2.4 Pore size distribution and BET specific surface area (SSA-BET)

Pore size distribution was determined in a well preserved fragment of the samples labeled D in Figure 10.

For the mercury intrusion porosimetry (MIP) and the physisorption tests samples of sizes lower than 1 cm^3 were cut and lyophilized in a Telstar LioQuest equipment for 24 h at a temperature of -50 °C under a vacuum of 0.2 mbar so that to eliminate the water in the pores. The porosimeter

used was a Micromeritics AutoPore Series IV 9500, which applied a maximum injection pressure of 33000 psia (228 MPa), what allowed the exploration of pore sizes between 0.003 and 360 µm. The equipment used for the physisorption tests was a Micromeritics ASAP 2020.

The external specific surface area (SSA) was analyzed in the sections labeled U in Figure 10. These sections were sampled for different sublevels by using cutters and steel scrapers under a conditioned glove box. The different sublevels samples for the six small cells, used in BET (SSA BET) and X-ray diffraction determination are listed in Table IV.

The separated samples were dried under vacuum in a dry (P_2O_5) and CO_2 free atmosphere (NaOH pellets) for 1 week. The dried samples were grinded by hand in an agatha mortar and stored in polycarbonate vials. 100-200 mg of these samples were heated to 90 ^oC 24 h in a sample holder and then outgassed in a nitrogen current for 2h in a degasification station. The SSA was then determined by nitrogen adsorption in combination with the BET equation in a Gemini V analyzer from Micromeritics™ using the 5-points isotherm method. The degassing phase, which takes place before the realization of the isotherm, was carried out from a 0.2 g sample heated to 90 ^oC for 18 hours (Norm UNE 22-164/94). The advance of this method is the reproducibility of measurements, which allows the comparison of data between different laboratories.

4.2.5 Mineralogical analysis by X-Ray Diffraction (XRD)

The XRD patterns registered from bulk randomly oriented powders and oriented < 2 µm aggregates were recorded in an angular range (2θ) of 3º-70º, and 3º-20º, respectively, in a θ/2θ X-PERT Panalytical instrument with an X-CELERATOR detector. This dispositive allowed taking measurements equivalent to -16º angular steps during 100 s each step. Voltage and intensity of the operated X-Ray Cu tube were 40 kV and 40 mA. The equipment uses monochromatic radiation provided by a primary graphite monochromator. Patterns for iron rich minerals were recorded in a SIEMENS 5000 instrument with a solid state SiLi detector discriminating energies and then avoiding high fluorescence background.

Prior to register the XRD patterns, the vials with dry powders prepared both for BET analysis and XRD were stored in a 50 % relative humidity chamber in order to rehydrate in comparable conditions the commonly hydrated clay mineral or CSH-like phases. Very small samples (< 50 mg) were taken at the interfaces or in special locations when the cells were dismantled (i.e., hydration source-mortar/bentonite contact). In order to study these small samples by XRD, the powder was pressed with a spatula in a zero background silicon wafer and then registered.

4.2.6 Scanning Electron Microscopy (SEM)

SEM-EDS characterization of the samples was done in two different equipments: at the UCM facilities with a SEM JEOL JM-6400 microscope coupled to a dispersive X-ray energy spectrometer X LINK LZ_5. Iron oxide samples were metallised with gold, whereas in the bentonite samples a

graphite coating was deposited on them. The equipment used at the UAM facilities was a SEM Hitachi S-3000N microscope and an INCAx-sight analyzer from Oxford Instruments.

Table IV: Samples taken at different sublevels. Numbering starts from the hydration source face. The first number of the samples is the cell number.

Sample UAM (U)	Description	Thickness (mm)	Analysis
1.1	Bentonite, from sample 1A*	**12**	RX, BET
1.2	Bentonite from sample 1B	**12**	RX, BET
2.1	Bentonite	**8**	RX, BET
2.2	Bentonite	**8**	RX, BET
2.3	Bentonite	**8**	RX, BET
3.1	Mortar-bentonite interface	**2**	RX, BET, SEM
3.2	Mortar upper face	**4**	RX, BET
3.3	Bentonite interface	**2**	RX, BET
3.4	Dark rim	**3.0**	RX, BET
3.5	Bentonite with 1 mm dark rim	**4.0**	RX, BET
3.6	Bentonita	**~5.5**	RX, BET
3.7	Bentonite-magnetite interface	**4**	RX, BET
3.Fe	Magnetite	**4**	RX, BET
4.1	Mortar	**~3.5**	RX, BET
4.2	Mortar lower face	**~3.5**	RX, BET
4.3'	Mortar interface	**<1**	**RX,SEM**
4.3	Mortar-bentonite interface	**2**	RX, BET
4.4	Bentonite crushed	**~7-8**	RX, BET
4-5.1	Bentonite	**5**	RX, BET
4-5.2	Bentonite	**5**	RX, BET
4.FeB	Bentonite-magnetite interface	**<1**	**RX-SEM**
4-Fe	Magnetite	**~2**	RX, BET
4-FeI	Magnetite interface	**~2**	RX, BET
5.I	Hydration Interface for SEM		**RX, SEM**
5.1	Mortar	**5.4**	RX, BET
5.2	Mortar lower face	**1.5**	RX, BET
5.2'	Mortar interface		**RX**
5.3	Mortar-bentonite interface	**4.1**	RX, BET
5.3'	Bentonite interface		**RX**
5.4	Bentonite	**3.8**	RX, BET
5.5	Bentonite	**3.9**	RX, BET
5.6	Bentonite	**6**	RX, BET
5.7	Bentonite	**4.1**	RX, BET
6.1	Bentonite	**6**	RX, BET
6.2	Bentonite	**6**	RX, BET
6.3	Bentonite	**6**	RX, BET
6.4	Bentonite	**6**	RX, BET
6.FB	Bentonite-magnetite interface	**~1**	RX
C6.Fe	Magnetite	**4**	RX, BET

*In cell 1, the U section was not separated. Then, A and B samples, used for water content analysis were used for XRD and SSA (BET) determination

4.2.7 Soluble salts

Each of the subsamples represented in Figure 8 and Figure 10 as DM, D and Fe was used to analyse soluble elements in aqueous extract solutions. Samples were dried overnight in an oven at 60 ^{o}C. They were ground and placed in contact with deionised and degassed water at a solid to liquid ration of 1:8 (1 g of clay in 10 mL of water), shaken end-over-end and allowed to react for 24 hours. Separation was made by centrifugation (30 minutes at 12500 rpm) and the supernatant was filtered by a 0.45-µm pore size filter. Duplicates were made for all the samples.

Cations and anions were analysed using ion chromatography (Dionex DX-4500i).

4.2.8 Adsorbed iron

The sample (just subsamples D) remaining after soluble salt extraction was used to extract the adsorbed iron. The procedure consisted on adding 10 ml of citric acid 0.3 M, shaking end-over-end and allow the sample to react for 24 hours. Separation was made by centrifugation (30 minutes at 12000 rpm) and the supernatant was filtered by a 0.45-µm pore size filter. Analyses were made by Inductive Coupled Plasma - Optical Emission Spectrometry (ICP-OES) in a Spectro ARCOS spectrometer.

4.2.9 Exchangeable cations

Before determining systematically the exchangeable cations in the different bentonite subsamples (D in Figure 8 and Figure 10) three of those subsamples were selected to analyse exchangeable cations by two different methods described below as Method A and Method B and compare results: natural FEBEX bentonite, sample C1D4 and sample C3D1 (both of pre-treated FEBEX bentonite). Duplicates were made for all the samples and cations were measured by ion chromatography in all the samples and by ICP-OES in all the samples except C1D4 Method A and C3D1 Method A.

Method A: a $CsNO_3$ solution was used to displace the exchangeable cations. Bentonite samples were equilibrated with $CsNO_3$ 0.5 N at pH 8.2 at a solid to liquid ratio of 0.25 kg/L (2 g of clay in 15 ml of $CsNO_3$ 0.5 N). After shaking end-over-end for 24 hours the phase separation is made by centrifugation (30 minutes at 12000 rpm), the supernatant solutions were filtered by 0.45 µm and the concentration of the major cations was analysed by ion chromatography and ICP-OES just for the natural FEBEX bentonite.

Method B: a $CsNO_3$ solution was used to displace the exchangeable cations. Bentonite samples were equilibrated with $CsNO_3$ 0.5 N at pH 8.2 at a solid to liquid ratio of 0.25 kg/L (2 g of clay in 15 ml of $CsNO_3$ 0.5 N). A magnetic shaker was used for 2 minutes and next an end-over-end shaker for 24 hours. Following 5 series of alternating ultrasonic dispersion for 5 minutes and end-over-end shaking for 5 minutes were made. The phase separation was made by centrifugation (30 minutes at 12000 rpm) and the supernatant solution was filtered by 0.45 µm and reserved. The process was repeated twice with the remaining solid. Finally, the three aliquots were mixed and

filled up to 50 ml with $CsNO_3$ 0.5 N and the concentration of the major cations was analysed by ion chromatography and ICP-OES.

The results obtained by both methods are shown in Table V. Based on the analyses of parallel samples denoted by 1 and 2, and comparing results from different methods and analytical techniques no significant differences were found. For this reason, the simplest method A and ion chromatography were selected for analysing exchangeable cations in all the samples.

Table V: Comparison of results of exchangeable cations obtained by two different methods A and B as described in the text.

Sample identification	Na^+ (cmol(+)/Kg)	K^+ (cmol(+)/Kg)	Mg^{2+} (cmol(+)/Kg)	Ca^{2+} (cmol(+)/Kg)
Natural FEBEX 1 Method A - IC	25,59	2,01	38,11	34,51
Natural FEBEX 2 Method A - IC	26,14	2,18	39,56	35,46
Natural FEBEX 1 Method A - ICP	26,20	2,09	38,37	35,29
Natural FEBEX 2 Method A - ICP	26,20	2,09	33,58	34,12
Natural FEBEX 1 Method B - IC	25,95	2,91	42,63	37,07
Natural FEBEX 2 Method B - IC	26,00	2,46	42,29	36,85
Natural FEBEX 1 Method B - ICP	25,62	2,12	33,19	36,51
Natural FEBEX 2 Method B - ICP	26,18	2,19	33,04	35,65
C1D4-1 Method A - IC	15,18	25,67	4,15	37,88
C1D4-2 Method A - IC	15,38	26,13	4,13	38,27
C1D4-1 Method B - IC	14,85	27,78	3,75	40,31
C1D4-2 Method B - IC	15,05	26,35	3,67	39,42
C1D4-1 Method B - ICP	14,66	26,12	3,75	40,15
C1D4-2 Method B - ICP	14,63	25,88	3,67	38,02
C3D1-1 Method A - IC	15,79	25,78	0,00	41,37
C3D1-2 Method A - IC	15,61	24,96	0,00	38,84
C3D1-1 Method B - IC	10,62	21,98	0,00	46,92
C3D1-2 Method B - IC	11,74	22,96	0,00	52,85
C3D1-1 Method B - ICP	10,06	21,19	0,00	47,15
C3D1-2 Method B - ICP	11,13	23,03	0,00	50,84

IC: ion chromatography; ICP: Inductive Coupled Plasma - Optical Emission Spectrometry

5 RESULTS AND DISCUSSION

5.1 Water intake

The deposits of all cells were periodically weighted and the loss of water in the deposits allowed inferring the water intake in the samples. Figure 15 shows these measurements. A quite fast

increase of water intake in cells 2 to 6 can be observed during the first two months of operation followed by the stabilization. The behavior of cell 1 is quite different. A leakage was detected from the first week of operation and it was not possible to correct the failure. It was usual to find a white precipitate of salts at the bottom part of the cell. Then, the measurements of water intake in that cell are not reliable in the sense of hydration behavior of the sample, although allow us to know exactly how the cell was functioning, which is important to interpret the final results. The same is true for cell 3. Although in this case the failure was corrected in a couple of weeks from start of operation, the first set of data appears unreliable.

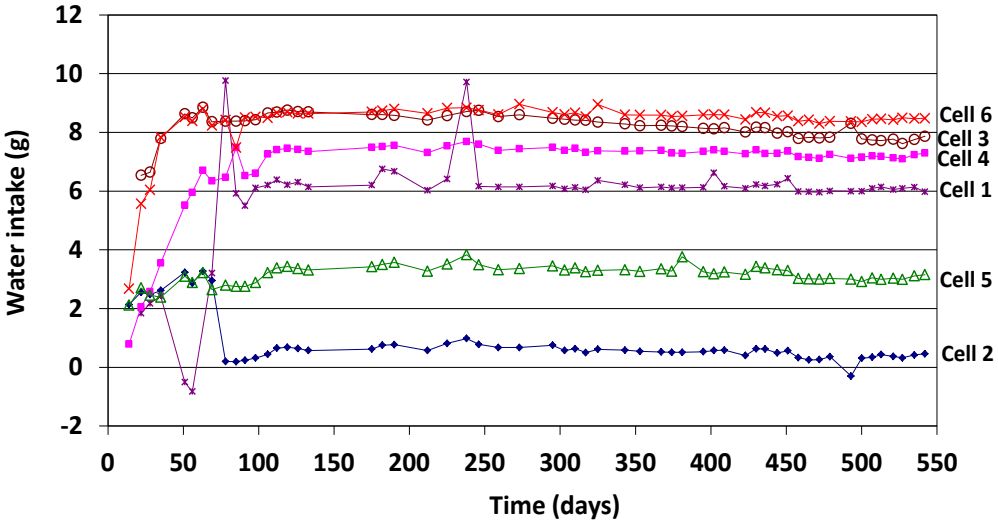

Figure 15: Graph representing water intake in the cells corresponding to the loss of water in the hydration deposits during the operation period of the tests.

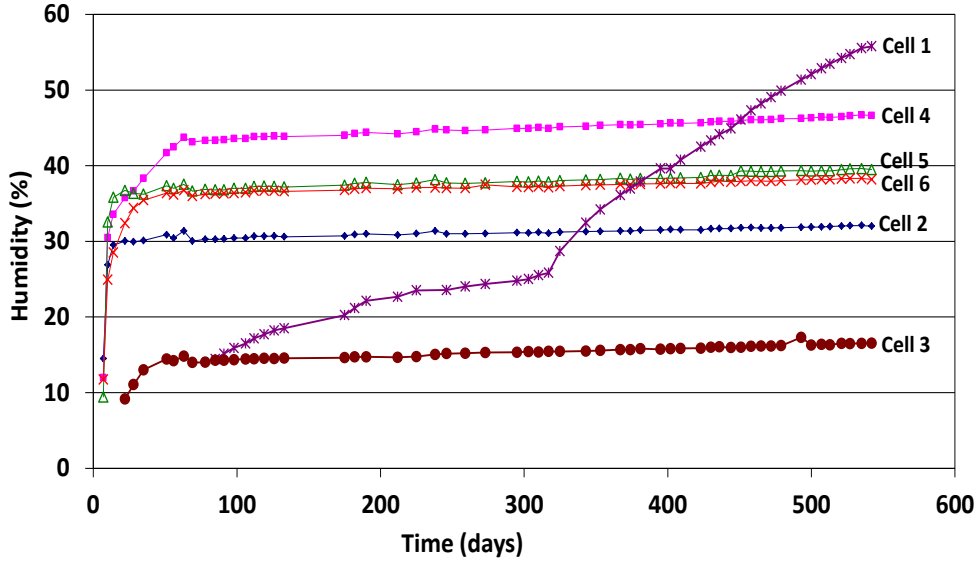

Figure 16: Evolution of relative humidity inside the cells 1 to 6 calculated from water intake measured during weekly during the 18 months of duration of the experiments. Results of the cell 1 and 3 are not comparable to the rest of cells due to failure during operation (see explanation in the text).

Figure 16 shows the evolution of humidity inside the cells during operation period of the tests. After approximately 63 days humidity become stabilized, except for cell 1. To mention that the evolution of humidity of cell 3 is not representative since, as described above, the data corresponding to the first weeks of operation are not representative of the real water intake of the cell.

5.2 Hydration water

Once dismantled the tests the remaining water in the hydration bottles was recovered for analyzing common anions and cations (Cl^-, SO_4^{2-}, Na^+, K^+, Ca^{2+}, Mg^{2+}) by ion chromatography (USEPA, 1991). Water was recovered from cells 2 to 6. Cell 1 was empty, probably due to leak during operation. Table VI shows the elemental composition of the remaining water in the cells.

Table VI: Elemental composition of the initial hydration water and the remaining water in hydration bottles of cells once dismantled.

	Cl^- (mmol/100g)	SO_4^{2-} (mmol/100g)	Na^+ (mmol/100g)	K^+ (mmol/100g)	Mg^{2+} (mmol/100g)	Ca^{2+} (mmol/100g)
Initial hydration water	2.33	7.06	13.15	0.08	0.91	1.11
Final hydration water Cell 1	no enough water for analysis					
Final hydration water Cell 2	5.50	7.17	14.02	0.36	1.12	1.19
Final hydration water Cell 3	2.33	6.96	13.33	0.19	0.43	1.04
Final hydration water Cell 4	3.30	5.31	12.71	0.10	l.d.	1.43
Final hydration water Cell 5	3.11	6.12	12.41	0.33	0.24	1.24
Final hydration water Cell 6	5.10	4.91	8.90	2.09	0.54	1.22

After analyzing the data it can be concluded that there is a solute transfer from the cells towards the hydration bottle. In general, the concentration of chloride and magnesium in the final hydration water is higher than that in the initial water. This is especially true in the cells without mortar (cells 2 and 6). In contrast, the concentration of calcium remained quite constant or showed only very small variations. Sulfate and sodium decreases in cells 3 to 6, although the lower concentration analyzed correspond to cell 6, that with the interface bentonite-magnetite. Potassium also increases in the final hydration water of all cells.

Cl^- concentration gradients between the bentonite (higher concentration) and the hydration bottle (lower concentration) favors the movement of these ions towards the bottle. Once the bentonite is fully saturated constant density and chemical composition values for the bentonite porewater is achieved and therefore it is acting as an impermeable barrier; then the flow, if it occurs, should be always towards the bottle. Thus, solute transfer from the bentonite to the bottle might justify the higher content of Cl^-.

Related to magnesium decrease in cells with mortar, mineralogical studies (see section 5.9 below) show that in the cells with mortar the precipitation of mineral phases such as brucite and Mg-rich silicate phases occurs and remove these ions from the water.

The decreasing of sulphate could be explained by the precipitation of mineral phases such as ettringite and gyspsum, as it will be explained in sections below.

Pre-treated bentonite is rich in potassium. Its increasing in the water could be due to release of potassium in the exchange complex of the bentonite by exchange with sodium (see section 5.6).

5.3 Water content and dry density

The 18th months experiments were fully saturated when the blocks were dismantled. Noticeable differences were determined in the cells which included pre-treated bentonite or natural bentonite. In general, pre-treated bentonite presented lower water content and higher dry density than natural (Figure 17). Table VII shows the values determined in the several slices tested according to labels in the drawings of Figure 10. The initial density of the bentonite was 1.65 g/cm^3. Then, in natural bentonite tests, the bentonite has expanded producing the deformation of the Teflon cell. The dry density is closer to 1.65 g/cm^3 in the pre-treated bentonite cells. The effect of partial dehydration of interlayer potassium induced by potassium exchange can be responsible for this different swelling behavior because high water content was achieved in natural bentonite with or without motar. The absence of mortar produces a relative high final water content and low density in the pre-treated bentonite–magnetite cell.

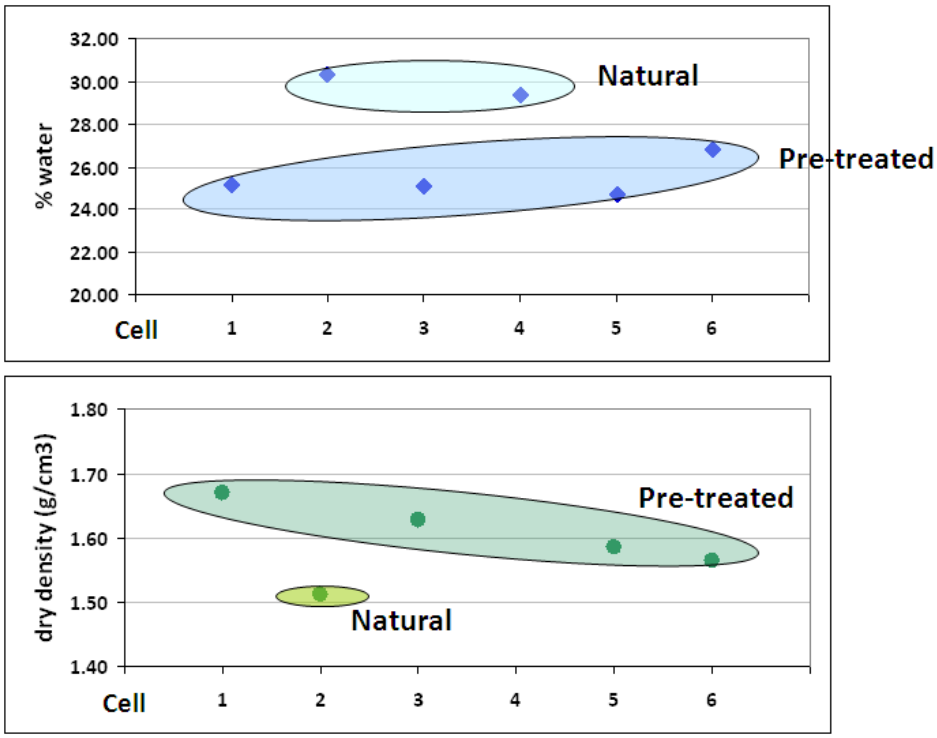

Figure 17: Averaged Water content and dry density determined in the small cell experiments. Different behavior of natural and pre-treated bentonite is shown in the graphs.

Table VII: Water content and dry density.

Cell	Description	Sample	Water content weight %	bulk density g/cm^3	dry density g/cm^3 (103 kg/m^3)
1	Pretreated FEBEX	1A1	25.40	2.04	1.63
		1B1	24.86	2.14	1.71
2	Natural FEBEX	2A1	30.76	1.98	1.51
		2A2	29.61	1.95	1.51
		2B1	30.40	1.98	1.51
3	Pretreated FEBEX+ lime mortar+ magnetite	3M1	16.30	1.93	1.66
		3A1	24.81	2.06	1.65
		3A2	25.18	2.05	1.64
		3B1	25.29	1.99	1.59
		3Fe1	31.64	2.50	1.90
4	Natural FEBEX+lime mortar+ magnetite	4M1	2--2	1.93	1.60
		4A1	23.54	*	*
		4A2	31.05	*	*
		4B1	33.45	1.84	1.38
		4Fe1	15.71	2.08	1.79
5	Pretreated FEBEX+lime mortar	5M1	18.28	2.14	1.81
		5A1	23.85	1.99	1.61
		5A2	24.94	1.97	1.58
		5B	25.37	1.97	1.57
6	Pretreated FEBEX+ magnetite	6A1	27.15	1.99	1.57
		6A2	26.98	2.00	1.57
		6B1	26.29	1.96	1.55
		6Fe	nd	nd	nd

*: samples for cell 4 were damaged and its integrity did not allowed the bulk density determination; nd: not determined in magnetite because it was powder.

5.4 Porosity distribution and BET specific surface area (SSA BET)

The porosity of bentonite samples, mortar and magnetite was measured at the end of the tests by mercury intrusion porosimetry (MIP) (Campos et al., 2013). Intact samples with respect to water content and dry density were used after liofilisation. The results from cell 3, at least samples C3D1, C3D3 and C3DM, should be used with caution due to problems with the sample size, too small to obtain reliable results and duplicates.

The results of the percentage of pores actually intruded are shown in Table VIII and Figure 18. The magnetite has an average total intruded porosity of 62% and the mortar has an average total intruded porosity of 36%, similar to the original one (see Table II).

Total intruded porosity of natural bentonite is slightly lower than total intruded porosity of pre-treated bentonite (Figure 18), related to higher water content and lower dry density of natural bentonite. This high water content is caused by water adsorption at the smectite interlayers, which are partially dehydrated in the pre-treated bentonite. Water at the interlayers is located at micropore (< 2 nm), which are not accessible to mercury intrusion. Then, the natural bentonite should contain a relative high proportion of very small pores regarding the pre-treated bentonite,

which has a higher population of mesopores (> 2 nm), presumably induced by the partial collapse of smectite layers. On the other hand, sections of bentonite in contact with mortar (named D1 in the three cells with mortar, 3, 4 and 5) seem to have lower total intruded porosity than sections far from the interface (Figure 18 right). The figure shows a similar trend in the three cells if the section D3 is left out. In addition, as already indicated, cell 4 with natural bentonite, has lower total intruded porosity than cells 3 and 5 with pre-treated bentonite. The data agree with the SSA BET values showed below. The high value of intruded porosity observed in the section close to the magnetite in cell 3 and 4 is attributed to a possible contamination of the bentonite by magnetite during dismantling, since magnetite readily separates and part of it disaggregates in powder as explained in subsection 4.2 and can be observed in Figure 7.

Table VIII: Total mercury intruded (%) for bentonite samples, mortar and magnetite in cells 1 to 6.

Reference	Total intruded (%)	Macro (%)	Meso (%)	Micro (%)
Cell 1_D1	25.2	16.5	8.7	74.8
Cell 1_D2	24.2	15.2	9.0	75.8
Cell 1_D3	25.0	16.4	8.7	75.0
Cell 1_D4	26.2	17.1	9.1	73.8
Cell 2_D1	22.6	19.1	3.5	77.4
Cell 2_D2	23.4	16.4	7.0	76.6
Cell 2_D3	23.7	17.5	6.2	76.3
Cell 2_D4	24.1	15.8	8.3	75.9
Cell 3_DM	40.0	64.1	35.9	
Cell 3_D1	24.4	21.5	2.9	75.6
Cell 3_D2	26.5	19.5	7.0	73.5
Cell 3_D3	39.1	39.1	0.0	60.9
Cell 3_Fe	66.7	99.9	0.1	
Cell 4_DM	32.4	35.4	64.6	
Cell 4_D1	22.0	14.6	7.4	78.0
Cell 4_D2	24.9	17.1	7.8	75.1
Cell 4_D3	28.5	22.3	6.2	71.5
Cell 4_Fe	62.3	99.4	0.6	
Cell 5_DM	35.3	43.1	56.9	
Cell 5_D1	24.2	15.5	8.7	75.8
Cell 5_D2	27.4	19.0	8.4	72.6
Cell 6_D1	26.7	20.5	6.2	73.3
Cell 6_D2	28.2	20.5	7.7	71.8
Cell 6_D3	25.6	16.5	9.1	74.4
Cell 6_Fe	58.2	99.4	0.6	

The mercury intrusion method allows access only to the macropores (< 360 µm) and to part of the mesopores (> 0.003 µm). The percentage of pores not intruded by mercury includes not only those pores whose sizes are below or above the technique limit, but also those whose entrance pore size is below the lower entrance limit of the equipment or those isolated, even if the pores themselves are larger. Nevertheless, assuming that the percentage of pores not intruded in the clay

corresponds entirely to the micropore size (< 3nm), an estimation of the percentage of micropores can be inferred from the percentage of pores intruded (Villar et al., 2012). This was done for all the samples of bentonite and the percentage of each pore size recalculated (Table VIII and Figure 19). The magnetite has a pore size distribution quite homogeneous, with a mean diameter of 258-287 nm. The mortar has a bimodal size distribution, the macropore size mode with a mean diameter of 53 nm and the mesopore size mode with a mean diameter of 19 nm. The micropores are dominant in all the samples of bentonite as expected in a fully saturated bentonite. However, there are differences between pre-treated or natural bentonite. In general, pre-treated bentonite presented slightly lower microporosity than natural as was anticipated. In the particular case of the sections of bentonite at the interface with mortar (named D1) it seems that there is a slight decreasing of the macroporosity. It could indicate a clogging of the porosity in the bentonite influenced by the mortar.

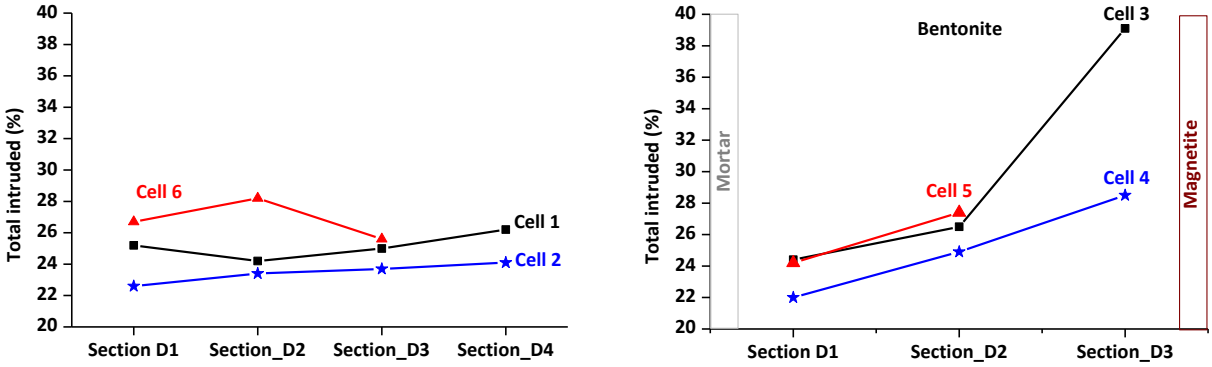

Figure 18: Total intruded pores (%) of the natural and pre-treated bentonite without mortar (left) and with mortar (right).

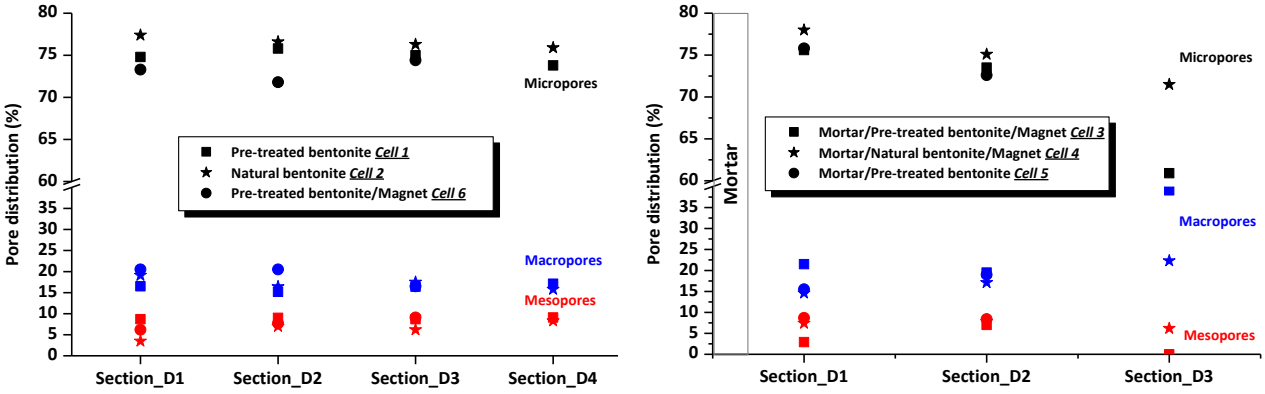

Figure 19: Pore distribution (%) of the natural and pre-treated bentonite without mortar (left) and with mortar (right).

Cells 3 and 4 both contained two interfaces and pre-treated and natural bentonites. Bentonite SSA is affected by the proximity of mortar. SSA decreases to 20-40 m^2/g at least in the first 8 mm measured from the mortar interface. There were no differences for the pre-treated or natural bentonite. The magnetite interface did not induce any remarkable change in the nearest bentonite

both cell 3 and 4 with typical values for the FEBEX bentonite (64 m^2/g). The mortar interface is characterized by crystallization and/or cementing processes affecting the aggregation mode of the bentonite.

Table IX: BET specific surface area (SSA BET) from small cells experiments

Cell.Sample	Description	Thickness (mm)	SBETm^2/g
1.1	Bentonite, from sample 1A	12	66
1.2	Bentonite from sample 1B	12	64
2.1	Bentonite	8	64
2.2	Bentonite	8	62
2.3	Bentonite	8	-
3.1	Mortar-bentonite interface	2	RX, SEM
3.2	Mortar upper face	4	25
3.3	Bentonite interface	2	27
3.4	Dark rim	3.0	18
3.5	Bentonite with 1 mm dark rim	4.0	37
3.6	Bentonite	~5.5	53
3.7	Bentonite-magnetite interface	4	64
3.Fe	Magnetite	4	9
4.1	Mortar	~3.5	24
4.2	Mortar lower face	~3.5	22
4.3'	Mortar interface	<1	RX,SEM
4.3	Mortar-bentonite interface	2	22
4.4	Bentonite crushed	~7-8	24
4.5	Bentonite	5	46
4.6	Bentonite	5	64
4.FeB	Bentonite-magnetite interface	<1	RX-SEM
4-Fe	Magnetite	~2	8
4-FeI	Magnetite interface	~2	RX
5.I	Hydration Interface for SEM		RX, SEM
5.1	Mortar	5.4	26
5.2	Mortar lower face	1.5	26
5.2'	Mortar interface		RX
5.3	Mortar-bentonite interface	4.1	39
5.3'	Bentonite interface		RX
5.4	Bentonite	3.8	49
5.5	Bentonite	3.9	57
5.6	Bentonite	6	66
5.7	Bentonite	4.1	49
6.1	Bentonite	6	68
6.2	Bentonite	6	73
6.3	Bentonite	6	72
6.4	Bentonite	6	71
6.FB	Bentonite-magnetite interface	*1	RX
C6.Fe	Magnetite	4	9

The SSA BET parameter lies within the FEBEX original sample values, near 60 m^2/g, for the small cells experiments 1 and 2 corresponding to pre-treated and natural bentonites respectively, hydrated and heated to 60 ^oC during 18 months (Table IX). These data imply to have similar

crystallite size for smectite phases and aggregate state (self-organization of clay platelets), not significantly affected by the potassium exchange effect.

Cells 5 and 6 contained pre-treated bentonite and a single interface, mortar and magnetite respectively. Mortar induced a decrease in SSA as was expected and the cell with magnetite showed relatively high SSA values near 70 m^2/g. This value is very close to the original one and thus confirms the negligible impact of magnetite to bentonite.

5.5 Aqueous extracts

The concentration of soluble elements was analyzed in the sections DM, D and Fe represented in Figure 9 and Figure 10. Average values obtained from the analysis of the soluble ions are displayed in Table X.

Table X: Soluble ions concentrations measured in the aqueous extracts (1:8 S/L) for cells 1 to 6. Analyses on material as received are also included for comparison.

	Ident	Cl mmol/100g	SO_4^{2-} (mmol/100g)	Na (mmol/100g)	K (mmol/100g)	Mg (mmol/100g)	Ca (mmol/100g)
Cell 1	C1D1	0.41	1.40	3.85	1.36	d.l.	0.22
	C1D2	0.05	0.55	2.65	0.83	d.l.	0.20
	C1D3	0.05	0.47	2.55	0.85	0.02	0.15
	C1D4	0.05	0.47	2.51	0.75	d.l.	0.16
Cell 2	C2D1	0.34	2.97	7.77	0.08	0.10	0.12
	C2D2	0.32	1.27	5.10	0.05	0.05	0.09
	C2D3	0.33	1.20	5.24	0.07	0.06	0.10
	C2D4	0.34	1.10	5.01	0.05	0.03	0.09
Cell 3	C3DM	2.02	1.88	0.50	0.34	0.04	20.04
	C3D1	0.28	1.06	5.52	2.33	d.l.	0.75
	C3D2	0.16	0.07	2.24	0.77	d.l.	0.28
	C3D3	0.20	0.08	2.07	0.71	d.l.	0.23
	C3Fe	0.83	0.29	1.46	0.56	0.04	0.88
Cell 4	C4DM	1.88	1.87	0.65	0.02	d.l.	19.18
	C4D1	0.41	1.49	11.92	0.13	d.l.	0.54
	C4D2	0.20	0.19	3.74	0.04	d.l.	0.18
	C4D3	0.26	0.36	3.83	0.05	0.03	0.10
	C4Fe	0.62	0.48	2.24	0.05	0.02	0.92
Cell 5	C5DM	2.63	0.34	0.21	0.11	d.l.	19.15
	C5D1	0.10	0.03	2.83	1.33	0.15	0.41
	C5D2	0.09	0.02	1.80	0.78	d.l.	0.33
Cell 6	C6D1	0.49	0.59	3.00	1.16	0.04	0.58
	C6D2	0.48	0.33	2.74	1.11	d.l.	0.34
	C6D3	0.40	0.26	2.55	1.03	d.l.	0.16
	C6Fe	0.83	0.54	2.51	0.23	0.37	1.40
Material as received	FEBEX natural	1.98	0.77	6.05	0.10	0.13	0.34
	FEBEX pret	1.76	0.01	1.57	1.44	0.15	0.24
	Mortar	0.05	0.09	0.07	l.d.	d.l.	18.99
	Magnetite (Fe)	0.03	0.28	0.74	l.d.	d.l.	0.61

d.l.: detection limit

5.5.1 Chloride distribution

The most relevant transport processes occurring in the cells may be deduced from the behavior of chloride. The distribution of Cl^- depends on the configuration of the experiment and is closely related to the interfaces (Figure 20 and Figure 21) and besides is affected by the type of bentonite, natural or pre-treated.

In the cell 1 containing pre-treated bentonite, the chloride concentration is higher in the section closer to hydration (0.4 mmol/100g) than in the rest of the sections, with values close to 0, and however, it is quite homogeneous (≈ 0.3 mmol/100g) along the bentonite column in cell 2 containing natural bentonite. At any case, chloride values in all cases are very low compared with the original value in FEBEX bentonite (see Table X). This fact is justified by a back-diffusion process occurring from the cells once saturated towards the hydration bottle (see previous chapter 5.2).

In the cells 3 to 6 the distribution of chloride concentration is linked to the formation of saline fronts of chloride moving towards mortar and/or magnetite. The penetration of chlorides into the mortar and magnetite occurs by diffusion through the pore system. Once the materials are fully saturated transfer of chlorides by concentration gradient in the pore solution of the different materials occurs. The mortar can react with chloride in diverse forms to form chloroaluminates or Friedel's salt, or adsorbed in CSH and mostly in Afm-like phases (Yuan et al., 2009; Florea and Browers, 2012), thus immobilizing the chloride and reducing the free chloride ions. That could be the reason of the lower concentration of chloride in the final hydration water of the dismantled cells with mortar (Table VI, section 5.2) and the sharp increase of chloride at the mortar as can be observed in Figure 20 and Figure 21. The Figure 22 shows a picture of the interface mortar-bentonite and an example of elemental composition of a zone of the mortar matrix in which the chloride was detected, confirming that mortar matrix is acting as sink of this element.

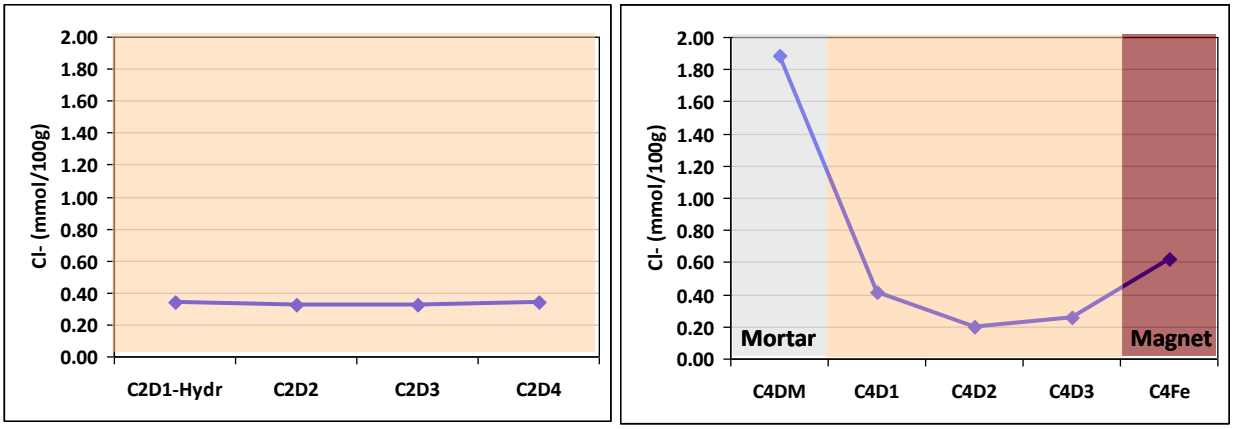

Figure 20: Chloride concentration along the bentonite block in cells 2 and 4, both with natural FEBEX bentonite (aqueous extract solid:liquid 1:8)

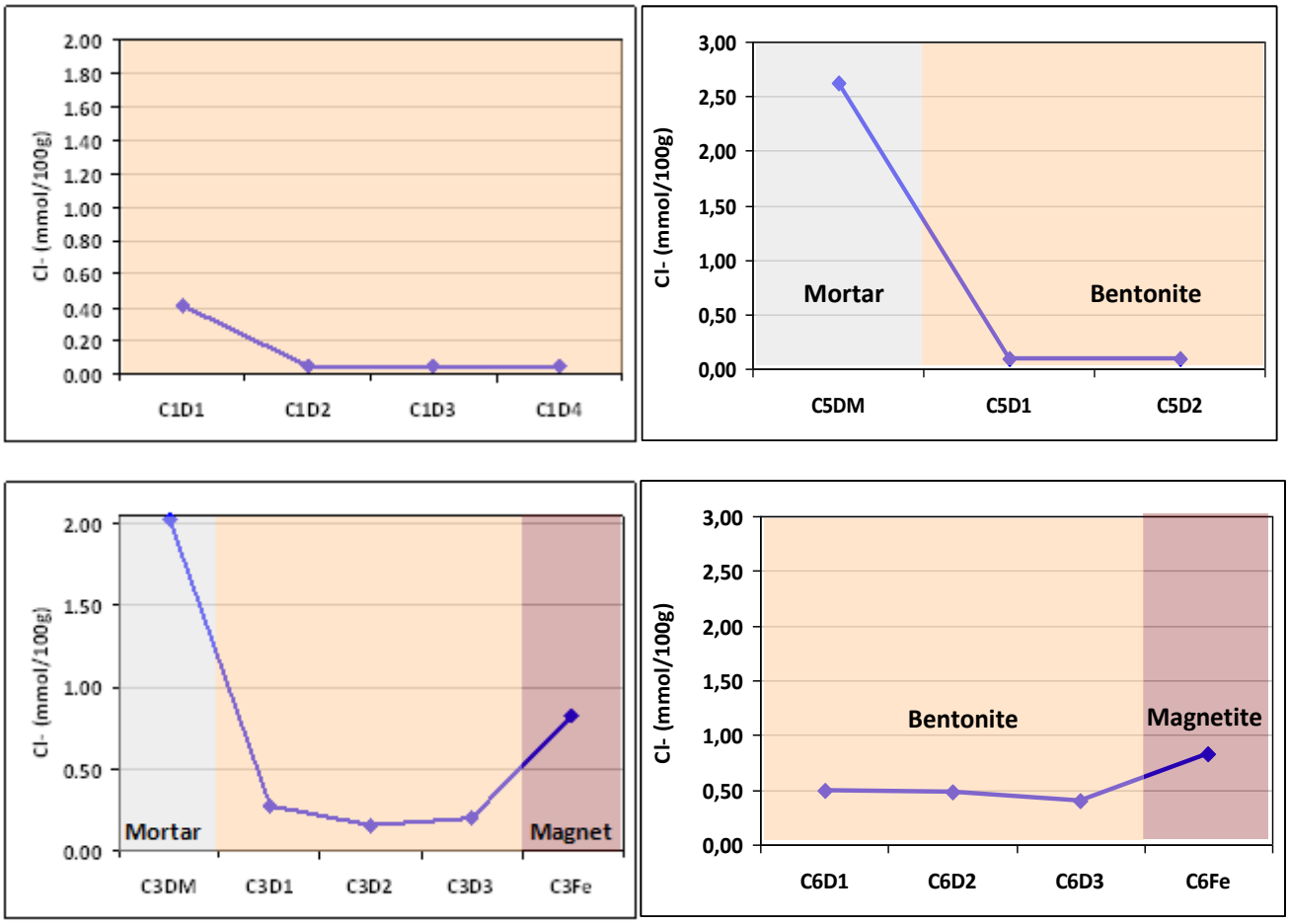

Figure 21: Chloride concentration along the cells 1,3, 5 and 6, all of them of pre-treated FEBEX bentonite (aqueous extract solid:liquid 1:8)

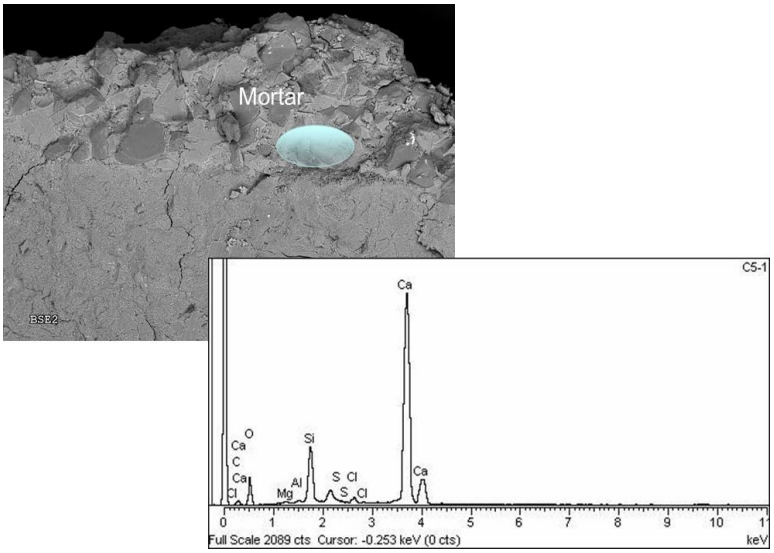

Figure 22: SEM-EDS image showing the presence of chloride and sulphate at the mortar in cell 5, evidencing that mortar matrix acts as a sink of both ions.

5.5.2 Sulfate distribution

The distribution of sulfate can be observed in Figure 23 and Figure 24. The sulfate profiles in the cells that contain only bentonite are not homogeneous. At the hydration front (section D1 in cells 1 and 2) the concentration of sulfate is higher than in the rest of the sections. Besides the concentration in natural bentonite is double than in pre-treated bentonite. The explanation could be in the lower initial concentration of sulfate of the pre-treated bentonite subjected to various leaching cycles to get the proposed exchangeable cation population. On the other hand, the continuous source of sulfate from the hydration water (which is higher than in the bentonite porewater) and the low mobility of sulfate, if compared to Cl^-, because of its retention on clay surfaces mainly by electrostatic repulsion (higher ionic charge/radii ratio than Cl^-) (Drever, 1988) can lead to those higher contents of sulfate just at the sections close to hydration.

When the interfaces are present mortar and magnetite acts as sink, as in the case of chloride, and ettringite and/or sulfate precipitates in the matrix of these materials removing this element from solution. Figure 25 on top shows a SEM-EDS image of the interface mortar-bentonite in which ettringite (S, Al) was analyzed. The bottom of the Figure 25 is a SEM-EDS image showing the presence of gypsum at the magnetite. Both cases evidence that mortar and magnetite matrix acts also as a sink of sulfate.

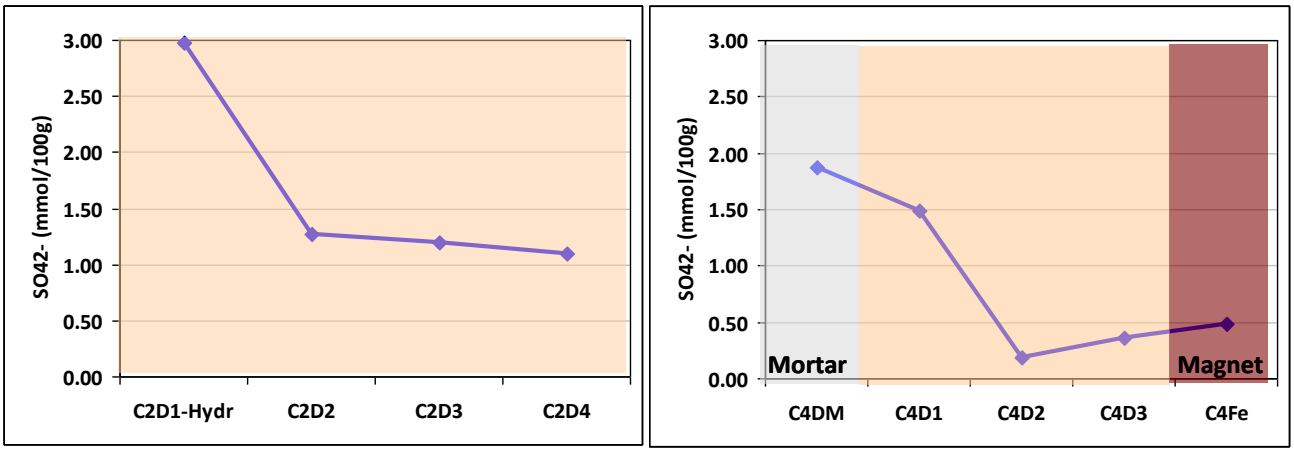

Figure 23: Sulfate concentration along the bentonite block in cells 2 and 4, both with natural FEBEX bentonite (aqueous extract solid:liquid 1:8)

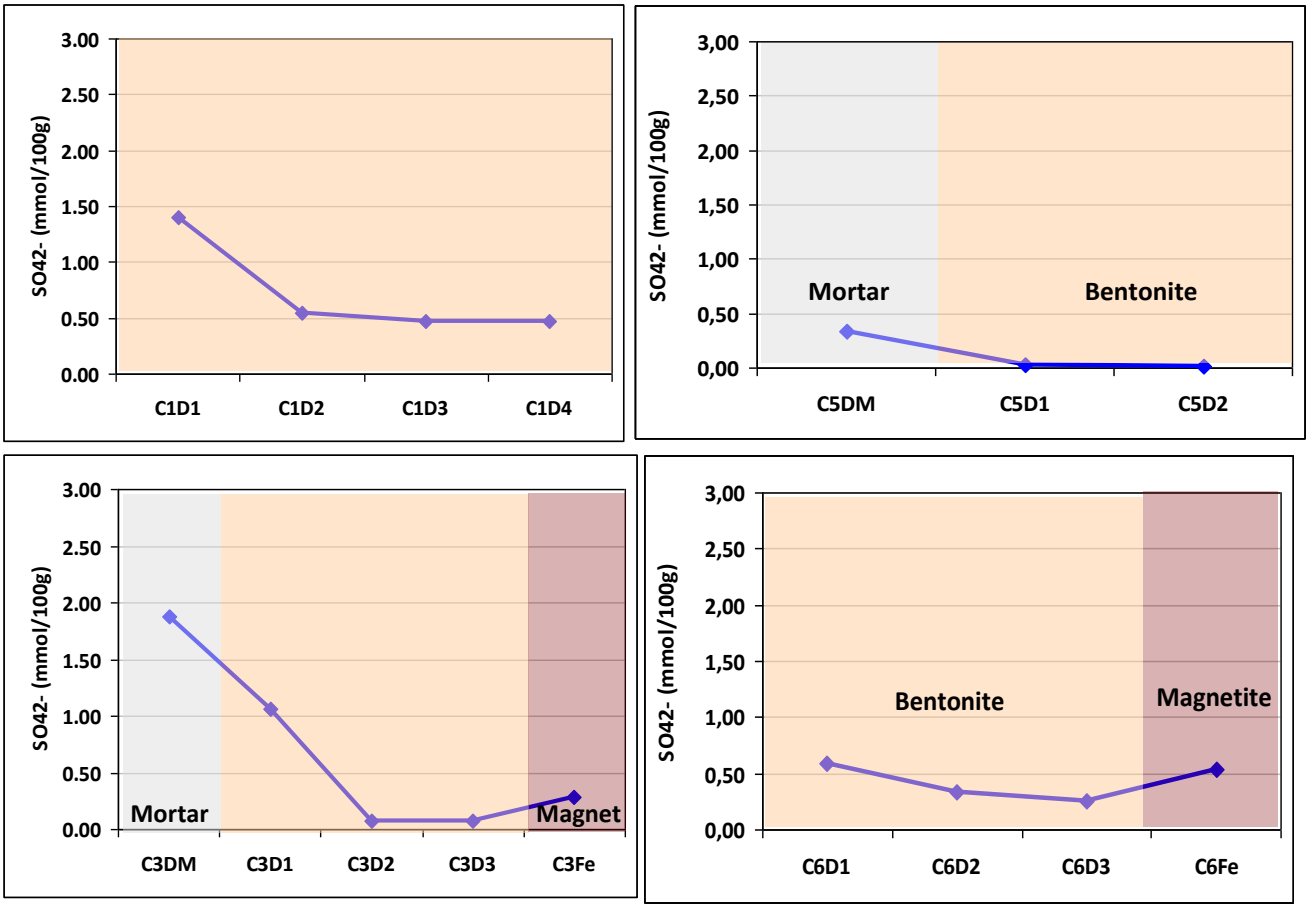

Figure 24: Sulfate concentration along the cells 1, 3, 5 and 6, all of them of pre-treated FEBEX bentonite (aqueous extract solid:liquid 1:8)

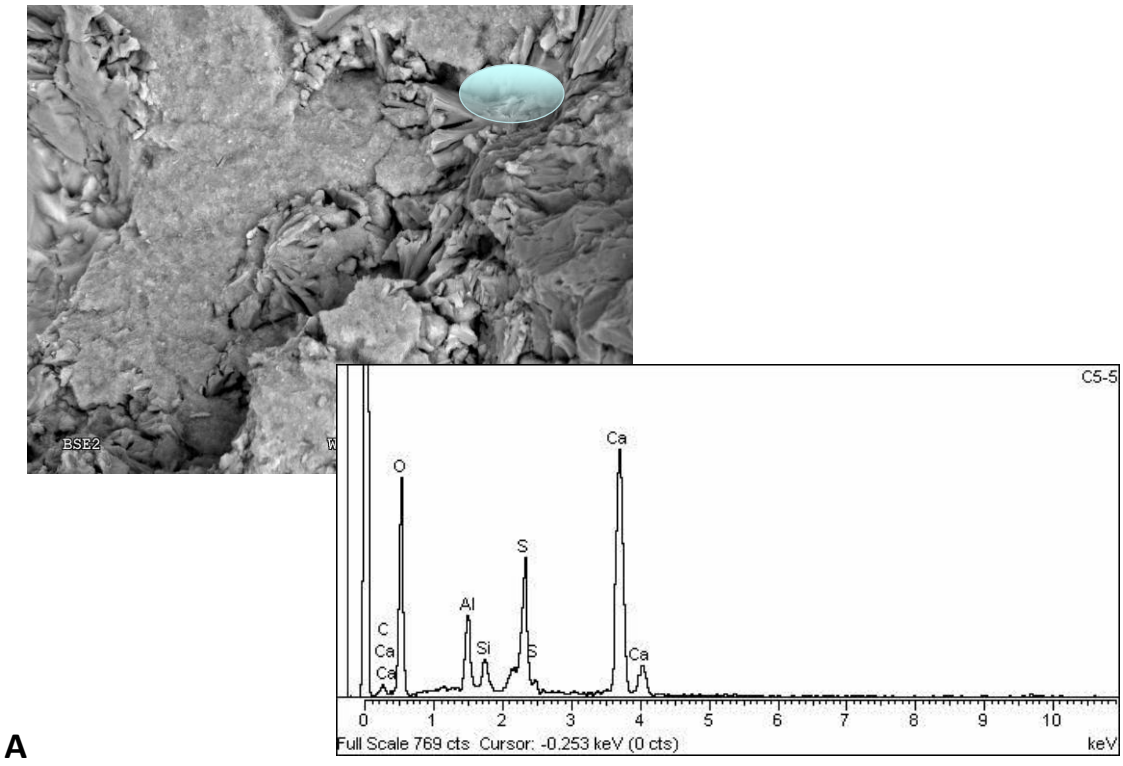

A

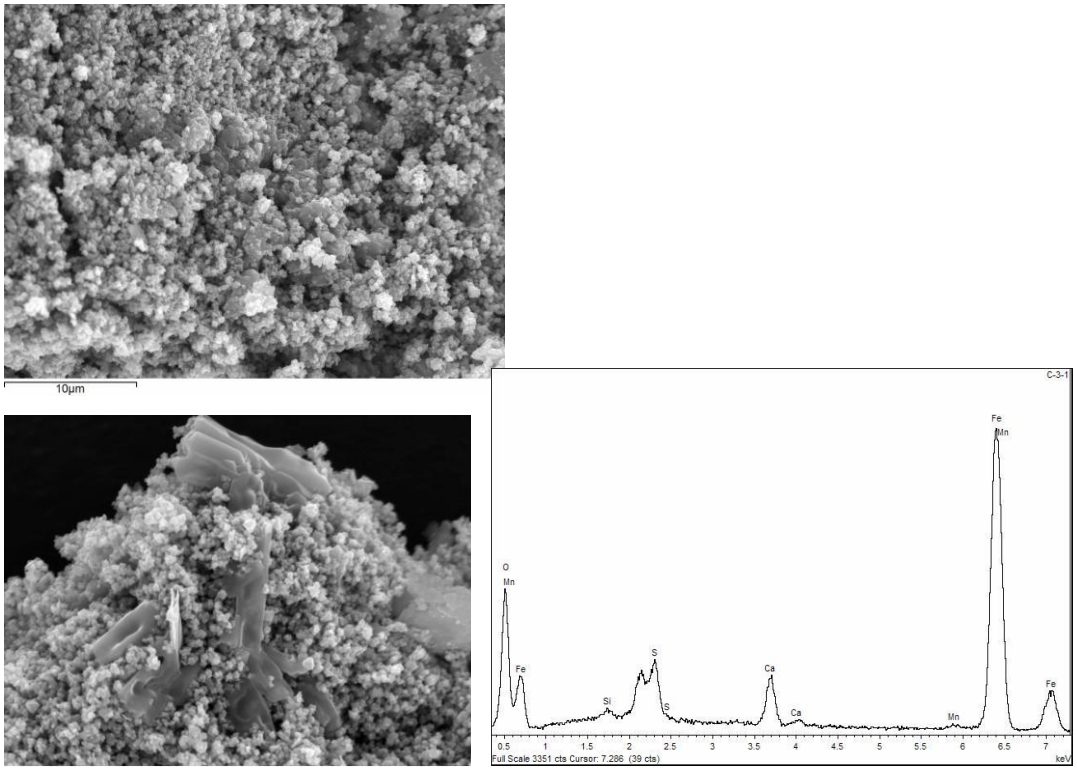

B

Figure 25: A - SEM-EDS image showing the presence of ettringite (S,Al) in mortar-bentonite interface, evidencing that mortar matrix acts as a sink of sulfate; B - SEM-EDS image showing the presence of gypsum at the magnetite, evidencing that magnetite matrix also acts as a sink of sulfate.

5.5.3 Cations distribution

Soluble cations values are displayed in Table X. The main counterion that followed sulfate in all the tests is sodium (Figure 26 and Figure 27). The source of sodium is the hydration water as it is for sulfate (see subsection 5.5.2) that leads to the higher contents just at the sections close to hydration. Regarding cell 1 and cell 2, which do not contain interfaces, the sodium concentration in the cell containing natural bentonite (cell 2) is double that in the cell with pre-treated bentonite (cell 1) and the opposite occurs with potassium. The explanation is a cation exchange process of sodium by potassium occurring in the pre-treated bentonite (enriched in potassium). This agrees with cation exchange data in Table XI. In the cell 1 sodium increases and potassium decreases compared to original cation exchange population of the pre-treated bentonite. The same can be extended to cell 4 (natural bentonite) compared to cells 3, 5 and 6 (pre-treated bentonite). In those cells containing mortar interface calcium content is very high in the soluble extracts of the mortar due to concrete leaching and increases very slightly in the magnetite.

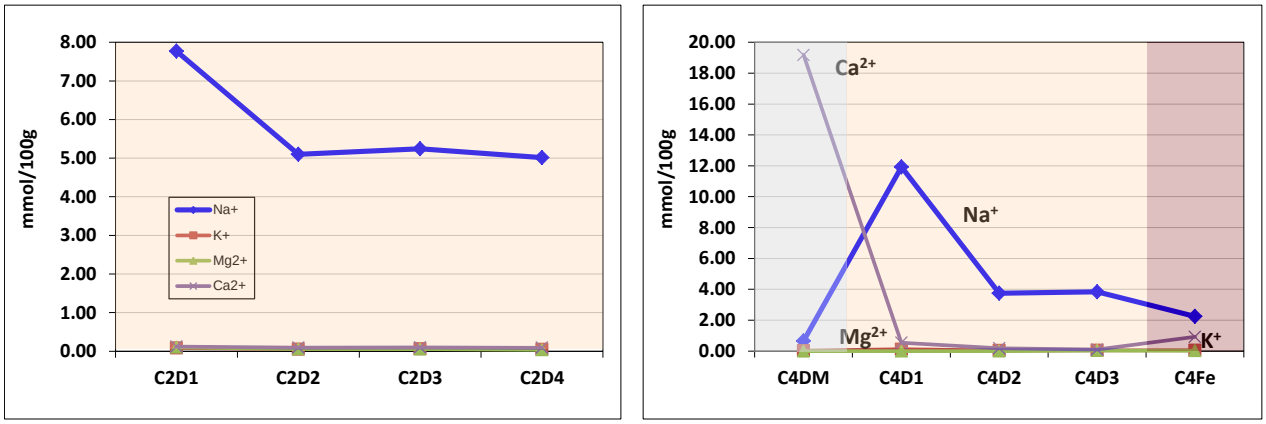

Figure 26: Soluble cations distribution along the bentonite block in cells 2 and 4, both with natural FEBEX bentonite (aqueous extract solid:liquid 1:8).

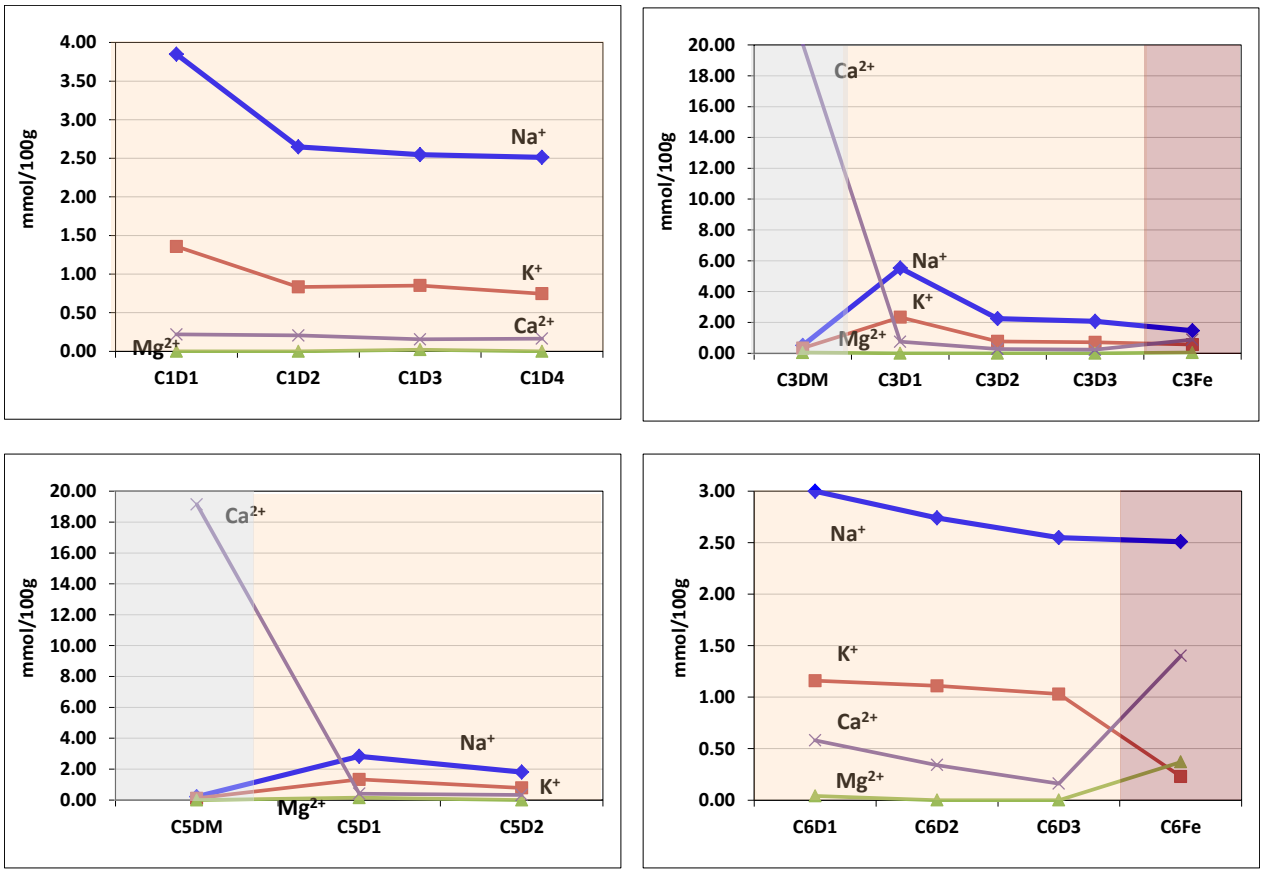

Figure 27: Soluble cations distribution along the bentonite block in cells 1, 3, 5 and 6, both with pre-treated FEBEX bentonite (aqueous extract solid:liquid 1:8)

5.6 Exchangeable cations

Table XI shows the average values of exchangeable cations measured in the different subsamples of bentonite for the cells 1 to 6.

The distribution of exchangeable cations does not vary along the bentonite column in cells 1 and 2. However, there are changes when the comparison is made with the distribution in natural or pre-treated bentonite before the experiment. Regarding to pre-treated bentonite the potassium decreases while the sodium increases in all the sections of cell 1. This is due to the input of sodium from the hydration solution. In the case of cell 2, containing natural bentonite, a slight increasing of sodium is observed but the most noticeable is the increasing of calcium and decreasing of magnesium. This general behavior can be extended to the cells with the mortar and/or magnetite interfaces. However, for these cells the most noticeable change is the decreasing in the content of exchangeable magnesium in the cells containing mortar either with natural or pre-treated bentonite, which is especially dramatic in the cell 4 containing natural bentonite with an initial content of exchangeable magnesium of 37 cmol(+)/Kg and a final concentration after dismantling of 0.0-0.3 cmol(+)/Kg. The magnesium is completely displaced by calcium and sodium replaces to potassium. As discussed in further sections Mg silicates and oxides are commonly found

precipitated at the mortar/bentonite interface. These mineral phases are responsible of the loss of magnesium in the solution and in the exchange complex.

Table XI: Exchangeable cations of bentonite samples from cells 1 to 6 determined by leaching with 0.5 N $CsNO_3$ at pH 7.

Ident	Na^+ (cmol(+)/Kg)	K^+ (cmol(+)/Kg)	Mg^{2+} (cmol(+)/Kg)	Ca^{2+} (cmol(+)/Kg)	Total
C1D1	13.24	26.59	3.99	44.51	88.32
C1D2	13.73	26.73	4.16	43.40	88.01
C1D3	14.07	22.31	4.12	43.99	84.50
C1D4	15.01	26.51	3.84	39.73	85.10
C2D1	30.05	2.28	33.33	40.50	106.16
C2D2	30.38	1.89	32.70	38.05	103.02
C2D3	29.27	2.36	32.47	37.03	101.12
C2D4	29.98	1.95	33.75	38.34	104.02
C3D1	12.12	23.29	0.00	47.89	83.30
C3D2	15.42	24.62	0.06	36.46	76.56
C3D3	16.16	25.69	0.14	39.16	81.15
C4D1	27.24	1.77	0.00	59.31	88.32
C4D2	33.28	2.36	0.31	67.70	103.65
C5D1	11.49	28.54	0.00	47.37	87.40
C5D2	11.60	27.89	0.09	46.75	86.33
C6D1	13.83	27.81	3.37	41.98	87.00
C6D2	13.36	27.02	3.32	40.41	84.11
C6D3	13.77	27.27	3.32	40.07	84.43

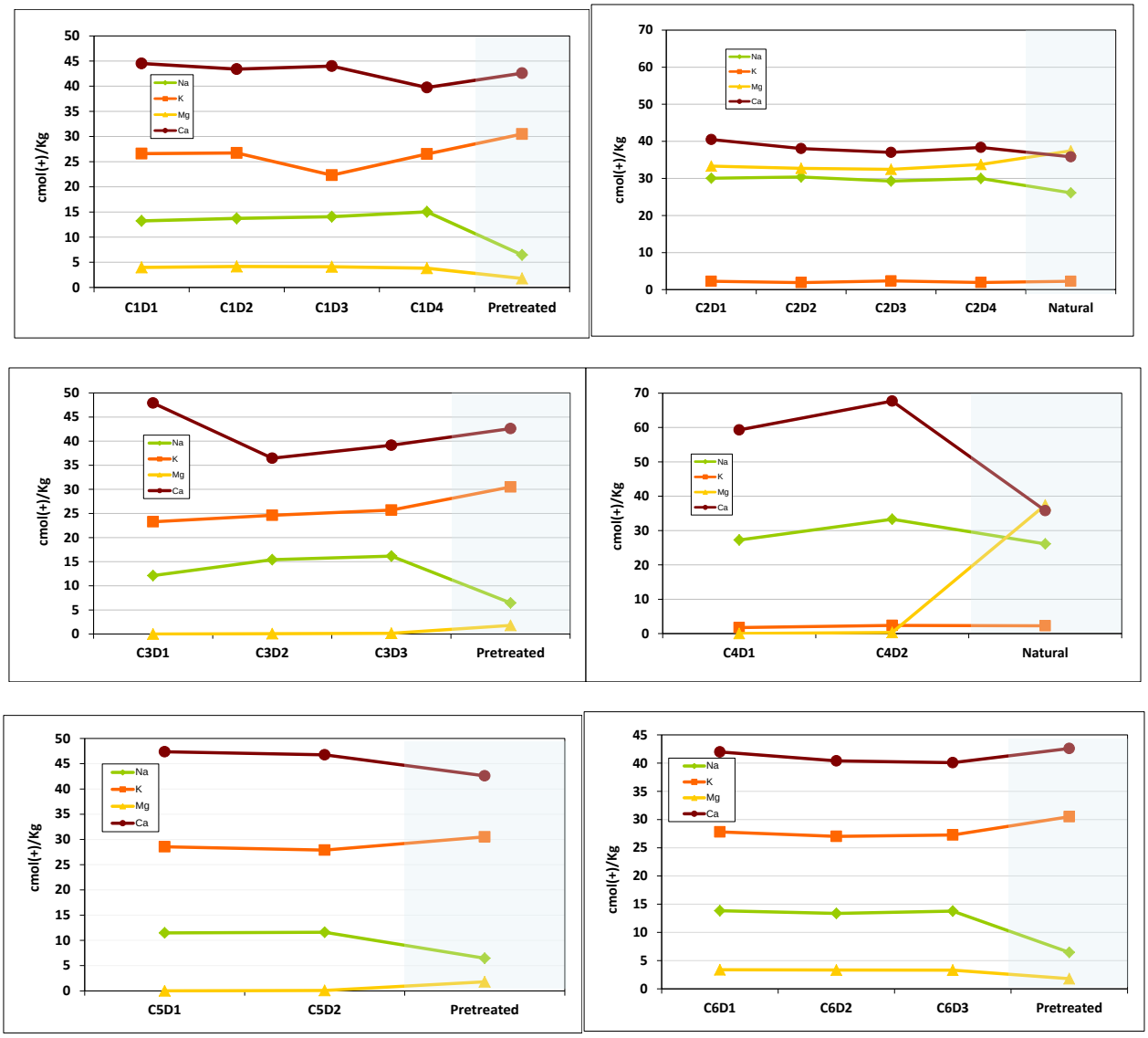

Figure 28: Distribution of exchangeable cations in the bentonite of the the cells 1 to 6 (CsNO3 0.5 N).

5.7 Iron distribution

The two major sources of iron in the planned experiments are the hydration solution and magnetite alteration. The concentration of the total extracted iron along the columns ranged from a peak of 2.24 mmol/100g localized at section named D1 in cell 3, which is adjacent to the interface with mortar, to background bentonite values (0.5 mmol/100g) or lower at sections away from hydration or the mortar interface (Figure 29). When the iron distribution of the different cells is compared a distinction between cells with or without mortar can be made. In fact, when cells were dismantled this distinction already could be made. As example Figure 30 shows a picture of cells 2 and 4, without and with mortar respectively, once dismantled. It can be observed the presence of Fe-oxyhydroxides precipitates in cell 2 just where hydration of cells occurs. This iron comes from the hydration solution and precipitation occurs before penetration of water into the

bentonite. However, the figure shows the cell 4, with mortar, in which the hydration zone appears very clean, without apparent remains of iron. This occurs in all the cells with mortar.

Usually calcium hydroxide alkaline environment protects iron against corrosion and just in the case of carbonation occurring this protection could fail. At the case of the cells with mortar, the presence of this alkaline environment in the closeness of hydration-mortar prevents the oxidation of the Fe^{2+} from the solution; this oxidation occurs when solution enters in the bentonite and then iron does not move further, being localized in sections close to mortar.

Total extracted iron is not detected at sections of bentonite close to the magnetite-bentonite interface suggesting that little or nothing of magnetite was altered. However, a chemical profile of iron at cell 6 shows iron enrichment just at the interface (Figure 31), with a Fe penetration front of < 0.2 mm. That also occurs in cells 3 and 4 (see section 5.8.2). This front is very small and has been possibly influenced by the difficulty to establish the exact position of the interface (Figure 39 in section 5.8.2)

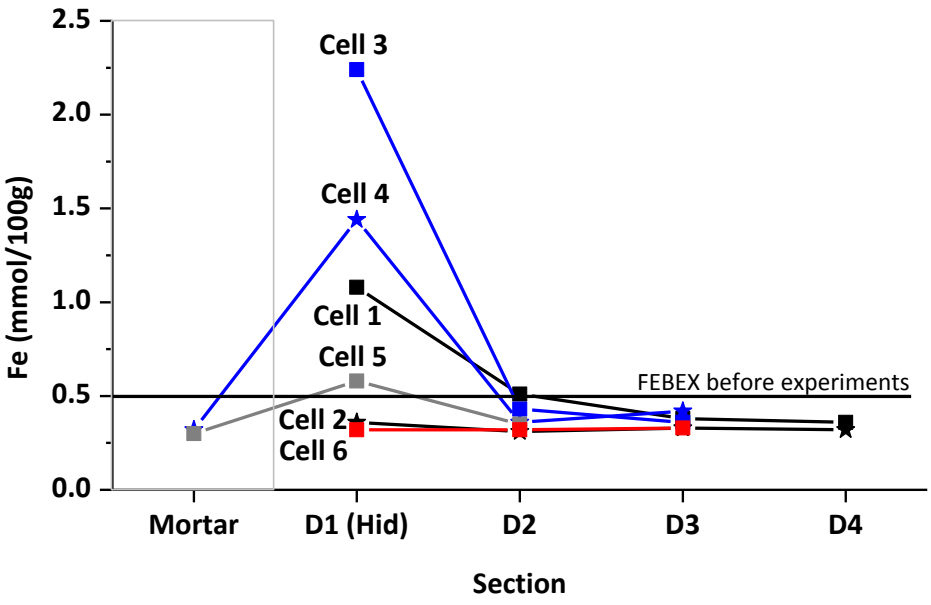

Figure 29: Distribution of the total extracted iron along the columns in cells 1 to 6.

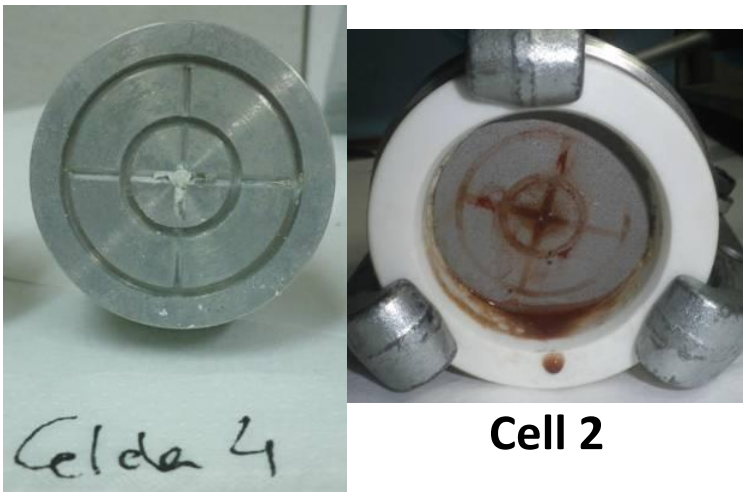

Figure 30: Picture showing the appearance of cells 2 (no interfaces) and 4 (both interfaces) at the hydration zone once cells were dismantled.

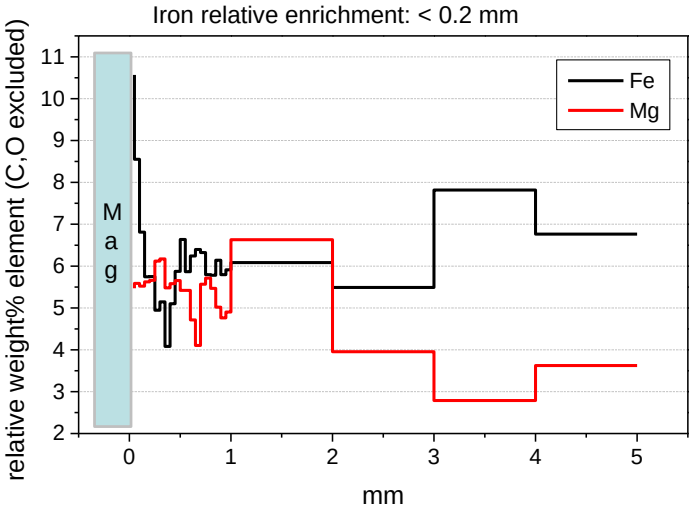

Figure 31: Chemical profile (Fe and Mg) in the magnetite-bentonite interface of cell 6.

5.8 Textural and elemental analysis at the interfaces

5.8.1 Natural and pre-treated FEBEX with two interfaces heated to 60 ºC.

Fresh fracture-samples

The texture at the mortar-bentonite interface is characterized by sharp contact between mortar (identified by the dark (under BSE mode) quartz-sand grains) and the bentonite with a very compact appearance (Figure 32, upper side). There were not apparent differences between the cell with pre-treated bentonite (cell 3) or natural (cell 4) in the appearance of the interfaces. The

interface with magnetite is not sharp as the compacted powder is slightly deformed when the compacted bentonite is pressed in the cell. This interface is easily distinguished by the bright magnetite powder adhered to the bentonite (Figure 32, lower side).

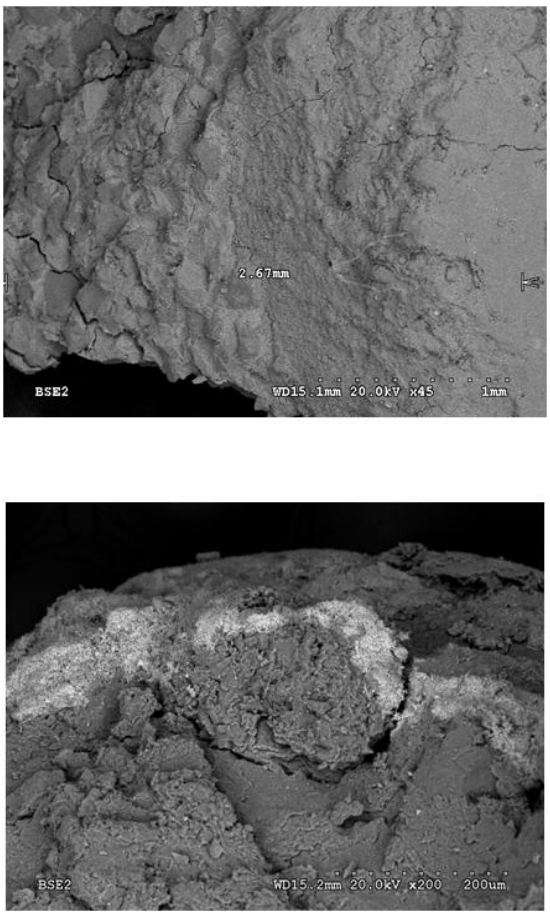

Figure 32: Typical aspect of the granulated mortar (upper left) to the compact bentonite (upper right) in cell 3. Irregular magnetite-bentonite contact in cell 3.

Some mineral phases produced during the hydration of mortar and the subsequent bentonite alteration has been identified. The most abundant new mineral in the lime mortar is a phase of aluminum sulfate of typical ettringite needles morphology containing significant amounts of carbon (Figure 33a). As will be described later in the XRD section, there were no evidence for ettringite sulfoaluminate presence (S/Al = 3/2). Instead of this, carboaluminate is detected and, with less confidence, Al-monosulphate. In consequence this phase seems to be complex. On the other hand it is frequent to find micellar or fibrous precipitates, rich in Mg silicates (Figure 33b), although they were not identified by XRD. These Mg phases use to have low crystal size and they are very difficult to characterize in these mixtures.

In previous sections it has been remarked that mortar seems to be a sink for chlorides and sulfates. This is confirmed by the visible chloride content in the mortar matrix and the ubiquitous precipitates of sulfate in the mortar pores (Figure 34).

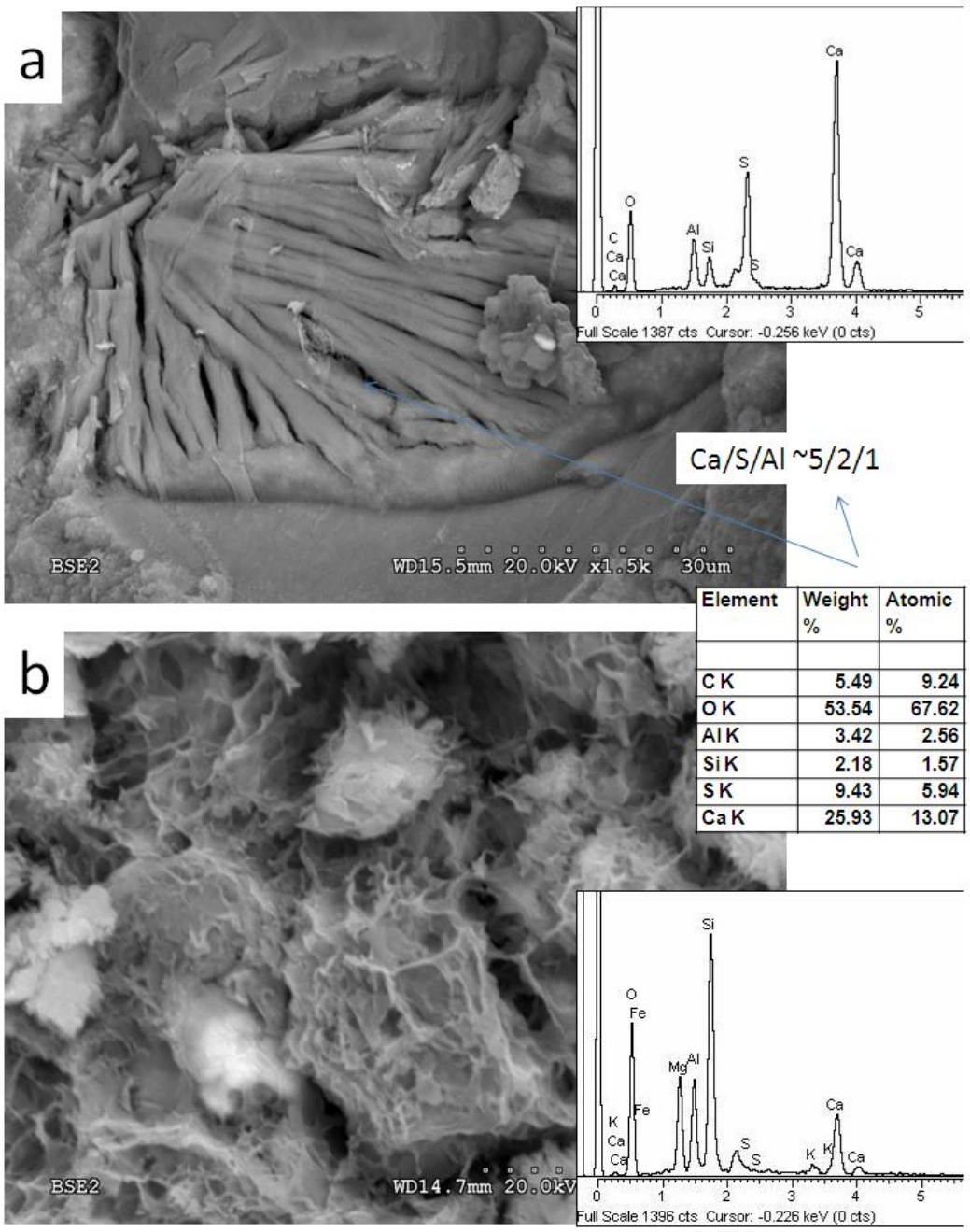

Element	Weight %	Atomic %
C K	5.49	9.24
O K	53.54	67.62
Al K	3.42	2.56
Si K	2.18	1.57
S K	9.43	5.94
Ca K	25.93	13.07

Figure 33: (a) Al-sulfates and (b) Mg-rich silicate phases (Mg-silicate hydrates: micelar and fibrous networks) in the mortar and in the mortar-bentonite interfaces, respectively.

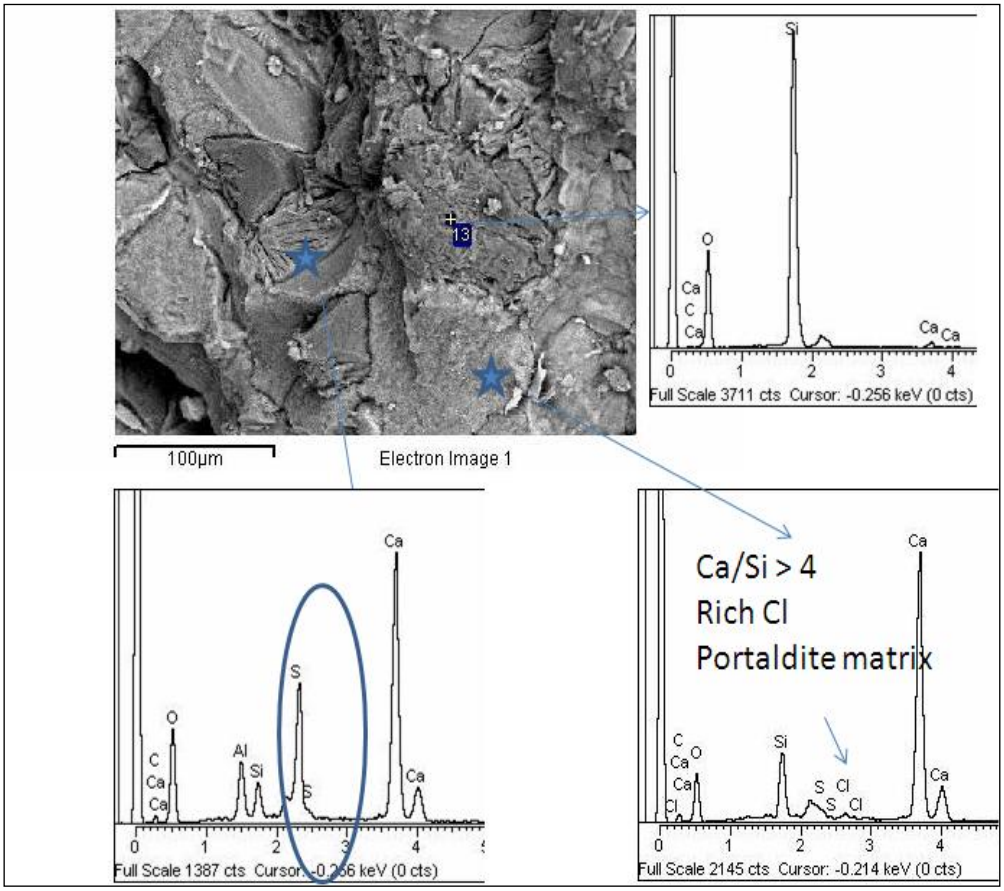

Figure 34: Lime mortar texture and elemental composition of grains.

Polished sections

a) Interface texture

Figure 35 shows a reconstruction of BSE images of cell 3 that were taken in the mortar-bentonite interface. Near the bentonite interface, the mortar matrix tends to darken, what it is indicative of the dissolution of the matrix. It is also significant that below the horizontal break, produced after the mortar-bentonite alteration band, the bentonite have its typical granular aspect due to a small retraction of smectite-rich grains. The micro-cracks in the alteration band and the absence of retraction indicate more a brittle than a plastic consistence of this zone. This band seems to be less developed in cell 4 (Figure 36, natural bentonite), but as it was mentioned, the cracks in this sample can be also an artifact of the mechanical deformation suffered during cutting.

Attending to the aspect of the mortar, the matrix darkens in cell 4 with more extension, and this dark zone often faces to preferential paths that end in micro-crack propagation direction in the bentonite. This can indicate preferential sources of alkaline alteration in zones were portlandite would be dissolved in a greater extent.

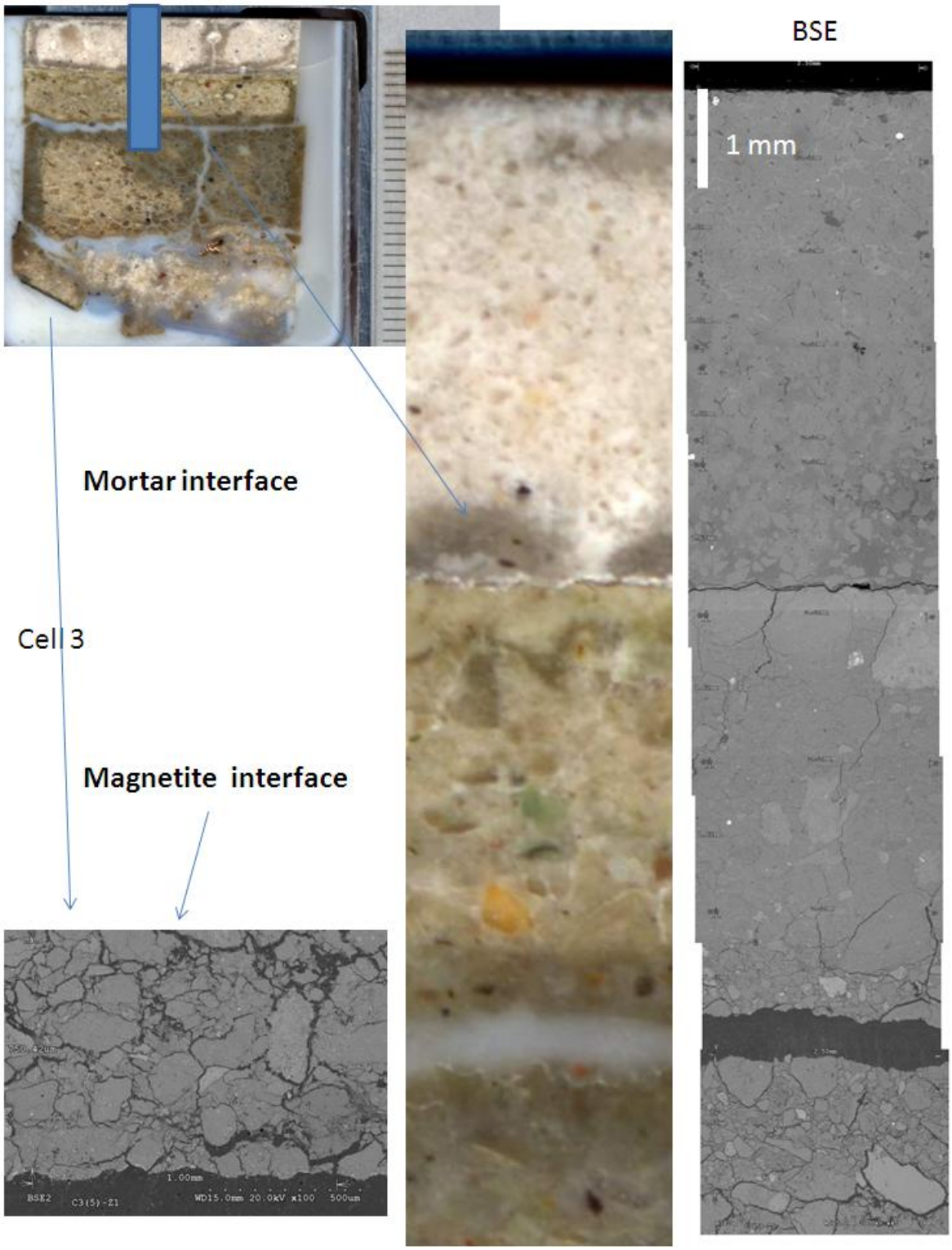

Figure 35: BSE images, compared to a digital scan of the polishes section in cell 3 (pre-treated bentonite).

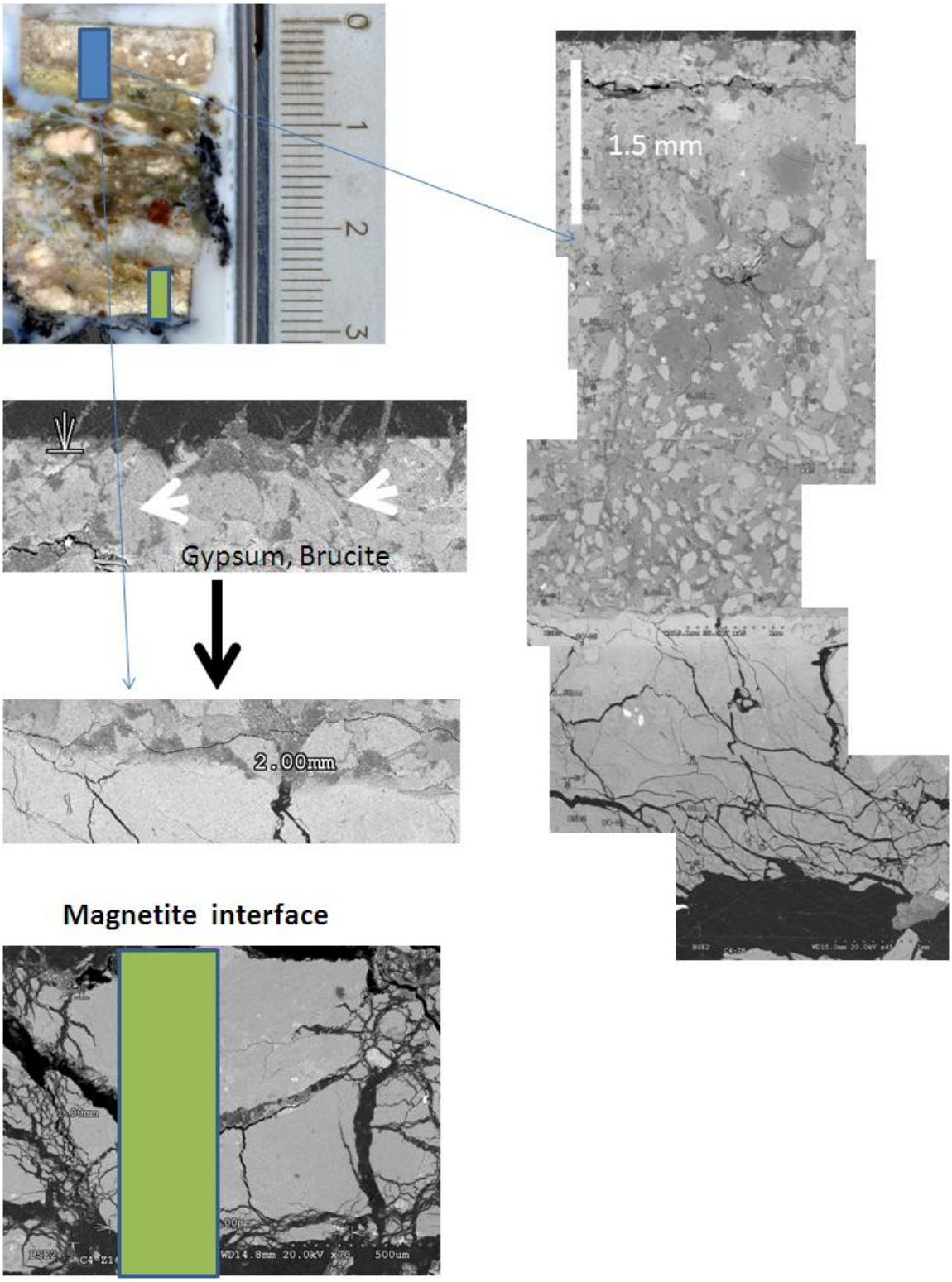

Figure 36: BSE images of mortar and magnetite interface of the polished section in cell 4 (natural bentonite).

b) Chemical profiles

A calcium front is developed from the mortar towards the bentonite. This is illustrated in Figure 37. Calcium in mortar is dissolved near the bentonite interface and the extent of dissolution towards the hydration source is more important in cell 4 (natural bentonite) than in cell 3 (pre-treated bentonite).

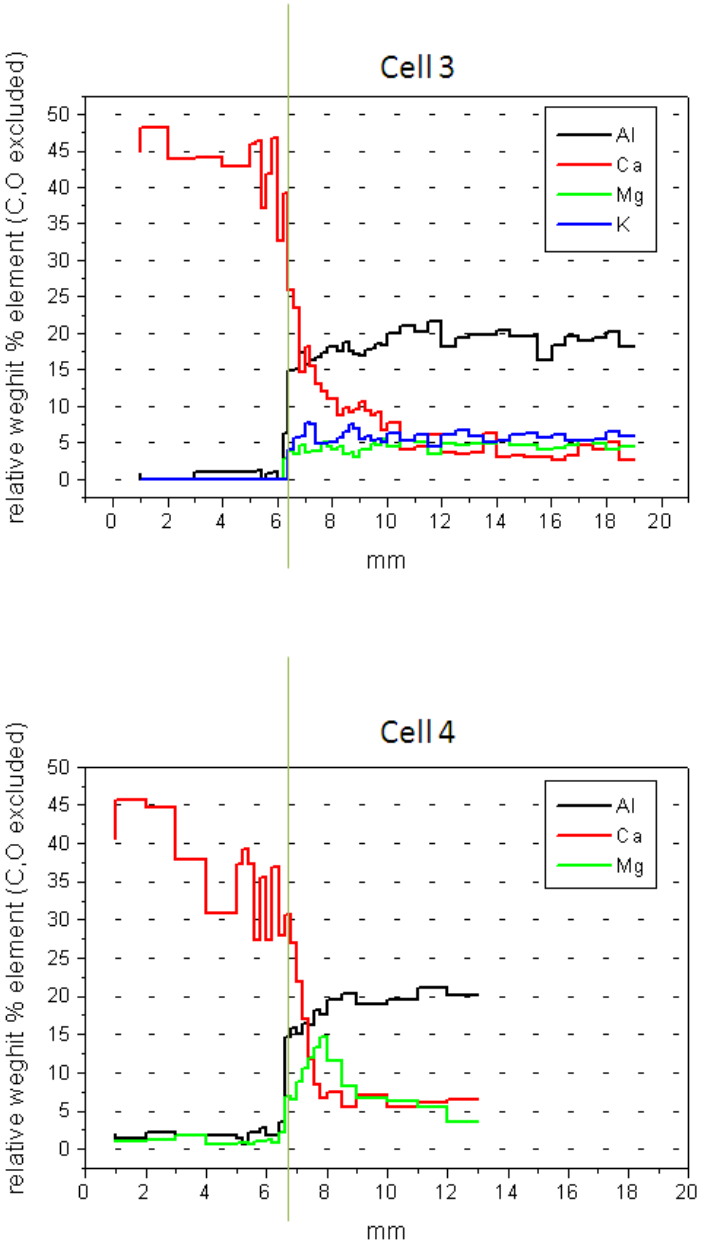

Figure 37: Chemical profiles (Al, Ca, Mg and K) in the bentonite-mortar interface of cells 3 and 4.

Aluminum penetrates in the mortar from the bentonite in accordance to the Al sulfate phases produced in the mortar. Magnesium is concentrated in the bentonite at the interface in cell 4, a phenomenon that is not observed in cell 3. Pre-treated bentonite has minor quantities of exchangeable magnesium and the precipitation front of Mg (as Mg-silicates) is not significantly produced. In turn, potassium, is visible in cell 3 and not in cell 4 (K is virtually absent from the exchange complex). The extension of K by Ca exchange in cell 3 is very small. However, the calcium front penetrates up to 3 mm in the bentonite compared to < 1mm in the natural bentonite. This confirms the less developed alteration band observed in cell 4.

The sulfur (sulfate) front is well detected by the EDX analysis and Cl is detected with less confidence (Figure 38).

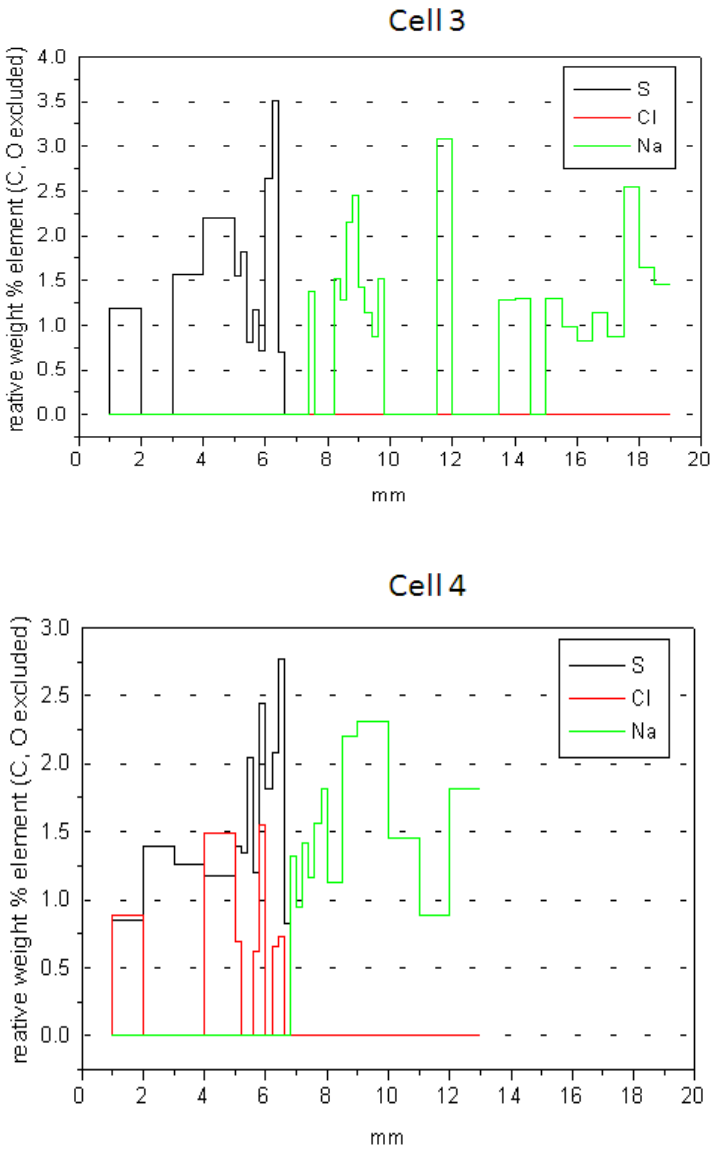

Figure 38: Chemical profiles (Na,S y Cl) in the bentonite-mortar interface of cells 3 and 4.

S is concentrated in the area of influence of the Al supplied by the bentonite. In consequence it is concentrated near the bentonite although it is present in the whole mortar thickness. Sodium is better detected in cell 4 than in cell 3 interfaces. This fact is due to the originally higher contents of sodium in natural bentonite.

The magnetite interfaces show a Fe penetration front of < 0.2 mm, less developed in cell 3. This front is very small and has been possibly influenced by the difficulty to establish the exact position of the interface (Figure 39).

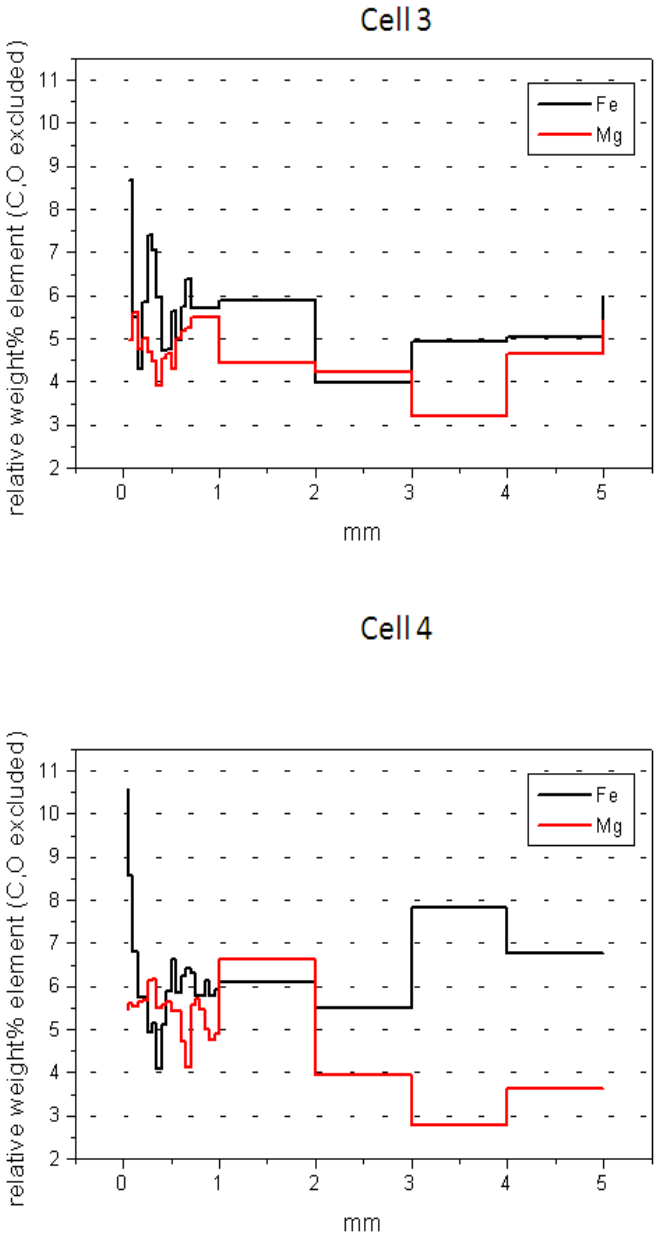

Figure 39: Chemical profiles (Fe and Mg) in the bentonite-magnetite interface of cells 3 and 4.

5.8.2 Pre-treated FEBEX with one interface heated to 60 ºC.

Fresh fracture-samples

The mortar in cell-5 has the aspect of a micro-conglomerate of dark quartz grains immersed in a bright cement matrix. This is due to the higher atomic weight of portlandite components ($Ca(OH)_2$) compared to quartz (SiO_2). The matrix, as it was observed in cells 3 and 4, is mostly portlandite. When its aspect is compact the matrix does not contain S or Cl, but in pores within the matrix filled with massive precipitates contain Al sulfate with C, and Cl. This kind of fillings, sometimes with columnar retraction, has been observed at the bentonite interface. These coatings do not contain Cl when they appear in tabular forms or needles (Figure 40). In consequence, Al-sulfates and carboaluminates are precipitated in pores where portlandite has been dissolved, and chloride is associated to non-differenced precipitates at the pores.

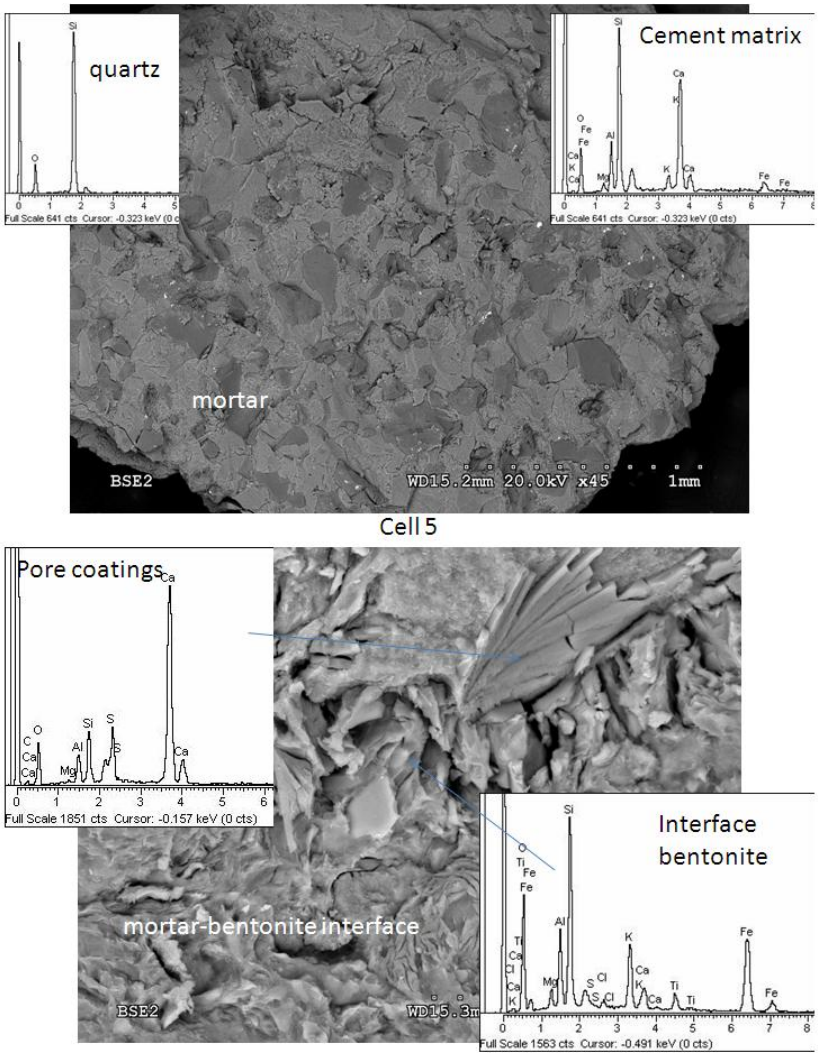

Figure 40: Mortar and bentonite-mortar interface in cell 5 (pre-treated bentonite with one mortar interface.

Cell 6 contains a magnetite interface. The analyses of the iron-rich coating at the bentonite interface are consistent with a Fe_2O_3 iron proportion rather than a magnetite composition (Figure 41). XRD of the bulk magnetite in cell 6 show the presence of hematite, then some oxidation process have been taken place at this interface. The clay aggregates of bentonite at the interface do not incorporate significant quantities of iron in their composition as can be deduced for the % Fe in the bentonite analyzed, which is typical or even lower than the non-altered bentonite, which exhibits a great variation in this parameter (0.5-2.0 %).

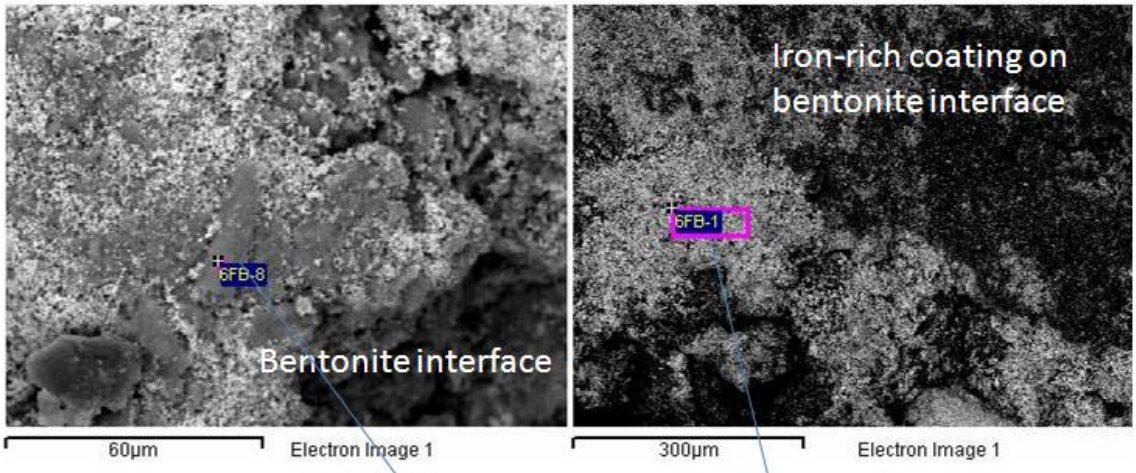

	Bentonite-interface	Iron-coating
Element	Weight%	
C	5.20	--
O	55.46	34.99
Mg	0.66	--
Al	6.13	0.48
Si	20.72	1.70
K	0.43	0.30
Ca	10.70	0.27
Mn	--	0.45
Fe	0.69	61.81

Figure 41: Magnetite interface in cell 6 (pretreated bentonite with one interface, magnetite)

Polished sections

a) Interface texture

The reconstruction in BSE images of the mortar to bentonite transition in cell 5 confirms the dissolution of mortar matrix near the bentonite (Figure 42). In this case the altered band developed up to 4. 5 mm and its compact cemented nature become evident. The bentonite below

the 4.5 mm band is extremely granulated in comparison to pre-treated bentonite in cell 3. The opposite case is the bentonite in cell 6, without mortar, in which the bentonite presents a very homogeneous aspect, without granulation (Figure 43). Magnetite grains appear with diffuse contours when a detailed BSE image is taken, but there is a sharp change in color and iron penetration seems to be virtually null.

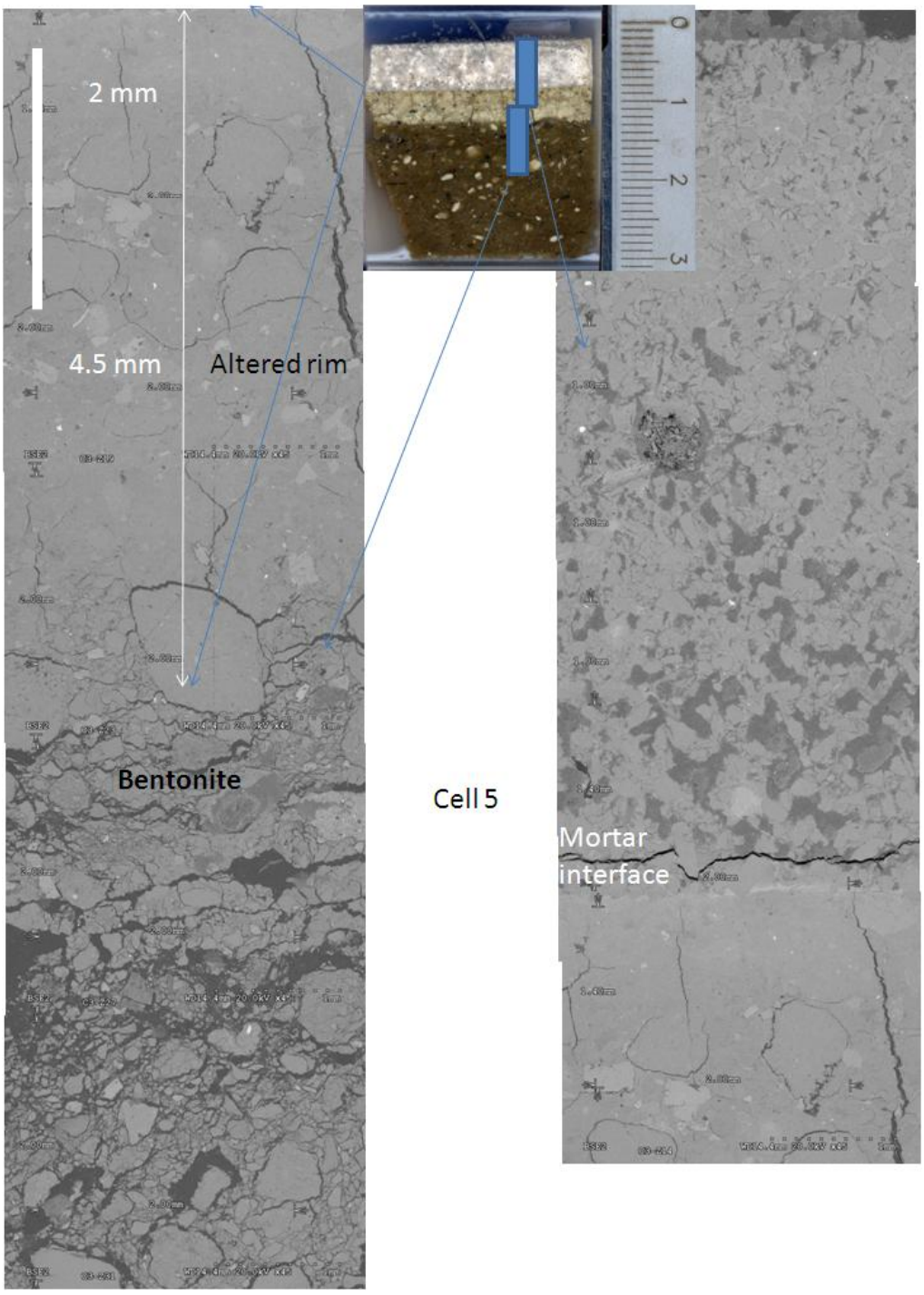

Figure 42: BSE images of mortar interface in a polished section of cell 5 (pre-treated bentonite).

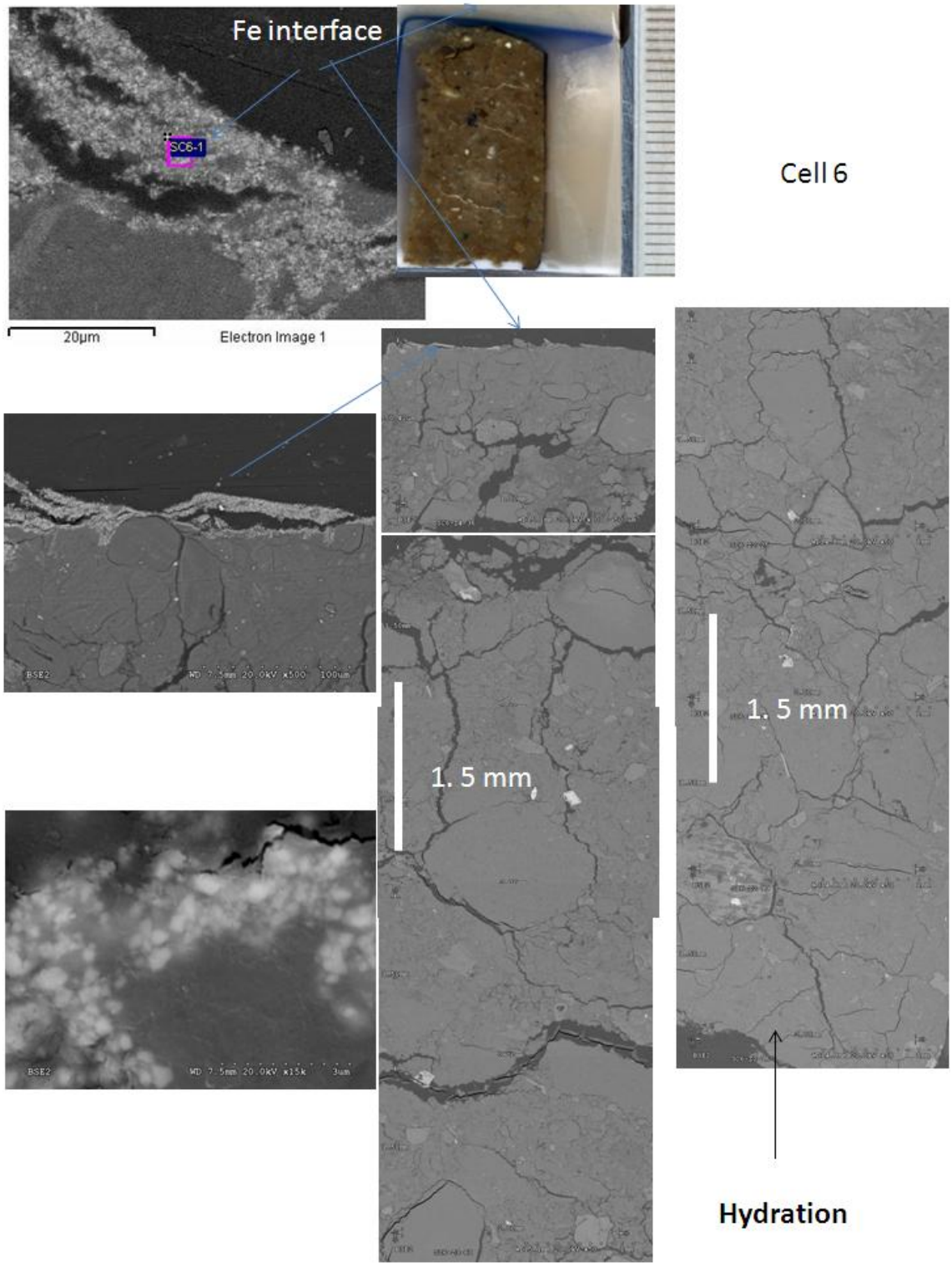

Figure 43: BSE images of magnetite and hydration interface in a polished section of cell 6 (pre-treated bentonite with one magnetite interface).

a) Chemical profiles

The calcium front in cell 5 (Figure 44) confirm the highest development up to 4-4.5 mm in the bentonite, compared to 3 or 1 mm measured in cells 3 and 4 respectively. As was expected S and Cl concentrations in cell 5 are measured in the mortar zone (Figure 45). By contrast in cell 6, mainly sulfate and some chloride are measured in the hydration sideThis means that in the magnetite side S and Clcan beconcentratedentrated or precipitated inside the 4mm thick magnetite powder. Figure 46 shows that iron does not penetrate in the bentonite in cell 6..

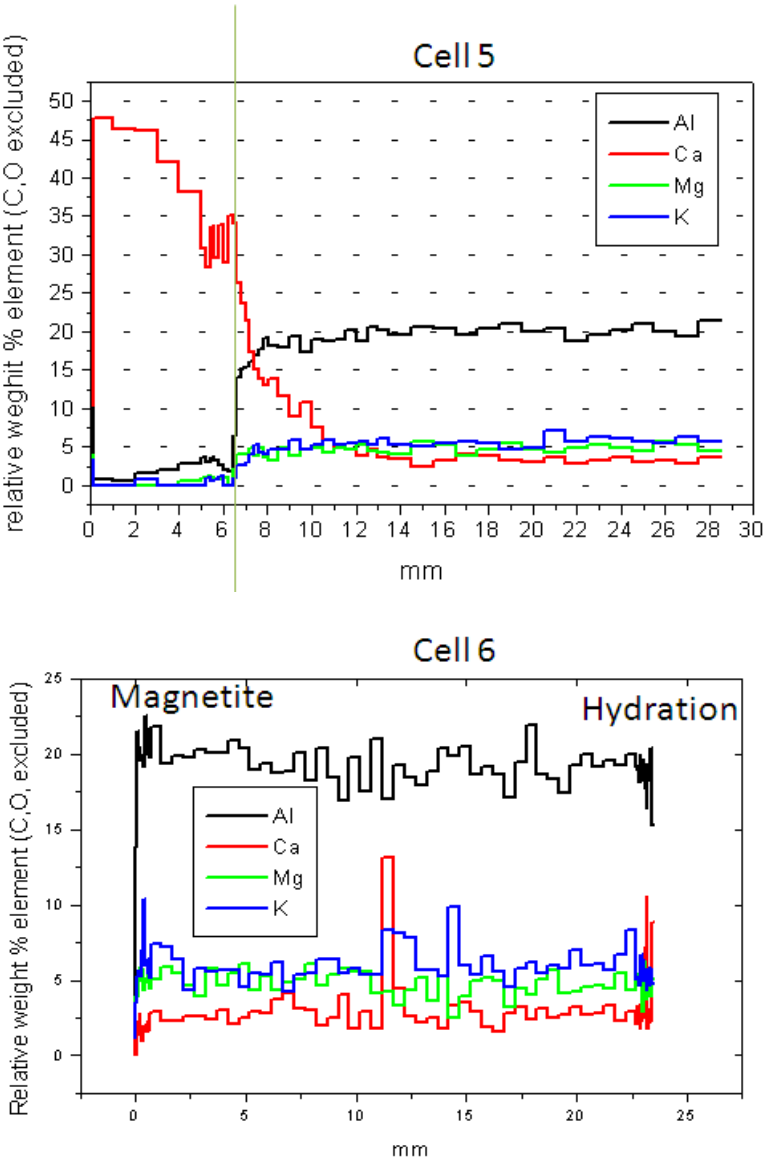

Figure 44: Chemical profiles (Al, Ca, Mg y K) in the bentonite-mortar interface of cells 5 and 6. Pre-treated bentonites with one interface: Mortar (5) and Magnetite (6). The vertical line situates the mortar interface.

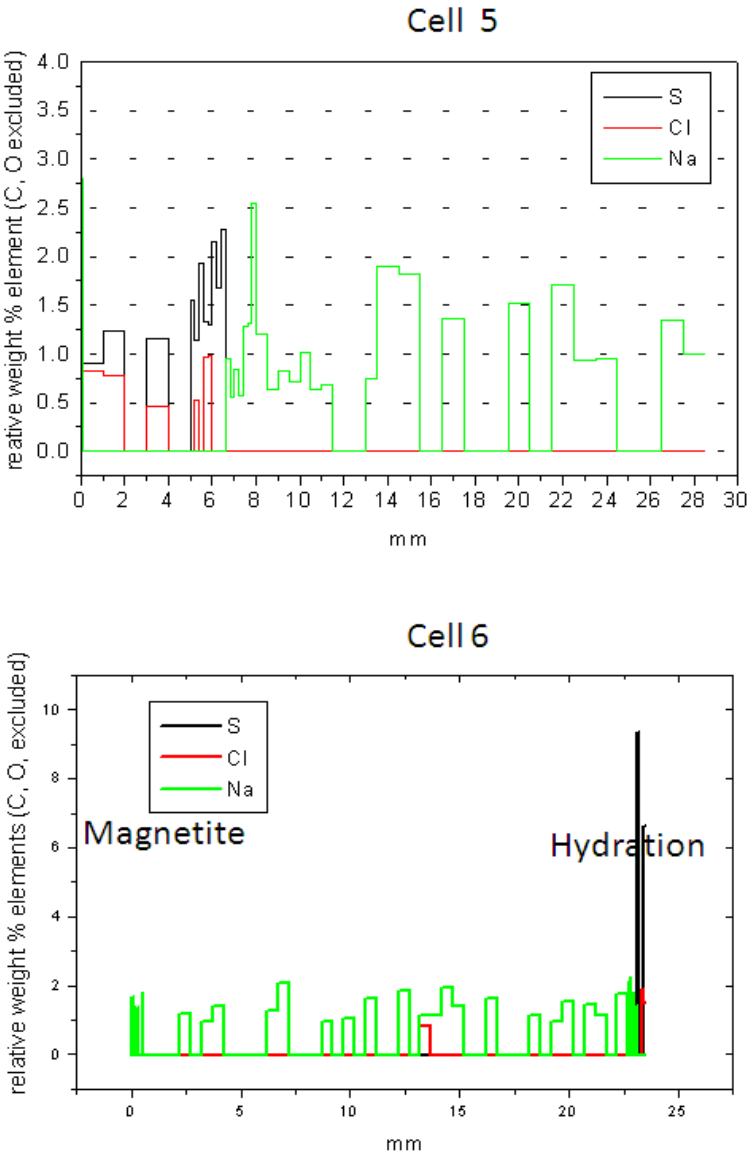

Figure 45: Chemical profiles (S, Cl, Na) in the bentonite-mortar interface of cells 5 and 6. Pre-treated bentonite with one interface: Mortar (5) and Magnetite (6).

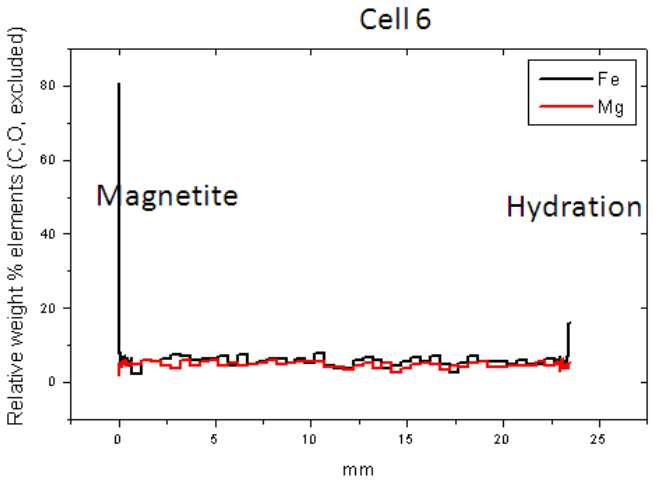

Figure 46: Chemical profiles (Fe, Mg) in the bentonite-magnetite interface of cell 6. Pre-treated bentonite with one interface.

5.9 Mineralogical transformations

The study of mineralogical transformations in the small cells experiments is carried out by the analysis of XRD patterns. This is focused to identify mineral phases, which allows us to link the observed physical, chemical and textural changes with the precipitation or dissolution of mineral phases.

5.9.1 Natural and pre-treated FEBEX with no interfaces heated to 60 °C.

X-ray powder patterns from bentonites after the experiments in cells with no interfaces are very similar to the originally emplaced bentonites (Figure 47). The first peak in the region near $^{0}6$ 2theta degrees (14-15 Å spacings) corresponding to the basal spacing (001 hkl Miller indexes or the repeating distance **c** between interlayers) of the smectite, remained in the values described in the materials paragraphs. These patterns have been semi-quantified in order to establish relative differences among them. Table XII shows the very similar wt% estimation (> 95 % smectite) for all this five samples. Differences in some accessory minerals as K-feldspars and plagioclase are not very meaningful as far as the size of these minerals can vary a lot in the samples (relative big crystal of plagioclase can be observed in SEM polished sections) and often cannot be grinded to very fine powder when they are mixed in a clay rich material. So, the intensities for their peaks are not very homogenous and show preferred orientation effects (some peaks are missing, but unfortunately not systematically in the studied samples). This seems not to affect in the same way to calcite or quartz. The case of cristobalite is greatly influenced but the presence of plagioclase because the most intense cristobalite peak (4.04 Å) is overlapped to a significant peak of plagioclase. The 060 (1/6 of the repeating distance in the **b** dimension) peaks are slightly displace form natural to pre-treated bentonite (1.500 to 1.501 Å).

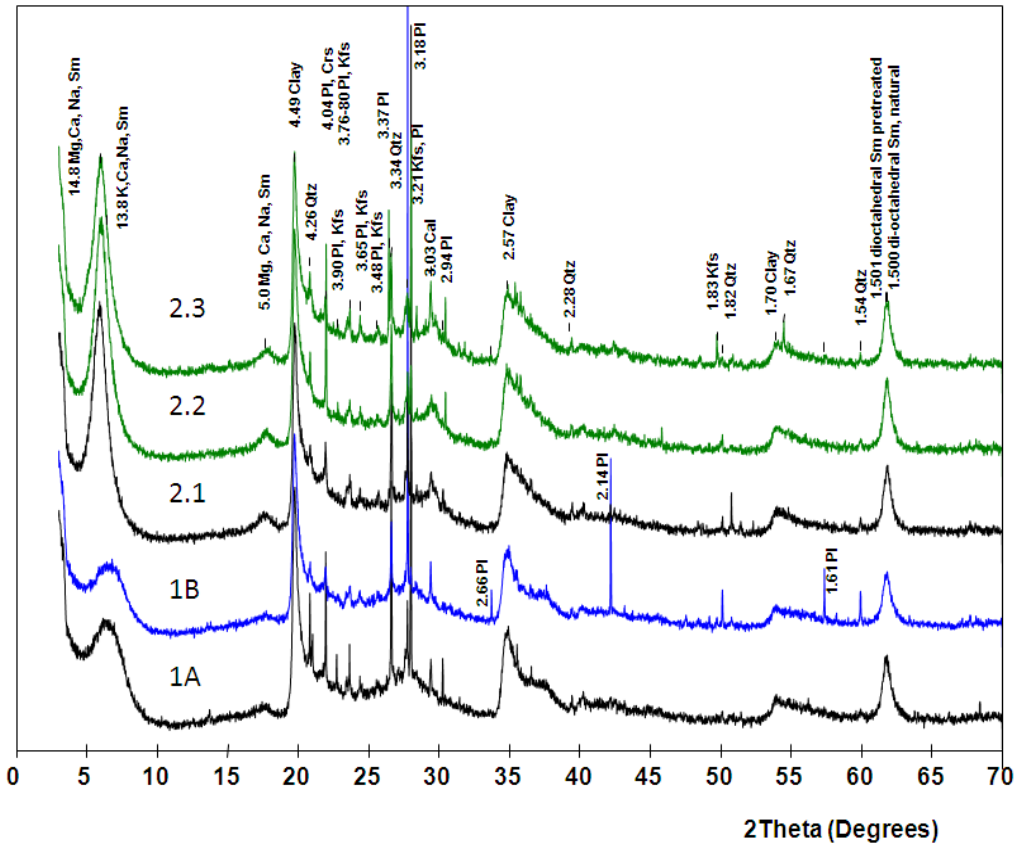

Figure 47: X-ray powder patterns for randomly oriented powder bulk samples for cells 1 (Pre-treated FEBEX, and 2: natural FEBEX. Sm: smectite, Clay: clay minerals, Qtz: quartz, Kfs: K-feldspars, Pl: Plagioclase, Cal: calcite. Numbers above the peaks are d-spacings in Å.

The very small alteration in these bentonites regarding the mineralogical phase changes as seen by XRD is confirmed by the study of clay oriented aggregates (Figure 48). Pre-treated FEBEX exhibits partial expansion in the same way as the same bentonite before the experiments. Just a very small peak of a collapsed 10 Å Ilite-like (Ilt) phase can be seen which was not detected in the initial pre-treated sample. Natural FEBEX showed the initial fully expandable behavior. In addition, in order to confirm the reversibility of the K-exchange induced partial collapse, samples were Mg-homoionized and re-expanded with ethylene-glycol. All of them re-expanded and showed a regular series of $d_{(00l)}$ basal spacings (Figure 49).

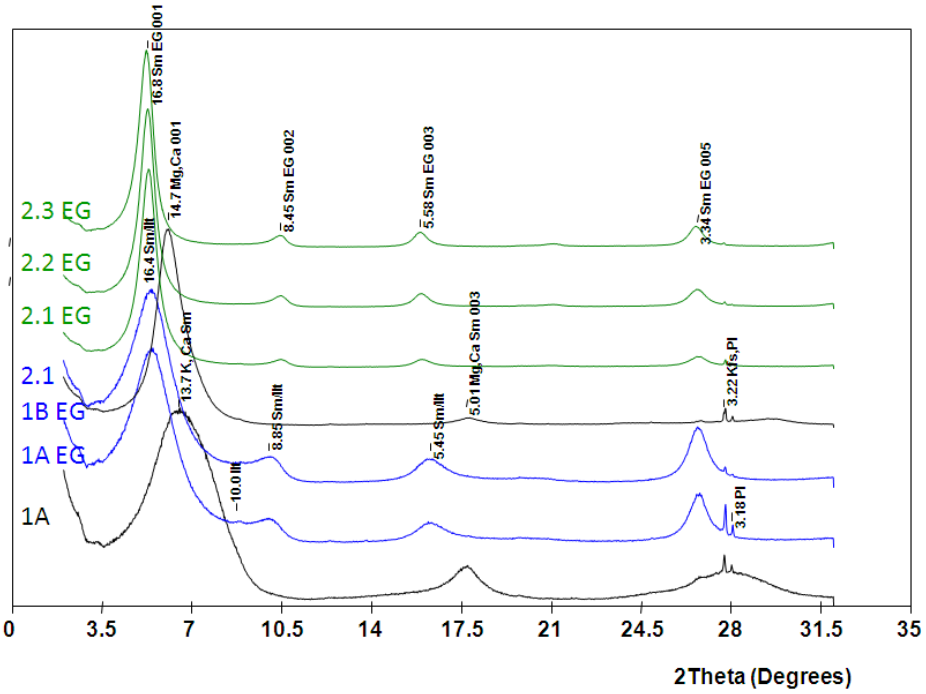

Figure 48: X-ray powder patterns for oriented and ethylene-glycol (EG) solvated aggregates for cells 1 (Pre-treated FEBEX, and 2: natural FEBEX. Sm: smectite, Qtz: quartz, Kfs: K-feldspars, Pl: Plagioclase. Numbers above the peaks are d-spacings in Å. Miller indexes (00l) for the regular EG solvated diffraction peaks are referenced.

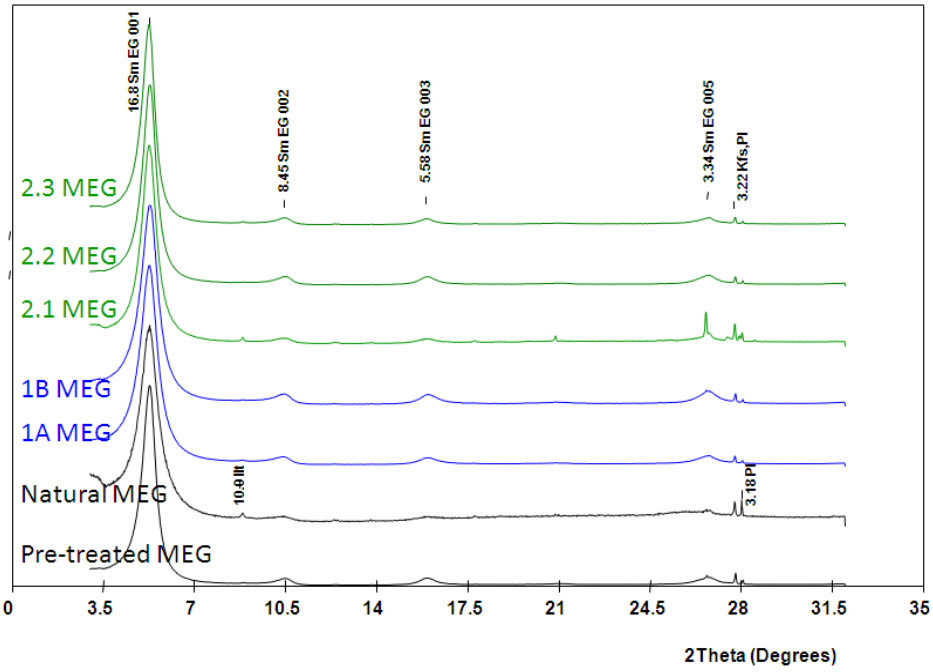

Figure 49: X-ray powder patterns for oriented and ethylene-glycol (EG) solvated aggregates after Mg-homoionization for cells 1 (Pre-treated FEBEX, and 2: natural FEBEX. Sm: smectite, Qtz: quartz, Kfs: K-feldspars, Pl: Plagioclase. Numbers above the peaks are d-spacings in Å. Miller indexes (00l) for the regular EG solvated diffraction peaks are referenced.

Table XII: Semi-quantitative weight % (wt) minerals in cells 1 (pre-treated) or 2 (natural) FEBEX samples in absence of interfaces. A relative error of, at least 10 wt.% should be considered. A decimal place is necessary in order to represent the relative abundance of some of the accessory or new formed minerals.

Sample	sheet-sil 4.45	Quartz 4.26	Cristobalite 4.04	Aragonite 3.39	Microcline 3.24	Plagioclase 3.18	CSH 3.07	Calcite 3.03	Portlandite 4.90	Ettringite 9.7	Monosulfate Al 8.9
	Clay	Qtz	Crs	Arg	Kfs	Pl	CSH	Cal	CH	Aft	C4ASH12
1.1	96.2	1.1	--	--	0.2	2.2	--	0.3	--	--	--
1.2	96.8	0.9	0.1	--	1.8	0.1	--	0.3	--	--	--
2.1	98.2	0.7	0.2	--	0.3	0.3	--	0.3	--	--	--
2.2	97.9	0.7	0.8	--	0.1	0.3	--	0.2	--	--	--
2.3	98.3	0.5	--	--	0.1	0.7	--	0.4	--	--	--

5.9.2 Natural and pre-treated FEBEX with two interfaces heated to 60 °C

Small cells 3 and 4 contained a compacted bentonite, pre-treated or natural respectively, with a 6 mm lime mortar facing the hydration source of the cell and 4 mm pressed magnetite powder at the opposite side. During the dismantling of the experiments white powder precipitates were sampled at the hydration source in contact with the lime mortar. The mineralogical composition determined was brucite, gypsum and aragonite (Figure 50). The powder is composed of small slates that contain a paste of brucite-rich material with inclusions of aragonite. Below this paste, big crystals of gypsum containing inclusions of Mg-silicates were detected (Figure 51).

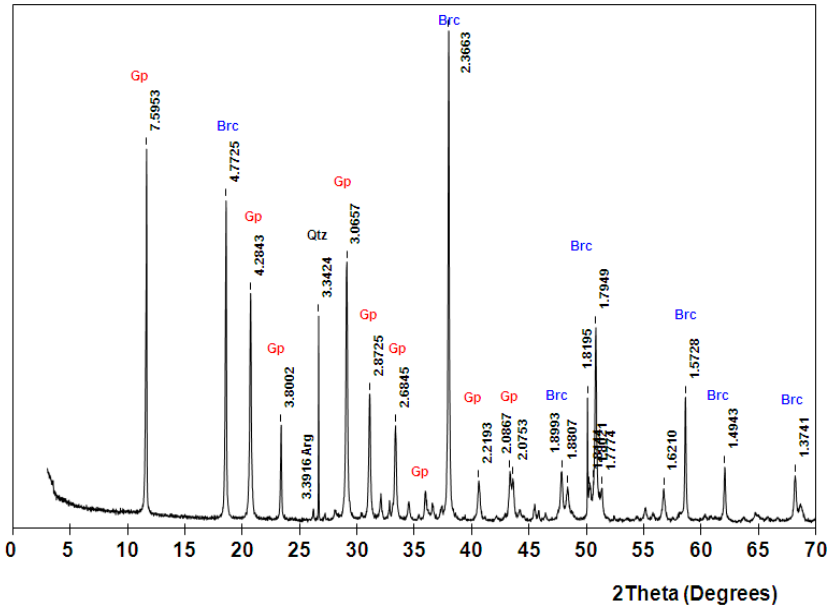

Figure 50: X-ray powder patterns for precipitated salts at the hydtation source in cell 4. Arg: Aragonite, Brc: Brucite. Gp: gypsum, Qtz: quartz. Numbers above the peaks are d-spacings in Å.

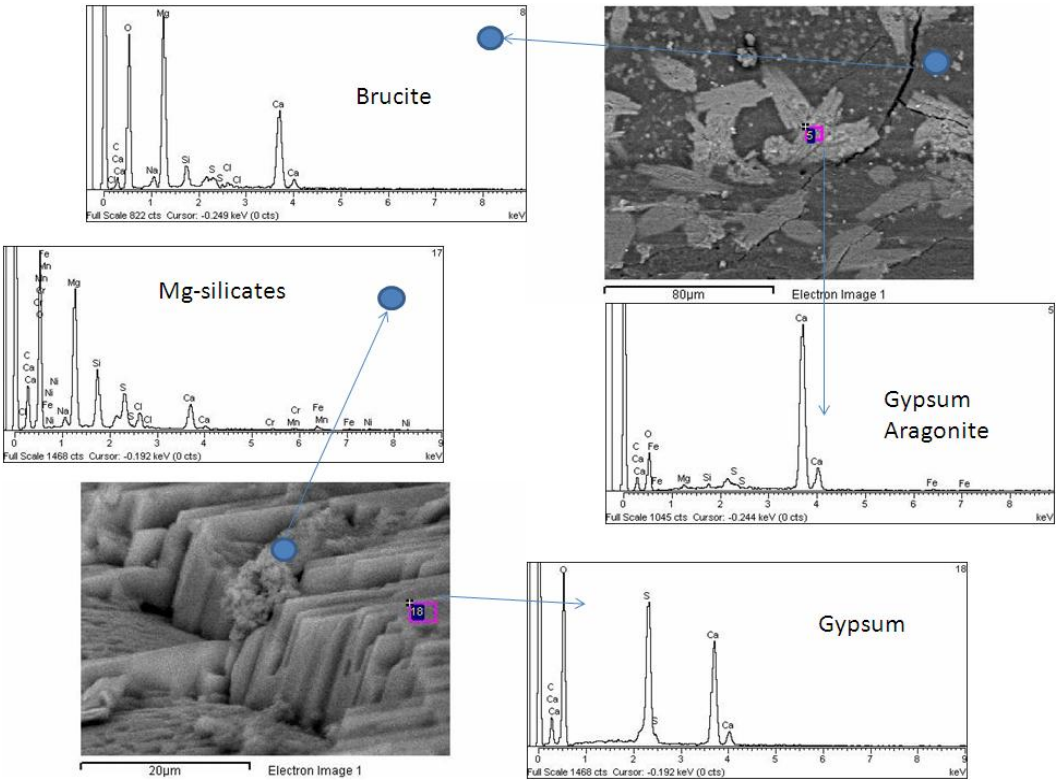

Figure 51: SEM photographs and analysis of the salts observed at the hydration source facing lime mortar in cell 4.

The XRD patterns for the samples near the mortar interface are represented in Figure 52. The mortar is composed of quartz and portlandite (CH). Portlandite is partially dissolved in the whole section of the mortar, but its dissolution is higher near the bentonite interface than in the hydration contact (Table XIII). More than a half of the initial portlandite has been dissolved in the whole mortar section. In the natural bentonite tests (cell 4) the portlandite dissolution is more important. There were very small amounts of new formed minerals detected in the mortar. Small peaks are identified as Al-monosulfates (cell 4) and carboaluminates have been detected in the mortar of cell 3.

Ettringite ($Ca_6Al_2(SO_4)_3(OH)_{12}$) was not detected. As far as we know from SEM-EDX observations that Al-sulphate is present, it is presumed to be mono-sulphate, but the overall quantities of this phase should be well below 1 %wt in the mortar.

The bentonite samples of cells 3 and 4 are represented in Figure 53. CSH phases (low crystalline) have formed in the interface samples (4.3' and 3.3). This is to say that its formation merely affected 1-2 mm thickness. Figure 54 shows a detail of the shoulder to lower angles regarding the 3.03 Å calcite peak, characteristic of the presence of CSH. These samples also maintain a 12-12.5 Å, for the first peak of the basal spacing, which is a very small value, taking into account the presence of calcium in the smectite. These peaks are very broad and overlap with the angles at which some CSH of tobermorite type (14-11-9 Å type) can be observed. Then, the low angle peak

of this region can be interpreted to be consistent with a mixture of clay and CSH phases. The bentonite samples in the magnetite contact have no evidence of any alteration.

The clays at the mortar interface have been extracted, oriented and EG-solvated all in absence of CO_2. They showed broad peaks because it was difficult to perform the orientation procedure. The materials have not the same dispersability than non- 60 ºC heated bentonite. However they exhibited smectite typical expansion. As it was mentioned, pre-treated bentonite partially collapsed, but this collapse have been reversed by calcim exchange because smectite expand with EG to a better grade (80 % smectite) than pre-treated (heated or not) bentonites (Figure 55).

Finally, magnetite is not significantly altered. A small quantity of hematite, and presumably siderite can be observed in the three samples analyzed. Not much difference has been detected when a magnetite has been analyzed near to the bentonite interface (Figure 56).

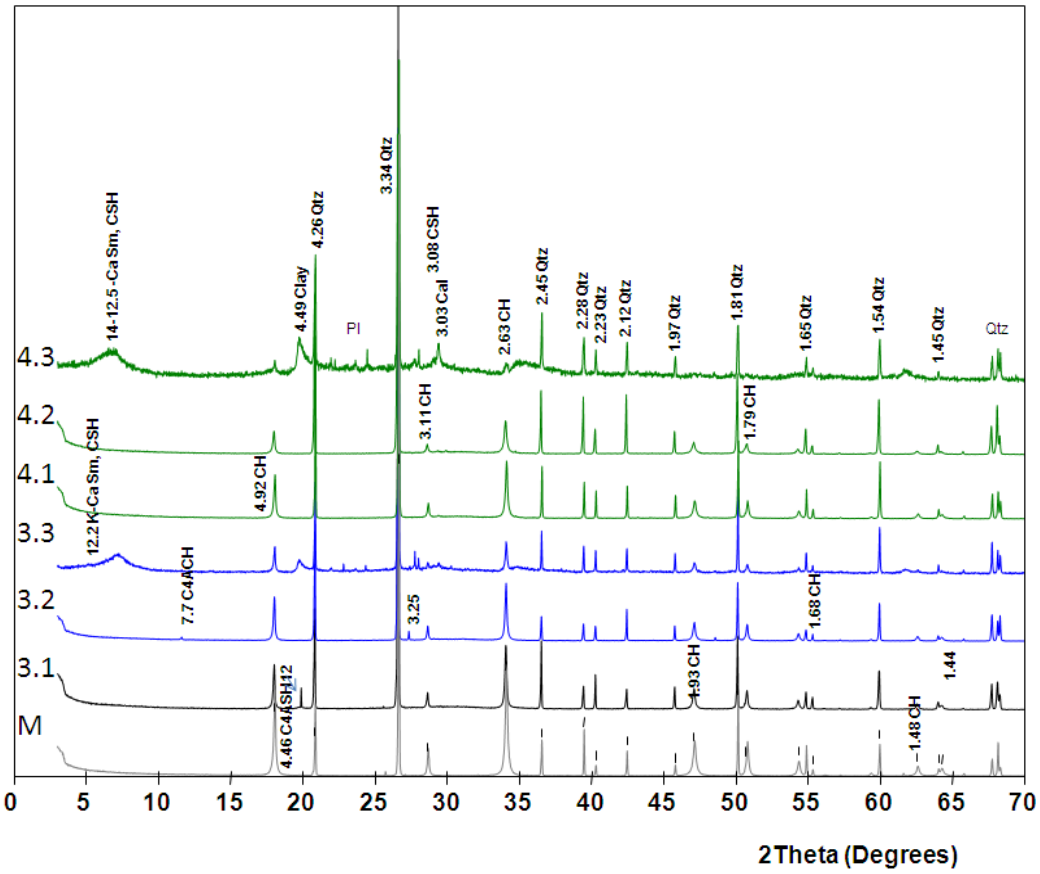

Figure 52: X-ray powder patterns for randomly oriented powder bulk samples for cells 3 (Pre-treated FEBEX), and 4: natural FEBEX at the mortar interface. See Table XIII. M: Original Morat, Sm: smectite, Clay: clay minerals, Qtz: quartz, Pl: Plagioclase, Cal: calcite. CH: portlandite, CSH: low crystalline Calcium silicate hydrate Ca/Si ~1. C4ACH11: carboaluminate 7.7 phases, C4SH12: monosulphate 4.46 phase. Numbers above the peaks are d-spacings in Å.

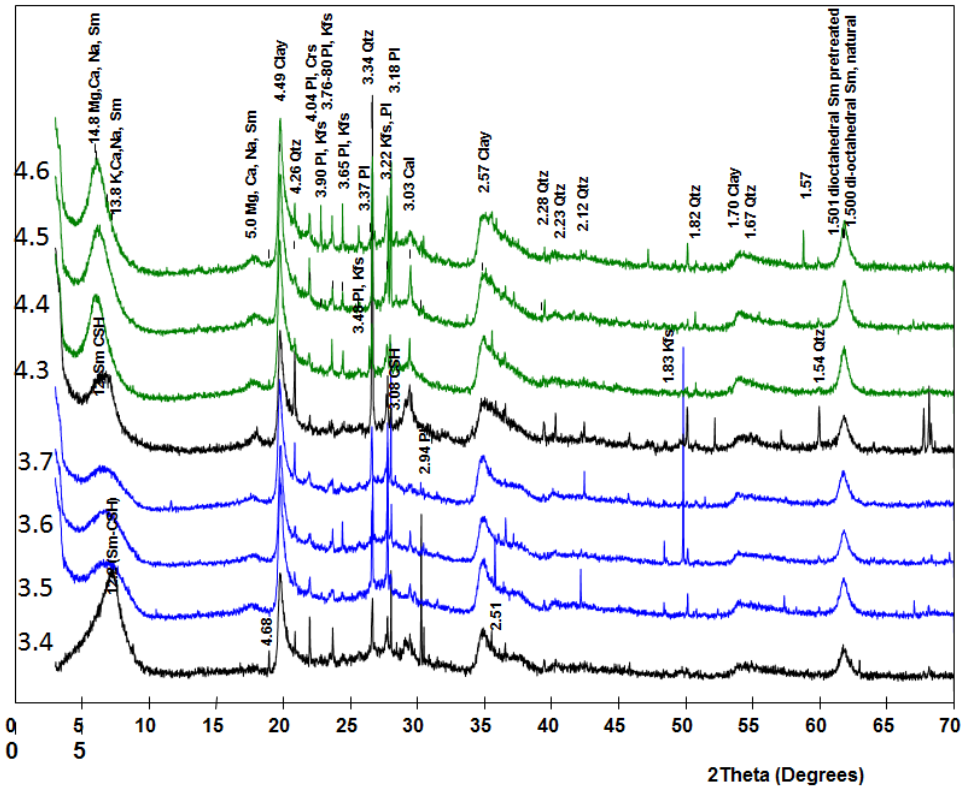

Figure 53: X-ray powder patterns for randomly oriented powder bulk samples for cells 3 (Pre-treated FEBEX), and 4: natural FEBEX bentonite. See Table XIII. Sm: smectite, Clay: clay minerals, Qtz: quartz, Kfs: K-feldspars, Pl: Plagioclase, Cal: calcite. CH: portlandite, CSH: low crystalline Calcium silicate hydrate Ca/Si ~1. Numbers above the peaks are d-spacings in Å.

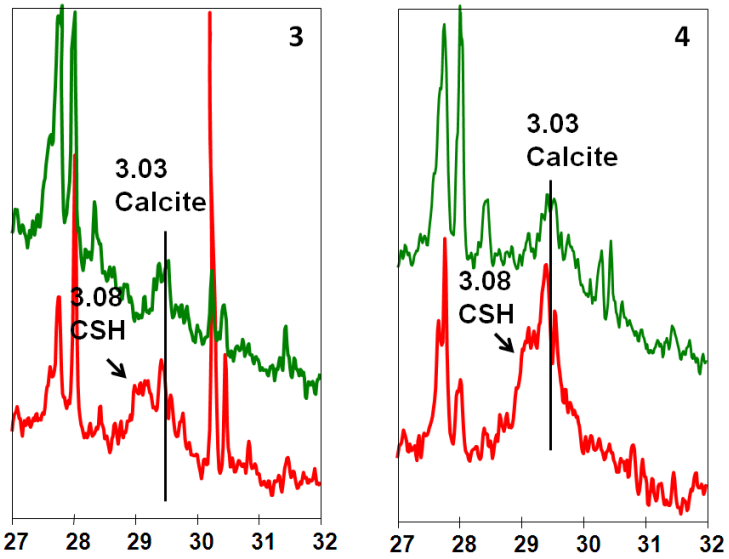

Figure 54: Detail of the 3.08 CSH XRD peak in the bentonite at the mortar interface in mortar interfaces of cells 3 and 4 (in red). Green lines are the bentonites in contact with the magnetite side. Numers in the Y axis are 2 theta angles and numbers referenced to the peaks are d-spacings in Å.

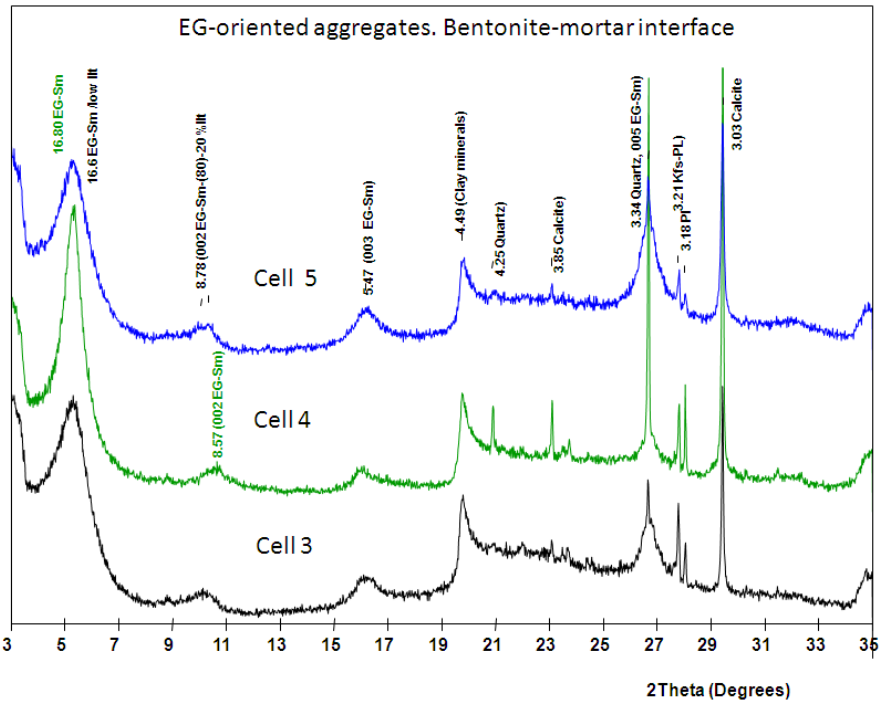

Figure 55: X-ray powder patterns for oriented and ethylene-glycol (EG) solvated aggregates for mortar interface samples in cells 3 (Pre-treated FEBEX), 4 (Natural FEBEX) and 5 (pre-treated FEBEX). Sm: smectite, Qtz: quartz, Kfs: K-feldspars, Pl: Plagioclase. Ilt: Illite-like mineral. Numbers above the peaks are d-spacings in Å. Miller indexes (00l) for the regular EG solvated diffraction peaks are referenced.

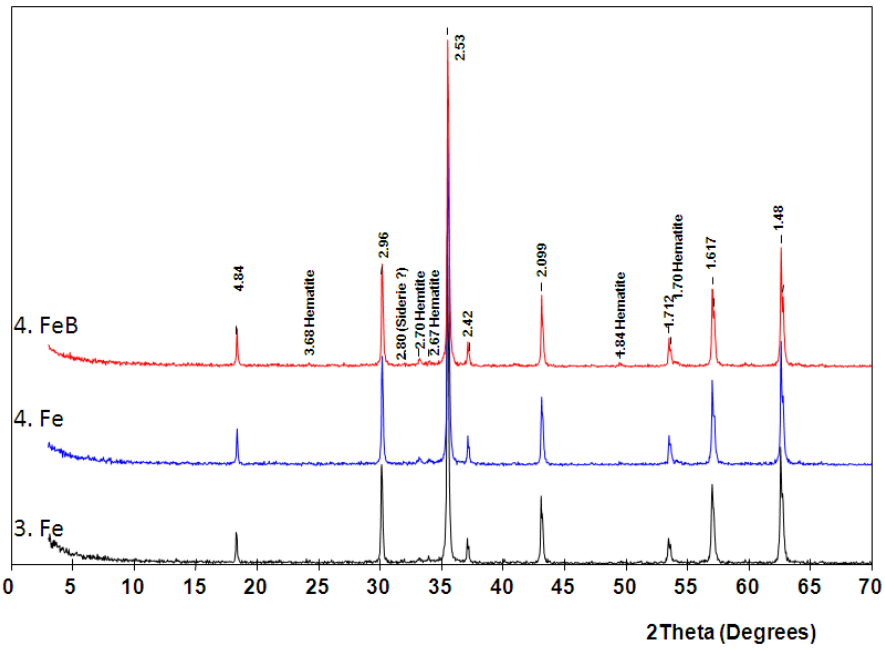

Figure 56: XRD diffraction patterns for magnetite in cells 3 and 4. Numbers without label are d-spacings for magnetite in Å.

Table XIII: Semi-quantitative weight % (wt) minerals in cells 3 (pre-treated) and 4 (natural) FEBEX samples with two interfaces. A relative error of 10 wt. % at least should be considered. A decimal place is necessary in order to represent the relative abundance of some of the accessory or new formed minerals. CH (portlandite) can be considered quantitative as has been related to the initial

Sample	sheet-sil 4.45	Quartz 4.26	Cristobalite 4.04	Aragonite 3.39	K-feldspar 3.24-22	Plagioclase 3.18	CSH 3.08	Calcite 3.03	Portlandite 4.90	Ettringite 9.7	Monosulfate Al 8.9
	Clay	**Qtz**	**Crs**	**Arg**	**Kfs**	**Pl**	**CSH**	**Cal**	**CH**	**Aft**	**C4ASH12**
Mortar	--	60.2	--	--	--	--	--	--	39.8	--	--
3.1	--	75.8	--	--	--	--	--	--	24.2	--	* 4.46, not 8.9
3.2	--	77.8	--	--	--	--	--	--	22.2	--	Carboaluminate 7.6,3.80
3.3	--	79.7	--	--	2.5	1.6	2.1	0.9	13.2	--	
3.4	93.1	1.6	0.5	--	0.3	0.6	3.0	0.8	--	--	--
3.5	98.2	0.6	0.1	--	0.7	0.2	--	0.2	--	--	--
3.6	97.8	0.8	0.1	--	0.8	0.2	--	0.3	--	--	--
3.7	97.3	1.6	--	--	0.3	0.6	--	0.2	--	--	--
4.1	--	81.3	--	--	--	--	--	0.2	18.5	--	--
4.2	--	85.9	--	--	--	--	--	0.2	13.8	--	--
C4.3	91.9	3.1	1.7	--	0.1	0.1	0.7	2.0	0.2	--	--
C4.3'	90.6	6.2	1.8	--	0.1	0.1	0.2	0.9	--	--	--
C4.4	96.4	0.8	1.5	--	0.3	0.4	--	0.6	--	--	--
C4.5	95.9	0.5	0.3	--	0.7	1.7	--	0.9	--	--	--
C4.6	96.3	0.9	1.2	--	0.4	0.8	--	0.5	--	--	--
C4.FeB	97.1	0.8	1.6	--	0.2	0.3	--	--	--	--	--

39.8 wt.% content. Numbers below the list of minerals are d-spacings in Å.

5.9.3 Pre-treated FEBEX with one interfaces heated to 60 ºC.

Cell 5: mortar interface:

As was performed in cell 4, some small samples of whitish crusts were taken during the dismantling at the hydration interface: The separated crusts were in fact scraps of mortar facing the hydration source. The matrix of this mortar is rich in chloride, sulfate and Mg. Nevertheless, portlandite predominates (very high values of C/S) and in some punctual cases CSH of composition C/S close to 1. Needles of Al sulphate of ettringite composition are frequent (Figure 57). However, ettringite is not detected by XRD (Figure 58) but carboaluminate peaks are present, so the Al-sulfate composition can be jeopardized.

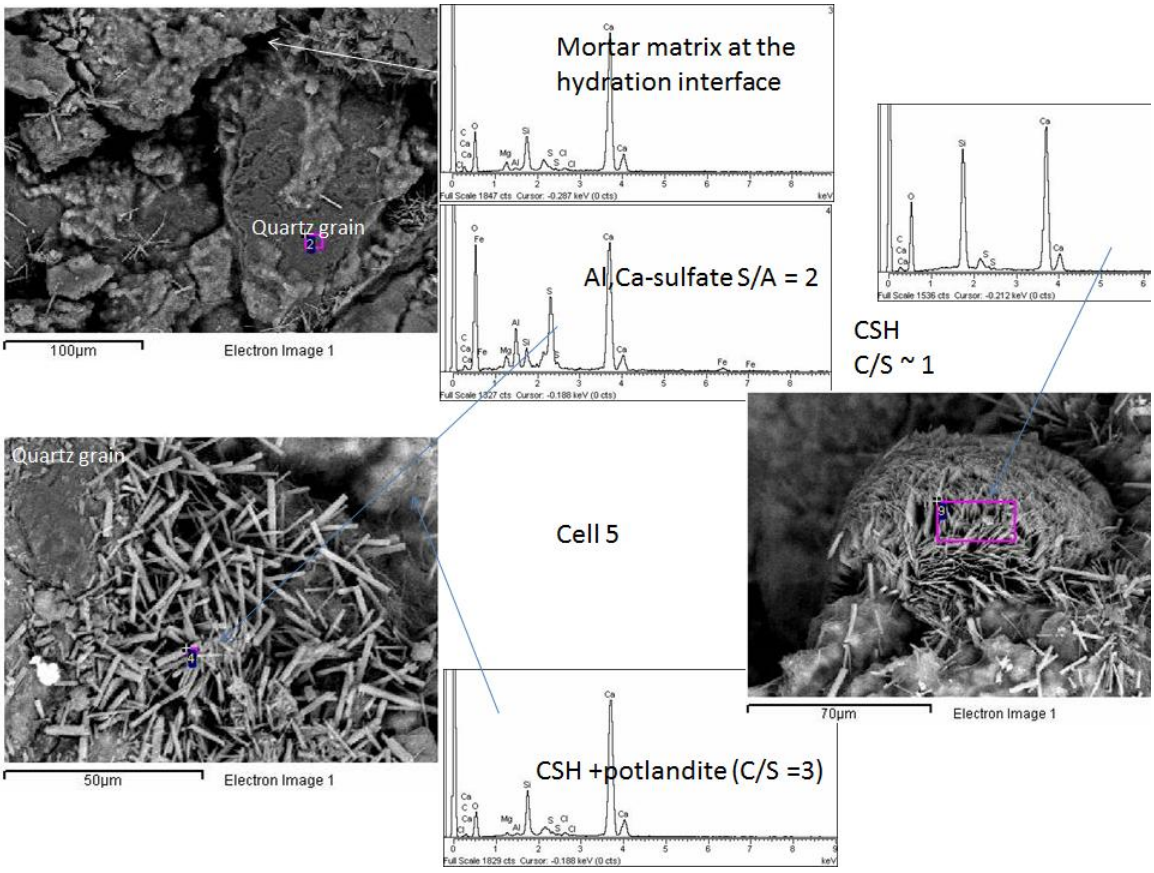

Figure 57: Photographs and analysis of the materials observed at the hydration source facing lime mortar in cell 5.

The behavior of the mortar interface in cell 5, as seen by XRD (Figure 59, Table XIV) is very similar to cells 3 and 4. CSH have formed in higher quantitities than in cells 3 and 4 and the main carbonate present is calcite, although aragonite has been detected in trace amounts. Based on these small differences there is not argument to establish different behavior comparing the mortar interface with or without the opposite magnetite interface.

Bentonite samples from the mortar to the magnetite interface showed also a similar alteration pattern than cells 3 and 4 (Figure 60). CSH is formed in the first 4 mm as the main alteration phase. The peak corresponding to the first order XRD reflection of the basal spacing of smectite is fixed to 12 Å. As has been shown in Figure 55, after clay separation and ethlylene-glycol treatment the smectite shows a virtually fully expandable behavior, so the consideration of this 12 Å peak as the result of an intimate CSH-smectite interaction is consistent with the observations.

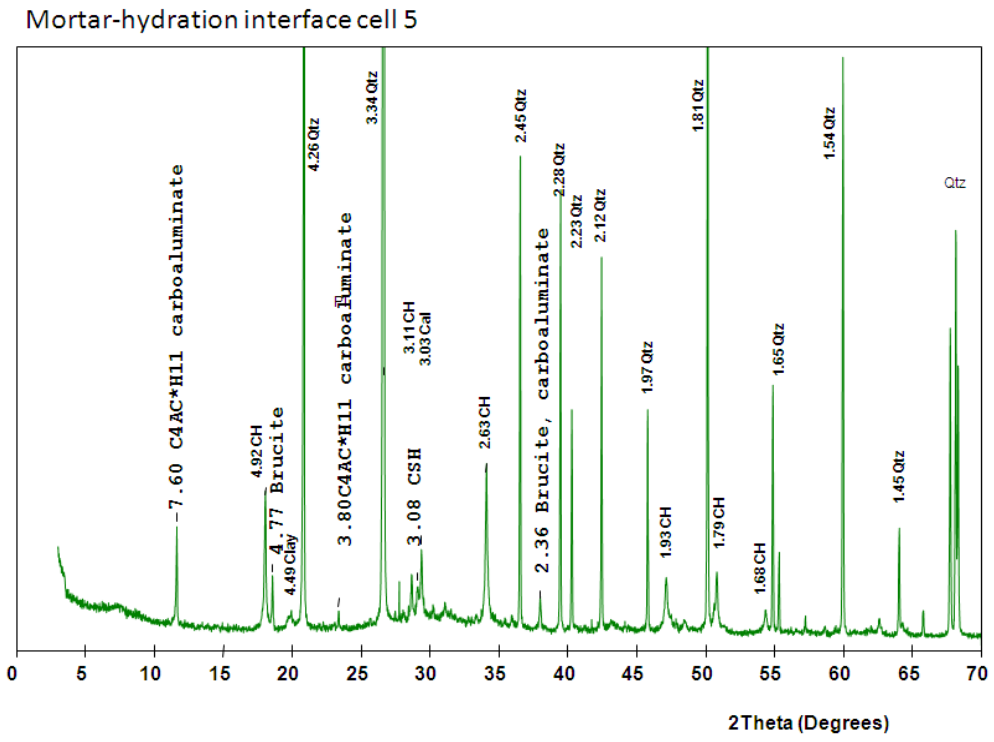

Figure 58: X-ray powder patterns for mortar scraps at the hydration source in cell 5. Qtz: quartz. CH: portlandite. Numbers above the peaks are d-spacings in Å.

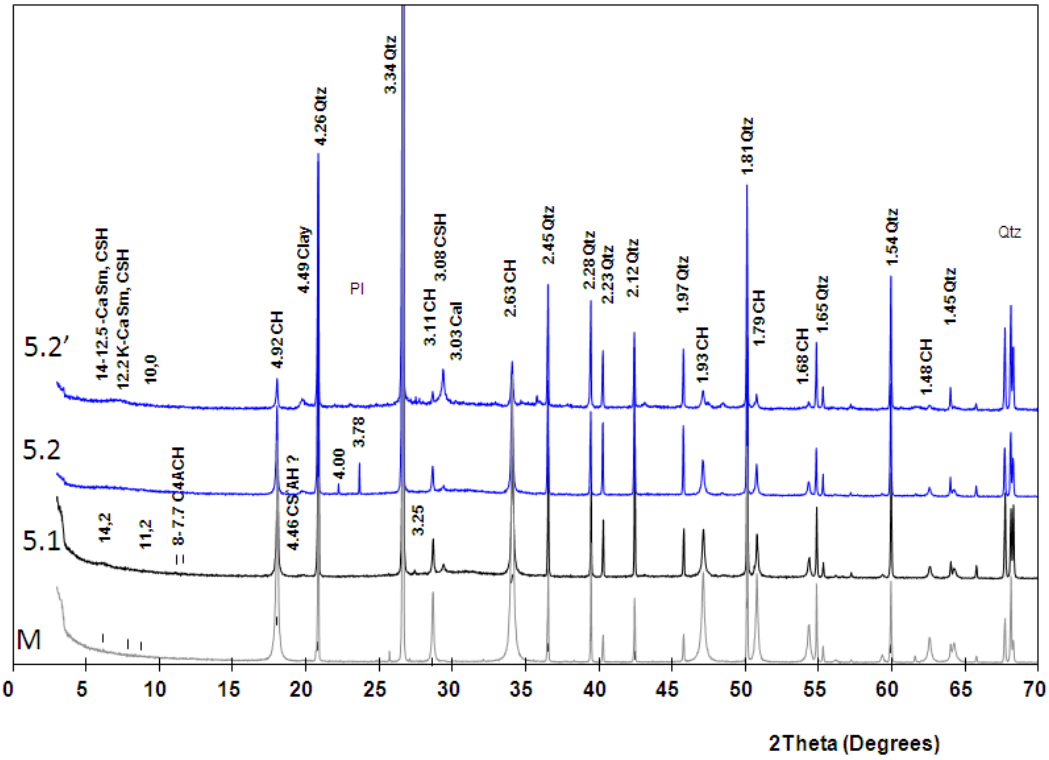

Figure 59: X-ray powder patterns for randomly oriented powder bulk samples for cell 5 (Pre-treated FEBEX) with a mortar interface. See Table XIV. M: Original Mortar, Sm: smectite, Clay: clay minerals, Qtz: quartz, Pl: Plagioclase, Cal: calcite. CH: portlandite, CSH: low crystalline Calcium silicate hydrate Ca/Si ~1. C4ACH11: carboaluminate 7.7 phases, C4SH12: monosulphate 4.46 phase. Numbers above the peaks are d-spacings in Å.

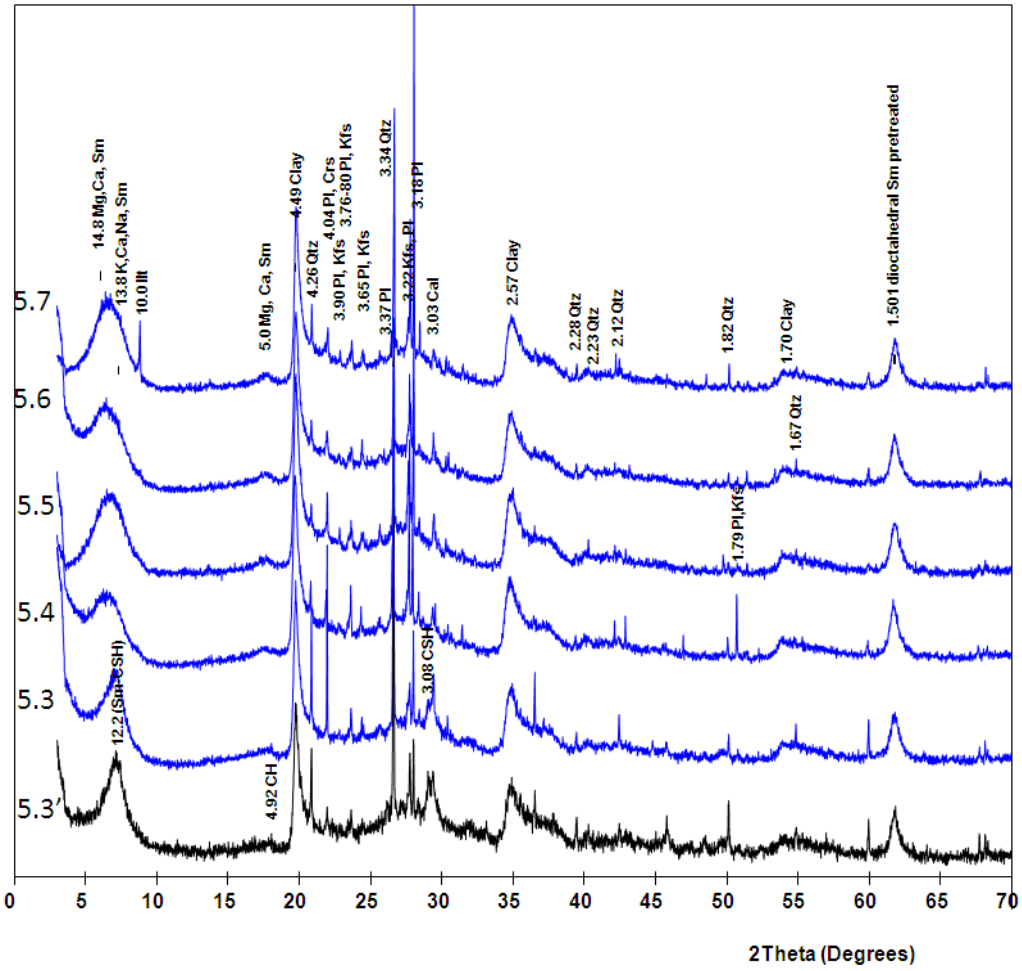

Figure 60: X-ray powder patterns for randomly oriented powder bulk samples for cell 5 (Pre-treated FEBEX) with a concrete mortar. See Table XIV. Sm: smectite, Clay: clay minerals, Qtz: quartz, Kfs: K-feldspars, Pl: Plagioclase, Cal: calcite. CH: portlandite, CSH: low crystalline Calcium silicate hydrate Ca/Si ~1. Numbers above the peaks are d-spacings in Å.

Bentonite outside the influence of the mortar interface have developed a double basal spacing peak at 14.8 (calcium) and 13.8 (calcium-potassium). This means that some of the interlayers have uptake more calcium than others in the interaction with the calcium front.

Cell 6: magnetite interface:

The nature of the hydration source-bentonite interface this time is characterized by the presence of crystallites and some crusts. The crystallites are well developed crystal of gypsum covered with a granular patina. The scraps are mixtures of clay and steel alteration products, rich in Cr and Ni. By far, gypsum is the main mineral formed at this interface (Figure 61).

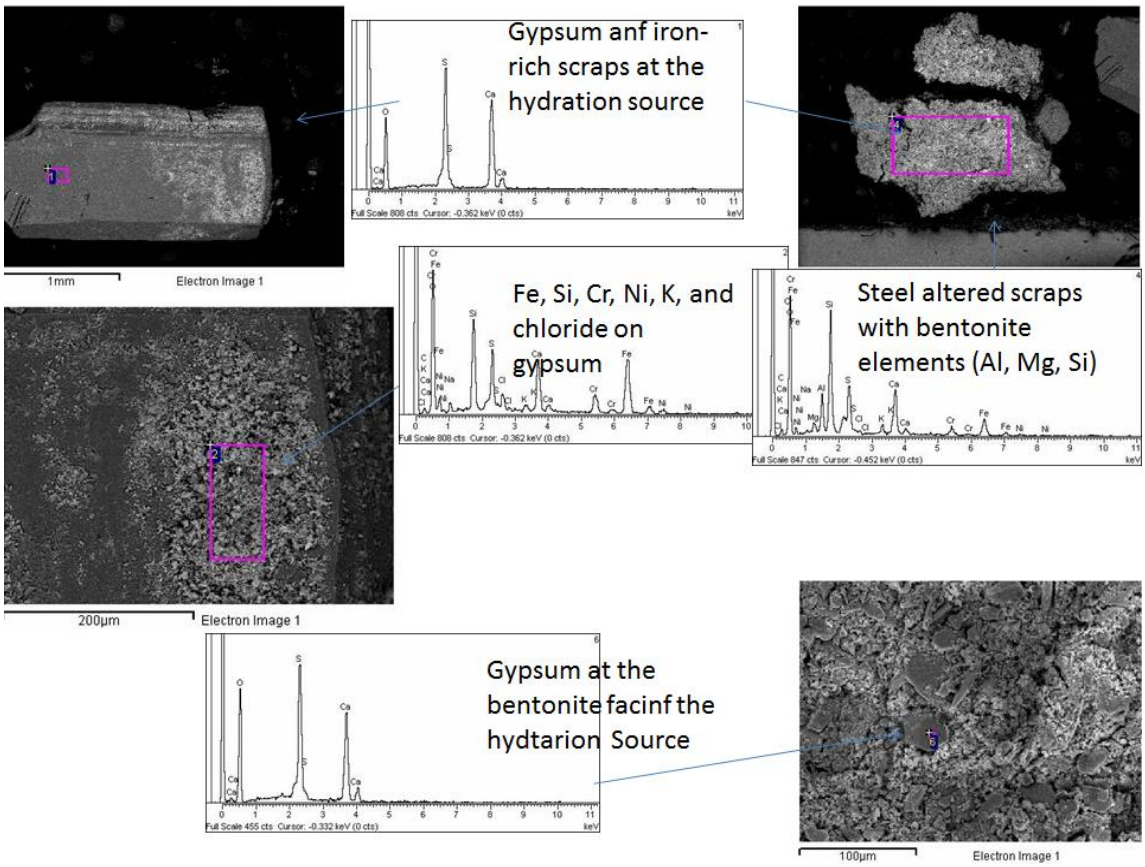

Figure 61: Photographs and analysis of the materials observed at the hydration source facing bentonite in cell 6.

Table XIV: Semi-quantitative weight % (wt) minerals in cell 5 (pre-treated) with a mortar interface. A relative error of 10 %wt at least should be considered. A decimal place is necessary in order to represent the relative abundance of some of the accessory or new formed minerals. Portlandite can be considered quantitative as has been related to the initial 39.8 % content. Numbers below the list of minerals are d-spacings in Å. Carboaluminate of A-sulfates are not quantified but is assumed to have < 1 wt.% contents.

Sample	sheet-sil 4.45	Quartz 4.26	Cristobalite 4.04	Aragonite 3.39	Microcline 3.24	Plagioclase 3.18	CSH 3.07	Calcite 3.03	Portlandite 4.90	Ettringite 9.7	Monosulfate Al 8.9
	Clay	Qtz	Crs	Arg	Kfs	Pl	CSH	Cal	CH	Aft	C4ASH12
Mortar	--	60.2	--	--	--	--	--	--	39.8	--	--
5.1	--	77.8	--	--	--	--	--	0.7	21.5	--	*4.46
5.2	--	83.7	--	--	--	--	0.3	0.6	15.5	--	carboaluminate 7.6,3.80
5.2’	12.5	73.3	--	--	--	--	1,5	5,4	7.0	--	--
5.3’	95.5	1.5	0.2	0.2	0.1	0.3	1,3	0,8	0.2	--	--
5.3	92.3	2.3	1.4	--	0.3	0.4	2,6	0,5	0.1	--	--
5.4	97.0	1.2	0.2	--	0.6	0.7	--	0.2	--	--	--
5.5	97.4	0.7	--	--	0.7	0.8	--	0.5	--	--	--
5.66	96.9	1.5	0.1	--	0.3	0.8	--	0.3	--	--	--
5.7	95.4	1.3	--	--	0.8	2.0	--	0.5	--	--	--

Bentonite in the several sections sampled in cell 6 has the same characteristics as the pre-treated FEBEX. They exhibit a single broad 13. 8 Å basal spacing peak and here were no evidence of alteration (Figure 62). Semi-quantitative wt% amounts calculated for the different minerals (Table XV) evidenced this small alteration impact. Magnetite is present in the magnetite interface sample (6.FB), but the general pattern profile is not different from the others. It is interesting to note how aragonite is present instead of calcite in the hydration source interface. The previous referenced anomalous expansion of the pre-treated FEBEX clay was preserved in the test (Figure 63).

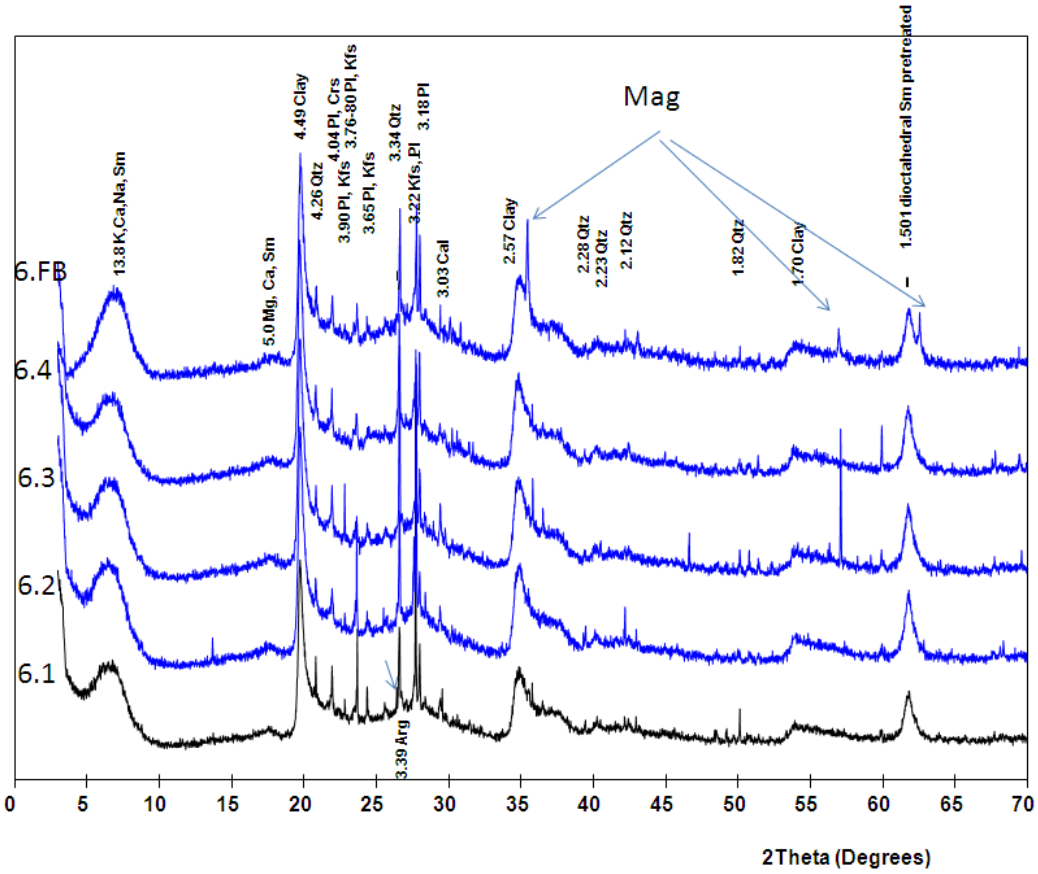

Figure 62: X-ray powder patterns for randomly oriented powder bulk samples for cell 6 (Pre-treated FEBEX) with a magnetite interface. See

Table XV. Sm: smectite, Clay: clay minerals, Arg.: aragonite, Qtz: quartz, Kfs: K-feldspars, Pl: Plagioclase, Cal: calcite. Mag: magnetite. Numbers above the peaks are d-spacings in Å.

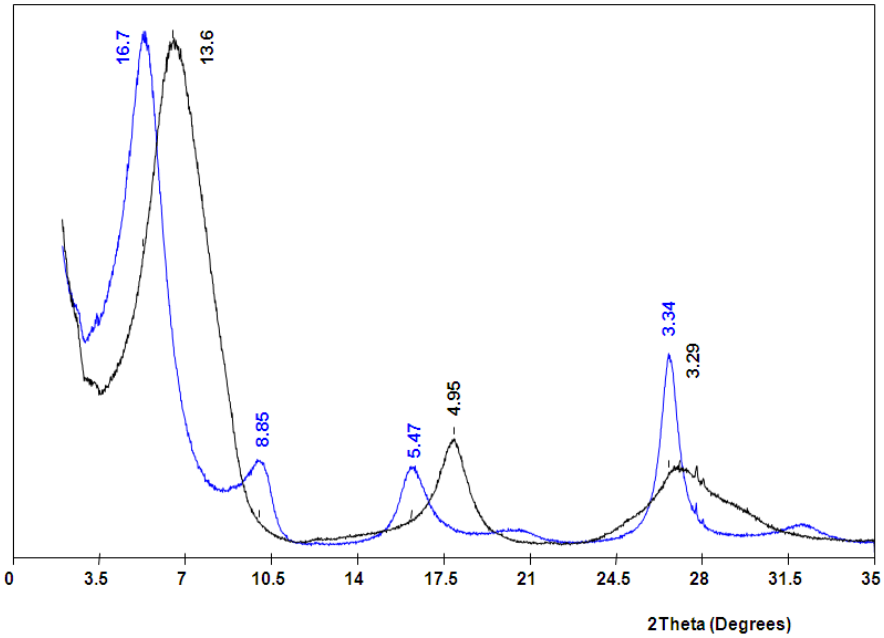

Figure 63: Oriented (Air dried, black) and Ethylene-glycol solvated (blue), XRD patterns from clay extracted from the 6.1 sample in cell 6 (hydration interface). Numbers are XRD peaks in Å.

*Table XV: Semi-quantitative weight % (wt) minerals in cell 6 (pre-treated) with a magnetite interface. A relative error of 10 %wt at least should be considered. A decimal place is necessary in order to represent the relative abundance of some of the accessory or new formed minerals. *: the sample contains trace amounts of magnetite.*

	Sheet-sil. 4.45	**Quartz 4.26**	**Cristobalite 4.04**	**Aragonite 3.39**	**K-felspar 3.24-21**	**Plagioclase 3.18**	**CSH 3.07**	**Calcite 3.03**
	Clay	Qtz	Crs	Arg	Kfs	Pl	CSH	Cal
6.1	97.2	0.7	0.4	0.1	1.2	0.4	--	--
6.2	97.7	0.9	0.5	--	0.4	0.2	--	0.3
6.3	97.1	0.8	0.7	--	0.6	0.4	--	0.5
6.4	97.9	1.0	0.2	--	0.3	0.3	--	0.3
6.FB*	98.0	0.9	0.2	--	0.3	0.3	--	0.2

6 Concluding remarks

Regarding the experiments performed in small cells which have been described in this summary of discussed results we can outline the following aspects:

- Long-term (3000 years) modified bentonite can experiment a potential partial collapse of K-substituted smectite. This will produce a higher density zone in comparison with natural bentonite when saturated. This aspect has to be revised in terms of reliable K-substitution grade in the system.

- Concrete and iron interfaces act as a sink of soluble salts (Cl, S) coming from the clay formation porewater or migrated through the bentonite. The specific Cl and S contained mineral phases has to be better addressed in order to understand their physicochemical behavior and process implication at the interfaces.

- Cell components corrosion is affected by the presence or absence of cementitious compounds. Cement preserves steel from corrosion.

- Cation exchange in bentonite in the concrete interface is characterized for Mg to be totally displaced. Then Ca and K will predominate, although the K cement source has to be carefully validated.

- The new formed minerals at the mortar-bentonite interface establish different altered thicknesses zones: CSH (1 mm), MgSH (2 mm), cemented (5mm). Magnesium concentrated at the interface with mortar in the natural bentonite, however, this was not observed in the pre-treated bentonite. It seems that the precipitation of Mg-phases in the natural bentonite buffers the C-S-H front (as determined by XRD), which is more developed in pre-treated bentonite. This means that natural bentonite has potentially higher buffering capacity to attenuate the calcium alkaline front than the pre-treated one. A low porosity bentonite-mortar zone was experimentally created. This should be carefully studied in order to predict the further development of a diffusive alkaline alteration front through the bentonite. This phenomenon can determine the reduction of hydration or alkaline alteration at long-term.

7 REFERENCES

Blake, CR. and Hartge, K.H., 1986. Bulk density.p. 363-375. In: Methods of soil analyses Part 1, 2nd edition. Ed. A. Klute. Agron. Monogr. 9. ASA and SSSA, Madison. WI

Campos, R., Barrios, I. González, A.M. (2013): Estudio de la porosidad en las Celdas C1 a C6: procesos de de corrosión/alteración en condiciones saturadas. Informe Técnico CIEMAT/DMA/2G210/6/13. 108 pp.

Cobeña, J., Cuevas, J., Martín, M., Ramírez, S., Vigil de la Villa, R. and Leguey, S. (1999). Estudio de la mineralogía y microestructura de una bentonita compactada. Efectos de calentamiento e hidratación. Boletín de la Sociedad Española de Mineralogía, 22, 235-247.

Florea, M.V.A., and Brouwers, H.J.H. (2012). Chloride binding related to hydration products Part I: Ordinary Portland Cement. Cement and Concrete Research, 42, 282–290.

Kaufhold S, Dohrmann R, Klinkenberg M, Siegesmund S, and Ufer, K. (2010): J Colloid Interf Sci 349: 275-282.

Kim, J., Peacor, D., Tessier, D. and Elsass, F. (1995). A technique for maintaining texture and permanent expansion of smectite interlayer for TEM observations. Clays and Clay Minerals, 43, 51-57.

Moore, D.M., Reynolds, R.C., Jr., 1997. X - Ray Diffraction and the identification and analysis of clay minerals. 2nd Edition. Oxford University Press. 378 pp.

Samper, J., Montenegro, L., Turrero M.J., Martín, P.L., Garralón, A., Cuevas, J. and Fernández, R. (2010): Technical Note 1: Design of new experiments. PEBS Internal Deliverable D 3.4.2. 10 pp.

Stefanidou, M. and Papayianni, I. (2005). The role of aggregates on the structure and properties of lime mortars. Cement & Concrete Composites, 27, 914–919.

Villar, M.V., Gómez-Espina, R., Campos, R., Barrios, I., Gutiérrez, L. (2012): Porosity Changes due to Hydration of Compacted Bentonite. En: Unsaturated Soils: Research and Applications, pp 137-144. Ed. Springer.

Yuan, Q., Shi, C., De Schutter, G., Audenaert, K., Deng, D. (2009). Chloride binding of cement-based materials subjected to external chloride environment – A review Construction and Building Materials 23, 1–13